Neural network models of slotted waveguide directional couplers

Martinette Müller

Thesis presented in partial fulfilment of the requirements for the degree of Master of Science (Engineering) at the University of Stellenbosch.

Promoter: Prof. Petrie Meyer

December 2001

Declaration

I, the undersigned, hereby declare that the work contained in this thesis is my own original work and that I have not previously in its entirety or in part submitted it at any university for a degree.

M. Müller

Summary

The application of artificial neural networks to microwave circuits is investigated. A neural network model is developed for two parallel waveguides coupled by a longitudinal slot in the common broad wall. Training data is generated through a moment method solution of the integral equations that describe the structure. A systematic investigation of training options is carried out and the development of the model is described in detail. The model is evaluated and compared with an Adaptive Sampling Interpolation (ASI) Technique. The neural network is found to be less accurate than the ASI Technique at a much greater expense of development time and required user supervision.

Opsomming

Die toepassing van neurale netwerke op mikrogolfbane is ondersoek. 'n Neurale netwerk-model is ontwikkel vir twee parallelle golfleiers met longitudinale gleufkoppeling in die gemeenskaplike breë wand. Data vir die opleiding van die netwerke is verkry deur 'n momentmetode-oplossing van die integraalvergelykings wat die struktuur beskryf. Verskillende ontwerpsopsies vir die netwerke is stelselmatig ondersoek en die ontwikkelingsproses van die netwerk is volledig beskryf. Die model is geëvalueer en vergelyk met 'n Aanpasbare Monstering Interpolasietegniek (AMI). Daar is gevind dat die neurale netwerk minder akkuraat is as die AMI terwyl die koste aan ontwikkelingstyd en gebruikerstoesig hoër is.

Acknowledgements / Erkenning

Verskeie mense het 'n rol gespeel in die voltooiing van hierdie tesis, en dis vir my 'n voorreg om hier op 'n klein manier my waardering te wys.

My studieleier, Petrie Meyer, was 'n groot aansporing wanneer ek dit nodig gehad het. Sy entoesiasme, insig en vertroue het my gehelp om deur te druk wanneer die vergelykings nie wou uitwerk nie of die foute nie wou kleiner word nie.

Met sy entoesiasme en gewilligheid om altyd nog 'n vraag oor Linux te beantwoord of nog 'n rekenaarprobleem te help oplos, het Thomas Stuart 'n onmisbare bydrae gelewer.

Vir praktiese ondersteuning, geduldige luister en moed-inpraat, 'n spesiale woord van dank aan my verloofde, Marius van der Merwe.

Ten slotte, my gesin en vriende se liefde en belangstelling word opreg waardeer. Hulle geduld en begrip, veral in die moeilike tye, het vir my baie beteken.

Contents

List of figures

List of tables

List of abbreviations used

ASI	Adaptive Sampling Interpolation
CEM	Computational Electromagnetic
CPW	Coplanar Waveguide
KBNN	Knowledge Based Neural Network
MLP	Multilayered Perceptron
RBF	Radial Basis Function
SNNS	Stuttgart Neural Network Simulator
SSE	Sum Squared Error

Chapter 1
Introduction

Many electromagnetic design problems require an optimisation stage. Optimisation often entails repeated computational electromagnetic (CEM) simulations to find the best solution. These computer simulations are usually time and memory intensive, and when an electrically large and complex structure is analysed using conventional numerical techniques such as Finite Element Methods (FEM), mode matching or Finite Difference Time Domain (FDTD) analysis, the problem places large demands on the available resources. These drawbacks of a brute force application of numerical techniques render it unsuitable for extensive design optimisation. The proper investigation of several parameters over a frequency band will require too much time and memory. For efficient design, a more elegant modelling approach is needed; one that will not rely so heavily on repeated simulation of the entire structure during optimisation.

Surrogate models, such as interpolation techniques and artificial neural networks, fit data points from CEM simulations. The advantages of these techniques are that they require less CEM simulations to create an accurate model and that the model is completely defined by the model coefficients – placing very little demands on computer memory. Once the model is established, it is fast to evaluate and therefore suitable for optimisation.

Artificial neural networks are increasingly being used to model microwave devices. Attractive features contributing to their current popularity include their ability to map input variables to output variables without any knowledge of the mathematics of the application, their ability to generalise by correctly interpreting data they have not been trained with, and the fact that they do not increase exponentially in size as the problem becomes more complex. But in spite of these advantages, neural networks are not yet being applied extensively to optimisation. A reason for this is the absence of a rigorous procedure for finding a good neural network model for a specific

application. For every problem many design decisions have to be made in order to find the best neural model, and there are few guidelines to making these decisions.

The purpose of this thesis was the investigation of artificial neural networks as a surrogate modelling tool for microwave applications. The specific application selected for experimentation was a directional coupler.

Directional couplers are four-port junctions used for power dividing and combining. These devices are used in microwave mixers, as input and output couplers in balanced microwave amplifier circuits, and for power monitoring in applications such as radar transmitters.

A general directional coupler is shown in Figure 1.1. In an ideal directional coupler, the input power P_1 divides in some ratio between port 2 and port 3, with no power reaching port 4. Both ports 1 and 4, and ports 2 and 3 are uncoupled. In addition, there is no reflection at the input port. Assuming input power P_1 at port 1, directional couplers can be characterised in terms of the following properties (with reference to Figure 1.1):

$$\text{Coupling} = -10\log\frac{P_3}{P_1} = -20\log|S_{31}| \tag{1.1}$$

$$\text{Directivity} = -10\log\frac{P_4}{P_3} = -20\log\frac{|S_{41}|}{|S_{31}|} \tag{1.2}$$

$$\text{Isolation} = -10\log\frac{P_4}{P_1} = -20\log|S_{41}| \tag{1.3}$$

Directional couplers implemented in waveguide consist of two waveguides with one or more apertures in a common wall. Waveguide couplers have the advantages of low loss and high power carrying capability. Several configurations are possible, depending on the shape and

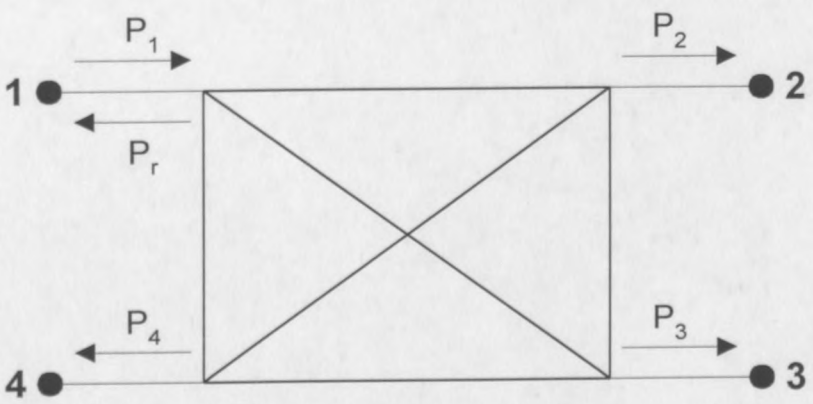

Figure 1.1: Directional coupler.

number of the apertures, and the relative position of the waveguides. Some of these configurations [Collin 1992] are illustrated in Figure 1.2 and listed here:

(a) Bethe-hole couplers consist of a small circular aperture in a common broad wall. If the aperture is centred, the waveguides are rotated with respect to each other in order to achieve directional coupling. For parallel waveguides, the aperture has to be off-centred.

(b) In the Schwinger reversed-phase coupler, each aperture radiates a field that is the negative of that radiated by the other. This leads to a coupler with very high directivity.

(c) The Moreno crossed-guide coupler makes use of crossed slots coupling between crossed guides. This is a very compact coupler, but the coupling is limited by the short length of the common wall [Kruger 1998].

(d) Riblet and Saad were the first to propose a pair of slots in the form of a T to be used [Riblet 1948]. This T-slot coupler can be designed to have very high directivity and flat coupling at its centre frequency. With several T-slots spaced quarter waveguide wavelengths apart along the length of the waveguide, both the coupling and the directivity-bandwidth can be increased.

When complex microwave devices such as these couplers are designed, there are no simple closed-form mathematical equations to describe exactly how the coupling or directivity of the coupler depends on parameters like aperture size, aperture position and (for multi-aperture couplers) frequency. An optimisation stage is usually necessary to refine the parameters to get

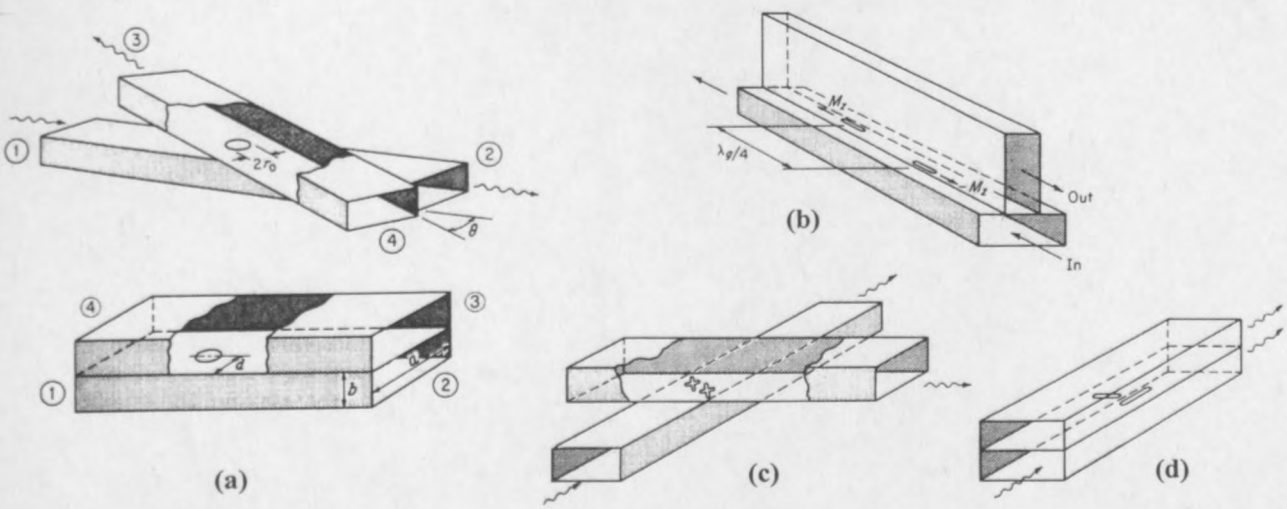

Figure 1.2: Different waveguide directional coupler configurations [Collin 1992, Chapter 6].

(a) Bethe-hole couplers. (b) Schwinger reversed-phase coupler. (c) Moreno crossed-guide coupler. (d) Riblet T-slot coupler.

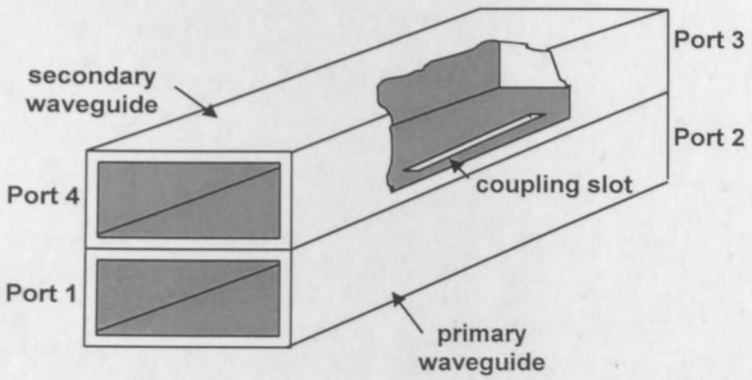

Figure 1.3: The problem configuration.

the desired response. This stage could be enhanced through the use of a neural network model.

This thesis presents a detailed exposition of the construction of a neural network model for a waveguide coupler consisting of two parallel waveguides coupled by a slot in the common broad wall. The aim was to establish a systematic design procedure and to measure its efficiency in terms of the development time and accuracy of the model. The evaluation of the model also includes a comparison with an interpolation technique, the Adaptive Sampling Interpolation Technique developed by Lehmensiek [Lehmensiek 2001].

The thesis comprises two main components: the generation of training data for the network model, and the systematic development of the model. The model had to provide the scattering parameters of the coupler as a function of the frequency, slot dimensions and slot position. The configuration of the coupler is shown in Figure 1.3.

The generation of the training data, a set of correct input-output pairs that can be used to train the neural network, is achieved by solving the fields in the waveguide using integral equations containing the waveguide Green's Functions. This is done with a Method of Moments (MoM) implementation. The equations for a general inclined slot are found to be of such complexity that they require the numerical solution of an infinite double summation of nested integrals. Therefore restrictions were placed on the orientation of the slot and these simplified equations were used for the generation of training data.

The neural network model development is carried out with consideration to several design options, such as the size of the network and the training parameters. An in-depth comparative investigation of the options is carried out and the results of the various stages of the development are presented. It is found that the development time of the model is one of its major drawbacks and that it is expected to increase for more complex modelling problems.

While neural networks are widely used in certain branches of engineering, their performance with respect to microwave circuits has not been documented extensively. The main contribution of this thesis therefore lies in the thorough investigation of a neural network implementation for a microwave structure with detailed attention to the design process itself. The comparison with interpolation models constitutes a completely original contribution.

A foundation for the use of neural networks is laid in Chapter 2. Several design aspects of neural networks are covered, along with references to the literature. The chapter concludes with a discussion of the software that is available for the implementation of neural networks.

The MoM equations are developed in detail in Chapter 3 and it is shown how these equations were used to generate the training data. Chapter 4 sets out the development of the neural model, giving full design details as well as results. Evaluation of the model and the designing process is done in Chapter 5, where conclusions about the project are also presented.

Finally, the Appendix contains mathematical detail omitted from the main part of the thesis.

Chapter 2
Overview of neural networks

One of the most fascinating parts of the human body is its brain. The capability of the brain to perform the most complicated tasks in fractions of seconds has motivated scientists to investigate exactly how it works, and to try to mimic its way of operation – to create artificial intelligence. One of the results of this research that has become useful in a wide range of fields is artificial neural networks, or simply neural networks. Similarities between neural networks and the structure and functionality of the brain are pointed out by this definition given by Simon Haykin [Haykin 1999, p. 2]:

> A neural network is a massively parallel distributed processor made up of simple processing units, which has a natural propensity for storing experiential knowledge and making it available for use. It resembles the brain in two respects:
>
> 1. Knowledge is acquired by the network from its environment through a learning process.
> 2. Interneuron connection strengths, known as synaptic weights, are used to store the acquired knowledge.

Although neural networks are essentially a mathematical tool, they can be visualised as physical networks containing neurons and links, analogous to the neurons and synapses that make up the anatomy of the brain. The neurons are the processing elements and the links are the connections between them.

This chapter will give an overview of how neural networks are used. Due to space constraints a strong emphasis will be placed on aspects of neural networks that were actually used in the current implementation. Other topics are only briefly mentioned.

2.1 Basic principles

2.1.1 The structure of a neural network

A neural network consists of neurons and the links that connect them. There are three kinds of neurons, namely input neurons, hidden neurons and output neurons. The input neurons receive input stimuli from outside the network. The output neurons deliver their output external to the network. Hidden neurons both receive their input stimuli from other neurons, and present their outputs to other neurons. These different kinds of neurons are illustrated in Figure 2.1.

By passing input signals from the input neurons through the hidden neurons to the output neurons, an input-output mapping is obtained. The processing of the signal is done inside the neurons. A neuron consists of two components: an adder and an activation function, illustrated in Figure 2.2. The adder sums all the input signals together with a threshold or bias signal, and presents the result to the activation (transfer) function. The activation function can be linear or non-linear. The non-linearity of the activation functions of the hidden neurons is essential in order to enable the network to model non-linear functions [Smith 1993]. The output neurons, however, are often assigned linear or even identical activation functions. The output of the activation function is the output of the neuron.

Input neurons differ from hidden and output neurons because they have only one input, so that no adder is necessary. They usually do not contain an activation function, so that they should

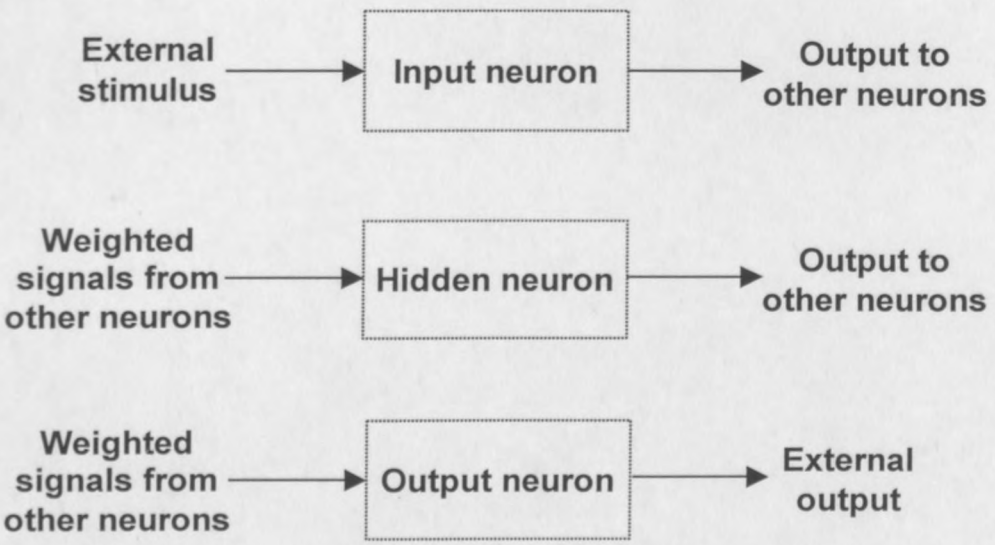

Figure 2.1: The connections of typical input, hidden and output neurons of a neural network.

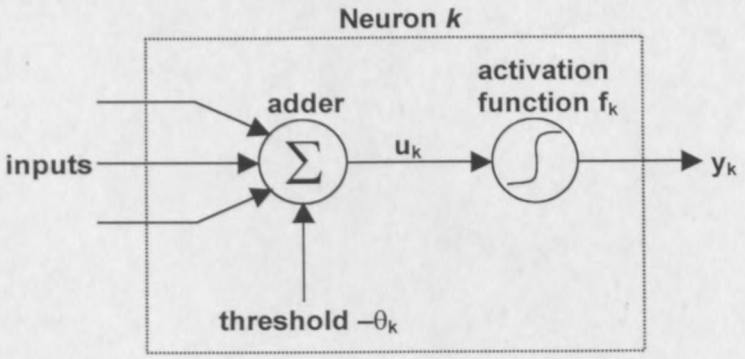

Figure 2.2: A typical neuron *k*.

rather be thought of as buffers between the external inputs and the hidden neurons.

Neurons are connected to each other with links. These links are associated with weight factors (synaptic weights). Signals travelling along the links are multiplied by these weights before they are summed into the destination neuron. Figure 2.3 shows a typical neural link with weight w_{kj}.

The above information can be summarised in the form of a mathematical description of a neuron k that is fed with the output signals x_j of J other neurons, to which it is connected through weights w_{kj}:

$$y_k = f_k\left(\left(\sum_{j=1}^{J} w_{kj}\, x_j\right) - \theta_k\right) \tag{2.1}$$

where the remaining symbols are defined in Figure 2.2.

A system such as that shown in Figure 2.4 is called a perceptron. One of the most frequently used neural networks, the multilayered perceptron (MLP), is formed by connecting perceptrons to each others in layers, like that shown in Figure 2.5. An MLP consists of an input layer, a number of hidden layers and an output layer. Neurons in each layer are connected to neurons in the next layer and the network is said to be fully connected if every neuron is connected to all the neurons in the next layer. MLPs are commonly trained with the backpropagation algorithm (see Section 2.3).

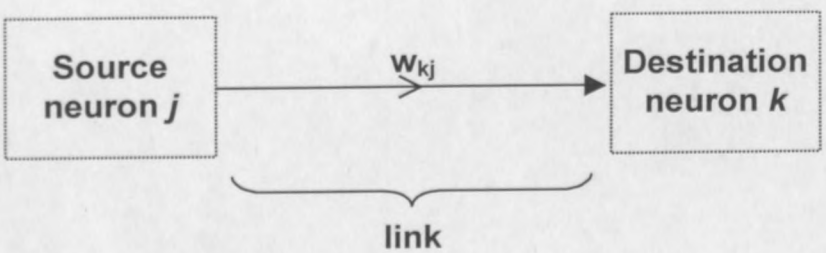

Figure 2.3: A typical link connecting two neurons with weight factor w_{kj}.

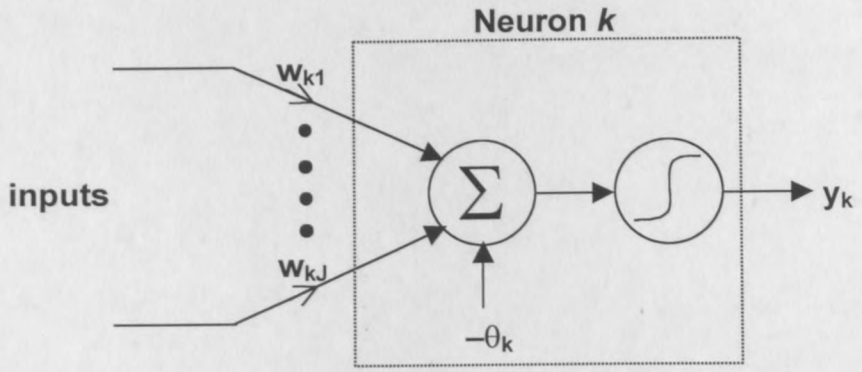

Figure 2.4: Single-layered perceptron.

The Universal Approximation Theorem states that *a single hidden layer is sufficient for a multilayer perceptron to compute a uniform ε approximation to a given training set represented by the set of inputs* x_1 .. x_p *and a desired (target) output* $f(x_1 .. x_p)$ [Haykin 1999, p.209]. The theorem does not state that this is the optimum configuration, however, and other architectures or MLPs with more hidden layers may give faster results. Some other network architectures are discussed in Section 2.2.1.

2.1.2 Applications of neural networks

The use of neural networks can be divided into two basic categories: classification and function approximation. Since function approximation is a more useful tool for the microwave engineer, this work focuses exclusively on that application.

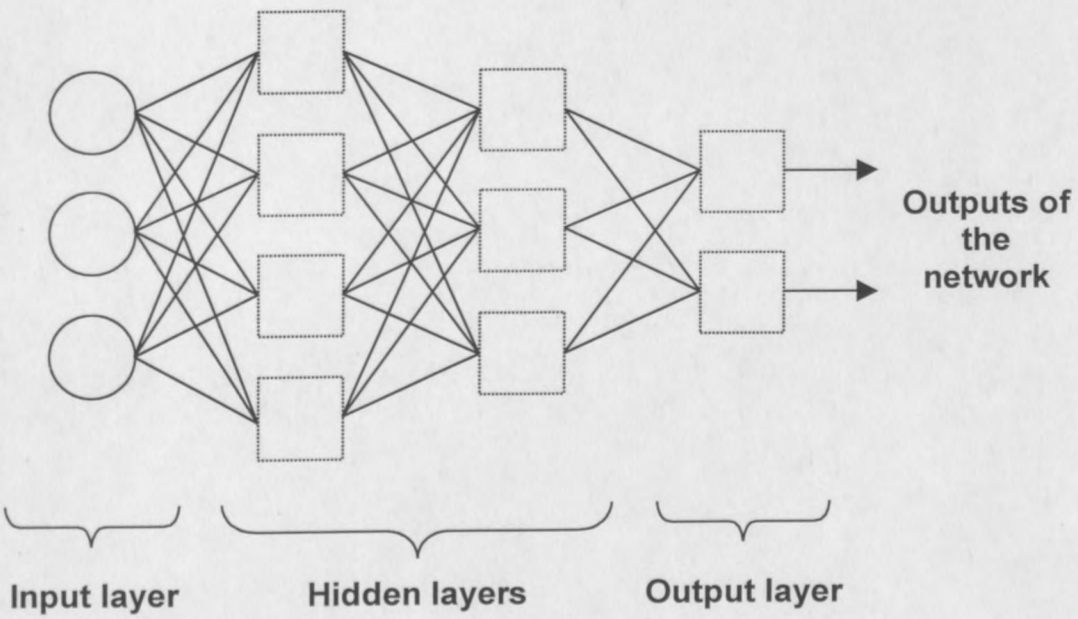

Figure 2.5: An example of a small multi-layered perceptron (MLP).

Neural networks as function approximators can find the underlying function when presented with a set of input-output pairs. They can learn to accurately model that data and can generalise the underlying function when presented with previously unseen input data. They are able to handle multi-dimensional non-linear problems. The size of a neural network does not increase exponentially with added dimensionality – unlike many other modelling methods.

Neural networks have been used for problems as diverse as that of engineering design, creating financial models and predicting social or natural phenomena. In the microwave field, neural networks have obvious applications with regard to system design. Having a library of neural network component models available will make system design and optimisation a much faster process. No knowledge about the underlying mathematical or physical principles is needed to create a neural model for a component. The only requirement is a set of training data; input-output examples that can be obtained either by measurement or computer simulation.

Once a network has learned to approximate the function, the model can be used repeatedly, each mapping taking place almost instantly. Depending on the accuracy of the neural network model, optimisation with the model can give an excellent starting point for final refinement through (expensive) measurement or simulation. Neural networks can also be used to directly model the entire system instead of subcomponents. Neural networks have even been implemented to facilitate the optimisation process itself [Vai 1998]: After training a conventional neural network model, another neural training process was used to select the best values for the input parameters to the model to yield the desired output for the design.

Several recent papers describe successful applications of neural networks in microwave engineering, a few of which are listed here:

- automatic impedance matching through stub tuning [Vai 1993]
- a microstrip corporate feed circuit [Horng 1993]
- MESFETs [Zaabab 1994, Goasguen 1999]
- stripline-to-stripline and microstrip-to-microstrip interconnects [Watson 1996-2]
- square spiral inductors [Creech 1996]
- microstrip vias [Watson 1996-1, Watson 1998]
- coplanar waveguide circuit components [Watson 1997]
- microstrip antennas [Sagiroglu 1997, Sagiroglu 1998]

- square patch antennas [Mishra 1998]
- transmission line parameters [Piel 1999]
- waveguide filter designs [Fedi 1998, Burrascano 1998, Wu 1999].

2.1.3 Neural network training

When input values are presented to the input neurons of a neural network, those values are propagated through the network and outputs are produced at all the output neurons. Initially, a neural network will model a random function, but a trained network will yield the correct output values, according to the function for which it was trained.

Training is the process by which the weights and thresholds, and possibly also the architecture, of a network are adjusted until the network output is not random any more, but represents a desired function. The value of a trained neural network lies in the fact that it will correctly evaluate data that it has never seen before, i.e. with which it has not been trained.

The training process can be described qualitatively as follows: Given a set of training data, i.e. matching input and output values of the function that needs to be modelled (the training set), every example in the training set is presented to the network-in-training one after the other. For every example, the network output is compared with the desired output and an error function is computed. The value of this error function is used to update the weights of the network in such a way that the error is minimised. This process is repeated for all the examples in the training set. The entire training set (epoch) is presented to the network several times, preferably in a different order each time, until the error produced by the network is small enough. The network is then ready to be tested for generalisation capability with unfamiliar data examples.

There exist several different training algorithms, some of which will be discussed in Section 2.3.

2.1.4 History of neural networks

Neural networks are currently an active research area and papers describing new developments appear regularly. Some of these, mostly from the last decade, will be referenced in the following sections. How it all started is the topic of this section and the remainder of the section contains brief historical notes, taken from [Zurada 1992] and [Haykin 1999]. The references cited in this section are also from those two sources.

It is generally held that 1943 was the defining year for neural networks. The first to describe a formal model of a neuron were McCulloch and Pitts [McCulloch 1943]. Their model contained 'all-or-nothing' neurons, and they showed that using enough of these neurons, with the proper synaptic connections, they were able to perform logic operations. Their ideas were used by Neumann in the design of the EDVAC (Electronic Discrete Variable Automatic Computer) that developed out of the ENIAC (Electronic Numerical Integrator and Computer) [Aspray 1986].

The first learning algorithm was presented by Donald Hebb in 1949. In his book [Hebb 1949], he described what is now known as the Hebbian learning rule and introduced his *postulate of learning*, stating that a synaptic connection is strengthened by repeated use.

In 1958 Frank Rosenblatt invented the perceptron, a trainable machine that could learn to classify patterns by modifying its connections [Rosenblatt 1958]. A different training procedure was presented by Widrow and Hoff who used a least mean-square algorithm (Widrow-Hoff learning rule) to formulate the ADALINE (Adaptive Linear Element), which was used for pattern recognition and weather forecasting at the time [Widrow 1960].

During the late 1960s and 1970s neural network research stagnated. Two of the reasons for this were the lack of sufficient computer resources and the doubts about the abilities of single-layered and even multi-layered perceptrons, advanced by the 1969 work by Minsky and Papert [Minsky 1969].

The 1980s saw renewed interest in neural networks. Two works that served to inspire this renaissance are a paper by John Hopfield [Hopfield 1982] that introduced a recurrent neural network architecture for associative memories and that formulated the properties of a fully connected neural network, and the two volumes on parallel distributed processing edited by Rumelhart and McClelland [Rumelhart 1986-1] that presented several new learning algorithms and other concepts. These works provided tools to solve problems that troubled the field since the 1960s.

Some other concepts that finally seemed to be presented in the right context – even though the fundamental ideas often originated as much as 20 years before – to gain attention and become popular are:

- self-organising maps [Kohonen 1982].
- reinforcement learning [Barto 1983].

- the Boltzmann machine [Ackley 1985] that was the first successful realisation of a multilayered neural network.
- the backpropagation algorithm [Rumelhart 1986-2]. This training method would emerge as the most popular to use until the present day.
- the use of radial basis functions [Broomhead 1988].

In the last decade the amount of work being done on neural networks has increased even more. Journals dedicated to neural networks have appeared, for instance *Neural Networks*, published by Pergamon Press since 1988, *Neural Computation*, published by MIT Press since 1989, and the *IEEE Transactions on Neural Networks* since 1990.

The mathematical and statistical bases of the principles are being investigated to find more efficient ways of utilising the networks. New or improved network topologies and training algorithms are being suggested and new applications demonstrated. The combination of neural networks with other techniques such as space mapping [Bakr 2000, Bandler 1999] is broadening the field.

Neural networks have stopped trying to mimic the human brain, but have become a valuable tool in modern science, even so in microwave engineering.

2.2 Designing the network topology

The success of a neural network model starts with proper design. The first main design decision is what the network should look like, what its structure should be. There are four issues to be dealt with: The network architecture, the network size, the neural activation functions and the representation of the problem variables.

2.2.1 Network architecture

Apart from the multilayered perceptron mentioned in Section 2.1.1, several other neural network structures can be used. A few of these are briefly discussed below.

Recurrent networks [Smith 1993, Appendix 1] contain feedback loops, i.e. connections going back from the neurons to themselves or to neurons in previous layers. This makes it possible to have temporal input sequences where the history of the neuron outputs also plays a role. Networks in which data only moves forward are called feedforward networks. The MLP is a feedforward network.

Kohonen self-organising maps [Haykin 1999, Chapter 10 and Zhang 2000, Section 3.8] divide the training examples into classes according to which examples possess similar outputs and then model the classes separately. This is very useful if the function reacts quite differently in different regions of the input space, for example a transistor that has linear, breakdown and saturation regions.

Radial basis function (RBF) networks [Zhang 2000, Section 3.4 and Smith 1993, Appendix 1] look exactly like MLPs with one hidden layer, but use radial basis activation functions for their hidden neurons.

If prior knowledge could be built into a network, less training data would be necessary to completely define the model, and the network would be able to extrapolate better after training. Prior knowledge is often available in the form of (inadequate) models. Knowledge based neural networks (KBNN) incorporate this knowledge into the neural network by feeding the input data of the training set through this model and computing the difference between the model output and the target output. These difference values are then used to train the neural network. This is expected to provide a simpler mapping for the network to achieve. This method is sometimes called the difference method [Wang 1999] or hybrid (ΔS) method [Watson 1996-2]. Other KBNN methods are described in [Wang 1997] and [Watson 1998].

New architectures are still being suggested in the literature. An example of this is the paper by Wu et al. [Wu 1999] that presents a neural network of which the connections are in the form of Finite Impulse Response filters.

2.2.2 Network size

For most network architectures the number of hidden neurons is not predefined and must be chosen by the designer. This discussion is based on the MLP, but most of the observations are applicable to other architectures as well.

The number of hidden neurons in a network can be quite critical to the success of the network. If a network has too few hidden units, it will result in high training error and low generalisation capability due to underfitting and high statistical bias. If there are too many hidden units, there will be a low training error but still low generalisation capability due to overfitting and high variance [Sarle].

Factors that influence the optimal size of the hidden layer include the number of input and output neurons, the size of the training set, the amount of noise in the target values, the complexity of

the function to be approximated, the activation functions used and also the training algorithm [Sarle]. Still, there exists no formula, and a common method to determine the optimal size is to experiment with networks of different size until the best one is found. Some more elegant methods exist:

- The best-known method is called pruning [Reed 1993]. It involves starting out with an excessively large network and then reducing it by letting weights decay to zero.
- Shirakawa et al. used a genetic algorithm to obtain the best network size [Shirakawa 1998].
- CasPer, a variation of the cascade-correlation network [Fahlman 1990, Treadgold 1999], is a constructive method that starts with a network without any hidden neurons and builds up to a larger network.

2.2.3 Activation functions

For every neuron, an activation (transfer) function must be selected. It was already stated in Section 2.1.1 that the activation functions of at least the hidden neurons must be non-linear. The most commonly used non-linear functions are the logistic function

$$f(u) = \frac{1}{1 + e^{-u}}$$

which maps u to the range [0, 1], and the hyperbolic tangent function

$$f(u) = \mathrm{Tanh}[u]$$

with outputs in the range [-1, 1]. These functions are shown in Figure 2.6.

Wavelet transforms are used as activation functions in so-called wavelet neural networks [Zhang 2000, Section 3.6]. This type of neural network and its training algorithms are described in [Bila 1999] and [Harkouss 1999]. Non-linear activation functions can also be used for input and output neurons, but it is more common to use linear or identity functions in those layers (especially the input layer). The function approximation is then handled by the hidden layers only.

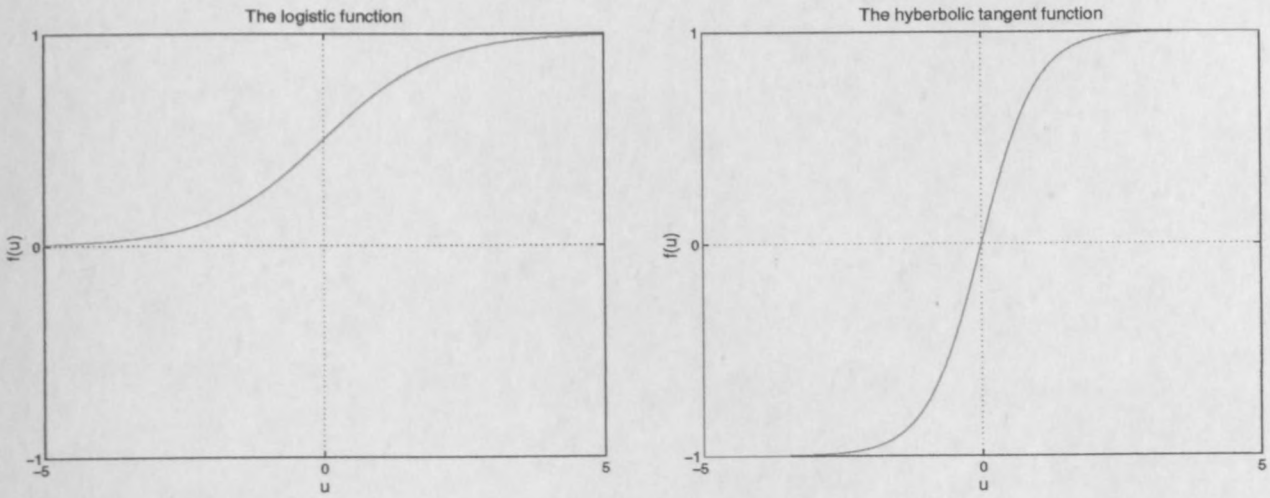

Figure 2.6: Examples of non-linear activation functions: the logistic function and the hyporbolic tangent function.

2.2.4 Representation of variables

It is important to find the best way to present the model parameters to the input neurons. There are different ways to do this for continuous input variables. One node (neuron) for each variable might seem to be the obvious way, but is not necessarily the best method.

Sometimes the influence of a specific variable can be spread over several nodes to localize the effect of its range and reduce the training time [Smith 1993, Chapter 10]. Figure 2.7 shows an example where nodes are 'turned on' when the value of the variable agrees with the value appointed to the node. In the figure, Node 2 is turned on completely and assigned a value of 1 when the input value is 10. When the input value is 15, Node 2 is half turned on, and so is Node

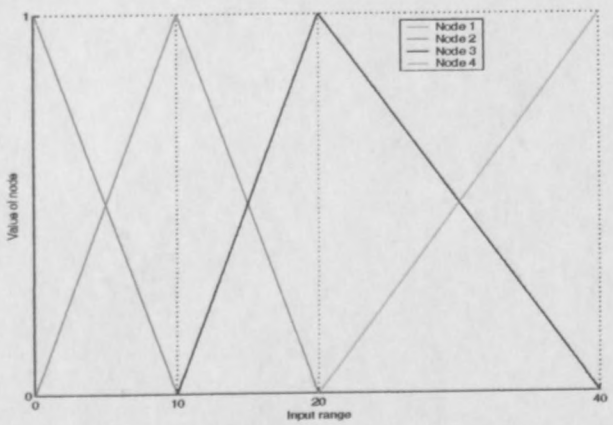

Figure 2.7: A different way to present variables to the network. Each node is fully 'turned on' when the input variable has exactly the value of that node. When the input value falls between two node values, those two nodes are partially turned on.

3, both assigned a value of 0.5. This approach is especially useful when values at the extremes of the input range should excite very different responses from the network.

The input and output variables can be normalised. Normalising the input variables is strictly speaking not necessary [Smith 1993, Chapter 10] since the weights can do the scaling as well, but it does make sense intuitively to at least make sure that the input variables are of the same order. It may take the weights longer to adapt if they need to give equal importance to one input variable with gigahertz values (10^9) and one with millimetre values (10^{-3}).

As far as the output variables are concerned, their normalisation will depend on the configuration of the output neurons. If the logistic activation function is used, for instance, the network can only produce outputs in the range [0, 1], and the output variables should be normalised to that range. In fact, since it is impossible for the logistic function to actually reach the extreme values 0 and 1, output variables should be normalised to a slightly smaller range, such as [0.1, 0.9].

Dimensional analysis [Langhaar 1980] is a method by which the number of variables of a problem can be reduced. This method has been used successfully in microstrip design [Mah 1998] and subsequently in neural networks as well [Watson 1999]. The advantages as set out by Watson et al. [op. cit.] are:

- The network is smaller and the number of training examples needed is reduced.
- Model accuracy is increased because an appropriate input variable space is defined.

2.3 Designing the training process

After a network topology has been established, the training process itself is the next important step. This is where the network will acquire its usefulness; where it will take shape as an accurate model.

2.3.1 Training algorithms for MLPs

The best-known and most widely used training algorithm for MLPs is error backpropagation. The basic principle of the method is simple and easy to understand. A few other methods that can be considered variations of standard backpropagation have also been developed. Standard error backpropagation, batch backpropagation and enhanced backpropagation will be described in this section. Other well-known training algorithms include

- RProp [Riedmiller 1993], which is another variation of backpropagation,

- second order gradient descent methods like scaled conjugate gradient [Shewchuk 1994], and quasi-Newton methods [Dennis 1983],
- the least-squares-based Levenberg-Marquardt algorithm [Levenberg 1944, Marquardt 1963, Zhang 2000],
- cascade-correlation [Fahlman 1990].

Improved or new algorithms have also been published recently, focusing on the problem of increasing training speed [Zaabab 1997, Devabhaktuni 1999] or decreasing the network error [Cavalieri 1999]. Specific algorithms are available for architectures like RBF networks, recurrent networks and self-organising maps [Haykin 1999, Zhang 2000].

2.3.1.1 Standard error backpropagation

In short, the standard error backpropagation training algorithm [Haykin 1999, Chapter 4] computes the network error for a certain training example and uses the gradient of the error surface to update the network weights.

After the network has been presented with an example input and has produced an output, a squared error function E is computed based on the difference between this actual output and the desired output, for example

$$E = \frac{1}{2}(T - A)^2 \tag{2.2}$$

where T is the target output and A is the actual output. The error E is then propagated backwards through the layers, while the weights are adjusted in such a manner as to minimize the error function. The weights w of the neurons are adjusted in accordance with the gradient descent method, i.e. in such a way as to move in the direction of sharpest descent on the error curve. The change in weight can be described with the following equation:

$$\Delta w_{kj} = -\eta \frac{\partial E_k}{\partial w_{kj}} \tag{2.3}$$

where Δw_{kj} is the amount added to the weight connecting neuron j with neuron k, and η is a constant called the learning rate.

To understand how this change in weight is computed, consider the following [Smith 1993] with reference to Figure 2.8:

For output neuron k:

$$\frac{\partial E_k}{\partial w_{kj}} = \frac{\partial E_k}{\partial A_k}\frac{\partial A_k}{\partial u_k}\frac{\partial u_k}{\partial w_{kj}} \tag{2.4}$$

$$= \frac{\partial}{\partial A_k}\left(\frac{1}{2}(T_k - A_k)^2\right)\frac{\partial}{\partial u_k}(f_k(u_k))\frac{\partial}{\partial w_{kj}}\left(-\theta_k + w_{k1}y_1 + w_{k2}y_2 + \ldots + w_{kj}y_j + \ldots\right)$$

$$= (A_k - T_k)A_k(1 - A_k)y_j \tag{2.5}$$

where it was assumed that f_k was the logistic function with derivative $A_k(1\text{-}A_k)$. For a threshold weight, only the last of the three derivatives changes and equation (2.5) becomes:

$$\frac{\partial E_k}{\partial \theta_k} = (A_k - T_k)A_k(1 - A_k)(-1)$$

For hidden neuron j not only the error of one output neuron k needs to be considered, but the sum of the errors of all the output neurons $[k = 1..K]$ connected to that hidden neuron:

$$\frac{\partial}{\partial w_{ji}}\left(\sum_{k=1}^{K} E_k\right) = \frac{\partial}{\partial y_j}\left(\sum_{k=1}^{K} E_k\right)\frac{\partial y_j}{\partial u_j}\frac{\partial u_j}{\partial w_{ji}}$$

$$= \left(\sum_{k=1}^{K}\frac{\partial E_k}{\partial A_k}\frac{\partial A_k}{\partial u_k}\frac{\partial u_k}{\partial y_j}\right)\frac{\partial y_j}{\partial u_j}\frac{\partial u_j}{\partial w_{ji}}$$

$$= \left(\sum_{k=1}^{K}(A_k - T_k)A_k(1 - A_k)w_{kj}\right)y_j(1 - y_j)y_i \tag{2.6}$$

where logistic activation functions were again assumed in both the hidden and the output layers. For a threshold weight, equation (2.6) changes to:

$$\frac{\partial}{\partial \theta_j}\left(\sum_{k=1}^{K} E_k\right) = \left(\sum_{k=1}^{K}(A_k - T_k)A_k(1 - A_k)w_{kj}\right)y_j(1 - y_j)(-1)$$

After the weights have been changed according to the above equations, the next example is

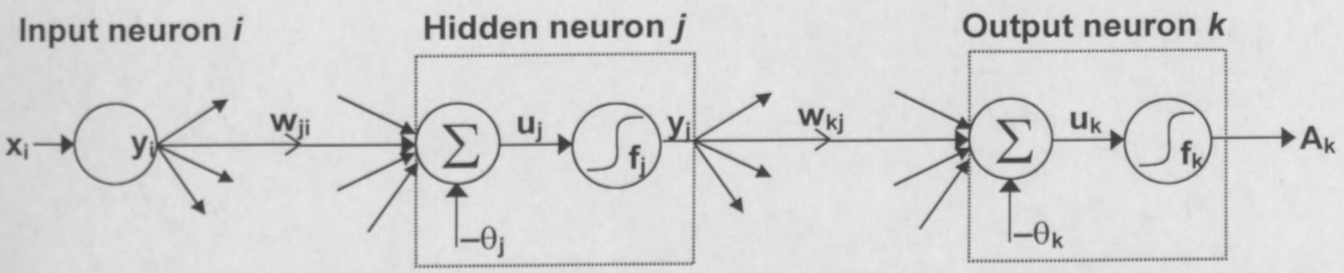

Figure 2.8: A typical signal path that is used to explain how the weights are updated.

presented to the network. Repeating this procedure several times with the entire set of training examples, the network can be trained to represent the training data to any sufficient level of accuracy, provided that a sufficient number of hidden neurons are available and that the function it approximates is continuous [Haykin 1999, Section 4.3].

The learning rate parameter η usually takes on a value between 0.1 and 1 [SNNS manual], and the optimum value will vary according to the problem at hand. It is also possible not to have one constant learning rate for the entire network, but to have a separate learning rate for each weight, and/or to adapt the learning rate(s) as training progresses.

One of the drawbacks of standard backpropagation is the function that is used to update the weights. The magnitude of the change in weights (the step size) is a function of the magnitude of the gradient at that point. This can cause slow convergence in problems with shallow minima. Some of the variations of backpropagation were designed not to have this large dependence on the magnitude of the gradient.

2.3.1.2 Batch backpropagation

Batch backpropagation [Haykin 1999, Section 4.3] uses the same formula as standard backpropagation to derive the weight changes. The difference lies in the time at which the weight values are updated. In standard backpropagation, weights are updated after every training example has been presented to the network. In batch backpropagation, the entire epoch (training set) is presented before the change is made.

The error that is used to determine the amount of weight change is the sum of the errors over all the outputs, averaged over all the training examples:

$$E_{av} = \frac{1}{N} \sum_{n=1}^{N} \sum_{k=1}^{K} E_k(n)$$

for training examples $n = 1..N$ and output neurons $k = 1..K$. It should be noted that the error E_k is already the *squared* error. The equation for weight update for batch backpropagation is then

$$\Delta w_{kj} = -\eta \frac{\partial E_{av}}{\partial w_{kj}}$$

Since the weight change follows the combined trend of many errors, it moves in a more efficient direction along the error curve, but it may also take longer than standard backpropagation because changes are made less often. Training time will increase for large training sets.

2.3.1.3 *Enhanced backpropagation*

Enhanced backpropagation is the name given in the SNNS manual for backpropagation with two added parameters, namely momentum and flat spot elimination.

The momentum parameter μ allows the previous weight change to influence the new weight change. If the previous weight change was large, the next one will tend to be large as well; if the previous change was in the opposite direction, the size of the next change will be decreased. This avoids oscillation problems as the error minimum is approached. The new weight change equation becomes:

$$\Delta w_{kj}(t) = -\eta \frac{\partial E_k}{\partial w_{kj}} + \mu \Delta w_{kj}(t-1)$$

where μ is the constant momentum and $\Delta w_{kj}(t\text{-}1)$ the previous weight change. The momentum μ is a positive constant smaller than 1. According to Murray Smith [Smith 1993], the training speed is not very sensitive for the value of μ, and he suggests a value of 0.9 for most applications. In an article by Ning Qian [Qian 1999] the optimal choice of the momentum parameter in gradient descent learning algorithms is investigated.

Flat spot elimination deals with the problem of large errors that induce only small weight changes when the error surface is flat and the derivative of the activation function is small. To solve this problem, a constant term c is added to the derivative of the activation function. The effect is that flat suboptimal error curves are traversed quickly. When flat spot elimination is included, equation (2.4) becomes:

$$\frac{\partial E_k}{\partial w_{kj}} = \frac{\partial E_k}{\partial A_k}\left(\frac{\partial A_k}{\partial u_k} + c\right)\frac{\partial u_k}{\partial w_{kj}}$$

The algorithm is very sensitive to the value of c, since large values will hide the information carried by the derivative. The SNNS manual suggests values up to 0.25.

2.3.2 The training process

The aim of the training process is to change the weights of the neural network until the network error is sufficiently small. A crucial question arises: what is the best time to end the training? The danger of continuing training for too long is that the network will start to overfit the data, i.e. although the training data will be approximated increasingly well, the generalisation ability of

the network will start to decrease. The network will be mapping the data instead of the underlying function.

The technique used to prevent overfitting is called early stopping or cross-validation. It involves dividing the available training data into three subsets: a training set, validation set and test set. The training set is used to train the network. The training error, based on this data set, should decrease during training. During training the validation set is used to periodically test the network and obtain the validation error. As the network accuracy increases, the validation error should decrease. However, as soon as overfitting starts to occur, the validation error will rise, even though the training error will continue to fall – so the validation error is used to determine when to end the training process. After training is completed, the independent test data set is used to measure the generalisation error of the network. Figure 2.9 illustrates the process.

Some other ways to prevent overfitting are [Sarle]:

- Choose the right size for the hidden layer. If there are too many hidden nodes, the network will be prone to overfitting. If the network is too simple, this may lead to underfitting, in which case the network cannot model all the trends in a complicated data set.
- Use a large training set to average out the noise. Many more training examples than weights are necessary.
- Make use of jitter; i.e. add small values representing artificial noise to existing training data, keeping the target output the same. This increases the size of the training set by

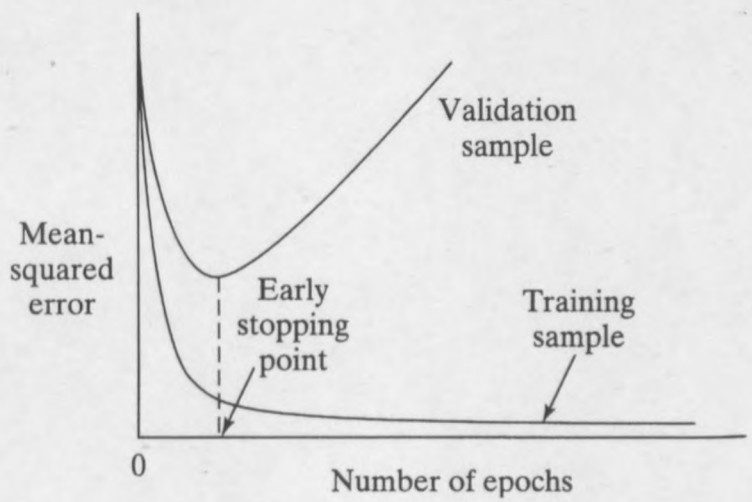

Figure 2.9 [Haykin 1999]: Typical curves showing the errors as training progresses. The training error will continue to fall as the network weights are adjusted, but when the validation error starts to rise it is an indication that overfitting is taking place.

adding new, noisy examples. A similar technique is described by Karystinos and Pados in a paper following a statistical approach to neural network modelling [Karystinos 2000].

- Add a weight decay penalty term to the error function in order to force weights to converge to smaller absolute values. Large weights can cause excessive variance of the output.

2.3.3 Initial values

Neural network software has built-in functions to initialise the weights of the network. Some principles to keep in mind are [Smith 1993]:

- Initial weights should be random; when corresponding weights start out equal, they will stay equal during training.
- If the output weights are made too small, the error derivatives of the hidden nodes will be too small for significant change.
- For every node the weighted sum of the inputs should be around zero to avoid extreme output values for the activation function.

2.3.4 The training set

Before a network can be trained, training data must be gathered, usually through numerical simulation or measurements – which are both very time-consuming. It is therefore desirable to keep the training set as small as possible, but not at the cost of poor accuracy or robustness against noise. It is also important that the training set be representative of the functional mapping. Because neural networks are generally poor at extrapolation, it is useful to have the range of the training data larger than the desired test range.

The size and composition of the training set can be determined using the Design of Experiments principle [Watson 1996-2] or other statistical methods [Sollich 1994, Fukumizu 2000]. When training examples are generated while training is in progress, the process is called active learning.

2.4 Summary of the design process

A neural network model is characterised by several parameters that need to be designed:

- Representation of the model variables
- Network architecture and size
- Neuron activation functions
- Initial weight values
- Training algorithm
- Size and composition of the training set
- End-of-training criterion

It should be clear that there are numerous choices to be made during the design process. These choices often seem arbitrary, since there are so many variables influencing them that it is impossible to deduce them logically. Yet the choices can be critical for the accuracy and training time of the model.

Investigating existing models can be a starting point, but even very similar applications may need very different models. Moreover, papers describing neural models tend not to detail the design process and mostly do not give full particulars about the model or the training process. Often the only available course of action is experimenting with different options until a good model is found. This makes the design process very time-consuming. The extent of the designer's background knowledge about neural networks will also greatly influence his or her ability to approach the process in a systematic and time-efficient way.

An example of such a systematic approach can be found in [Shirakawa 1998]. Shirakawa et al. describe how they determined the network parameters by first experimenting with a simple network and then used pruning and a genetic algorithm to obtain the optimal network size.

2.5 Neural network software

There exist at least two major software packages for implementing neural network models. They are SNNS and NeuroModeler. Apart from that, users can write their own programs using available modules like Matlab's Neural Network Toolbox.

2.5.1 *NeuroModeler*

NeuroModeler is a Windows-based program that has been developed recently by Professor Q.J. Zhang and his team at Carleton University. The program is intended to make the creation of neural models as easy as possible for the typical RF or microwave engineer. It has an intuitive graphical user interface guiding the user through the steps of creating a network and it suggests parameters like the size of the hidden layer and a suitable training algorithm based on the user's input. Data files containing training data can be imported and output data can be exported to applications such as Matlab for post-processing.

2.5.2 *SNNS*

The Stuttgart Neural Network Simulator (SNNS) was created by the SNNS Group at the Institute for Parallel and Distributed High-Performance Systems at the University of Stuttgart and the SNNS Group at the Wilhelm Schickard Institute for Computer Science at the University of Tübingen. The program was originally written for a Unix environment, but a Windows version has also been released. Both versions as well as the user manual are freely available on their website.

SNNS is not as intuitive to use as NeuroModeler and requires extensive reading of and reference to the user manual. It is very comprehensive, though, and contains twenty-three different architectures / training algorithms for the user to choose from (notably absent is KBNN). Two of the main attractions of SNNS (as opposed to NeuroModeler) for the current application were the superior stability of Linux over Windows, and the existence of the program *batchman* that enables the user to write batch files to facilitate the training process.

Chapter 3
Moment method solution of slot-coupled waveguide

In this chapter equations for the scattering parameters of slot-coupled waveguide are derived using the moment method. The problem was solved for a slot of arbitrary rotation and position in the common broad wall. To test the validity of the final equations, the simplified cases of the longitudinal slot and the transverse slot were compared with published results. The longitudinal slot was chosen as the test problem for the evaluation of the neural network.

3.1 Waveguide slots in the literature

The problem of coupling through small apertures in walls of zero thickness was solved by Bethe [Bethe 1944], making use of equivalent electric and magnetic dipoles. A limitation of the method was that the aperture had to have electrically small dimensions and a simple shape. A modification to this theory made by Cohn [Cohn 1952] made provision for large apertures and to some extent for finite wall thickness. A wall thickness correction factor was only rigorously derived by McDonald [McDonald 1972]. Later Levy [Levy 1979, Levy 1980] made use of a slightly modified Bethe-Cohn theory and included McDonald's correction factor to obtain excellent results.

A different approach suitable for apertures of any size makes use of an integral equation formulation where Green's functions are used to find the field in the waveguide in terms of the field in the aperture. This fundamental theory of slots in waveguides was first presented by Stevenson [Stevenson 1948]. He considered rectangular waveguide with perfectly conducting walls of zero thickness with only the TE_{10}-mode propagating. The slots were narrow and close to resonance and were radiating into free space, although he also briefly mentioned waveguide-

to-waveguide coupling. Because of his assumption that the slots were resonant, Stevenson could assume a simple sinusoidal field in the slot aperture and compute the fields in the waveguide relatively easily.

For a more general solution, several other methods have been implemented, including variational methods [Sangster 1965], a quasi-static method based on antenna principles [Lewin 1960] and the concept of self-reaction [Pandharipande 1978, Sangster 1979, Pandharipande 1979]. The method that finally seemed to emerge as the method of choice was the method of moments. It involves approximating the field in the aperture in terms of basis functions and then solving the integral equations of the boundary conditions. The advantages of the moment method are that wall thickness and higher mode coupling are accommodated quite naturally into the analysis, and the shape of the aperture can theoretically be arbitrary.

Several authors described the application of the moment method to waveguide slots. Vu Khac and Carson solved longitudinal and transverse narrow slots coupling two parallel waveguides with finite wall thickness [Vu Khac 1972], as well as longitudinal narrow slots radiating into free space [Vu Khac 1973]. Lyon and Sangster [Lyon 1981] solved both longitudinal and transverse radiating slots and included finite wall thickness in their analysis. Whereas Vu Khac and Carson used pulse basis functions, Lyon and Sangster used sinusoidal basis functions that led to smaller matrices.

Josefsson [Josefsson 1987] analysed narrow longitudinal radiating slots. He used the model of an equivalent shunt admittance, thus disregarding the asymmetrical scattering in the forward and backward directions. He briefly mentions a correction factor for rounded slot ends. Rengarajan in three papers [Rengarajan 1989-1, Rengarajan 1989-2, Rengarajan 1989-3] treated longitudinal, transverse and centred-inclined slots coupling crossed waveguides, as well as radiating slots with arbitrary orientation and offset. Datta et al. [Datta 1995] considered transverse and longitudinal narrow slots for the more general case of dissimilar parallel waveguides.

Attention has also been given to improved computation. The double infinite summations resulting from the waveguide Green's Functions are slowly convergent and recent papers such as [Park 1998-1, Park 1998-2] have discussed this issue.

3.2 Overview of the moment method

The method of moments (MoM) is a well-known numerical method used in computational electromagnetics. It is used in the frequency domain and is integral equation-based. An introduction to the application of MoM can be found in most books on numerical computation. A brief overview is given here, based on a description given by Stutzman and Thiele [Stutzman 1998, Chapter 10].

The MoM provides a solution to an integral equation by converting it to a set of simultaneous linear algebraic equations. Consider an equation of the form

$$\int F(z')\,G(z,\,z')\,dz' = H(z) \tag{3.1}$$

where z' is the source point, z is the field point, H(z) is the field excited by the unknown source F(z') and G(z, z') is the Green's Function giving the field excited by a source of unit strength. The first step in solving (3.1) is to approximate the unknown in terms of basis (expansion) functions such that

$$F(z') \approx \sum_{p=1}^{N} A_p f_p(z'), \tag{3.2}$$

where f_p are the expansion functions and A_p are the unknown complex coefficients. By substituting (3.2) into (3.1), the problem becomes:

$$\sum_{p=1}^{N} A_p \int f_p(z')\,G(z,\,z')\,dz' \approx H(z).$$

This is an equation in N unknowns. In order to solve the system, N equations are needed. This can be done by enforcing the exact equation at N values of z, a procedure that is known as point-matching. The system of equations then becomes:

$$\sum_{p=1}^{N} A_p \int f_p(z')\, G(z_1, z')\, dz' = H(z_1)$$

$$\sum_{p=1}^{N} A_p \int f_p(z')\, G(z_2, z')\, dz' = H(z_2)$$

$$\sum_{p=1}^{N} A_p \int f_p(z')\, G(z_3, z')\, dz' = H(z_3)$$

$$\vdots$$

$$\sum_{p=1}^{N} A_p \int f_p(z')\, G(z_N, z')\, dz' = H(z_N)$$

Point-matching enforces the boundary conditions only at N points on the boundary – i.e. the residual is forced to be zero only at those N points. The residual R(z) is the difference between the actual value of the equation and the approximated value:

$$R(z) = H(z) - \sum_{p=1}^{N} A_p \int f_p(z')\, G(z, z')\, dz' \tag{3.3}$$

Instead of point-matching, the residual can be forced to be zero on the boundary in a weighted average sense. This is the principle of the method of weighted residuals. Mathematically, for a residual R(z) and a weighting (testing) function W_q, this means that:

$$\int W_q(z)\, R(z)\, dz = 0, \quad q = 1..N \tag{3.4}$$

where the integral is taken over the same boundary as in (3.1). If (3.3) is applied to (3.4), it yields:

$$\sum_{p=1}^{N} A_p \int W_q(z) \int f_p(z')\, G(z, z')\, dz'\, dz = \int W_q(z)\, H(z)\, dz, \quad q = 1..N. \tag{3.5}$$

Equation (3.5) can be written in matrix form and solved.

The choice of basis functions and weighting functions can greatly influence the accuracy of the solution. For example, basis and weighting functions can be pulses or can be global (across the entire boundary). When the weighting functions are equal to the basis functions, the method is called the Galerkin method.

3.3 General moment method formulation for slot-coupled waveguide

In this section a detailed description will be given of how the moment method was used to solve the coupling slot system. In order to clarify the notation used for the mathematical derivations in the remainder of this chapter, some notational conventions are set out here:

- **Bold** type refers to vectors and normal type to scalars.
- Dyadics are indicated with bold type and an overbar, e.g. $\bar{\mathbf{G}}$.
- Unit vectors and unit dyadics are simply indicated by their symbols in bold type, e.g. $\boldsymbol{\xi}$, $\mathbf{x}_1$ and $\mathbf{xy}$.
- $\mathbf{E}_t$ and $\mathbf{H}_t$ refer to the tangential electric and magnetic fields respectively.
- E_x and H_x refer to E and H field components in the x direction.
- $\mathbf{E}^{(i)}$ and $\mathbf{H}^{(i)}$ refer to **E** and **H** fields in region i, where the regions are defined in Figure 3.2.
- $\mathbf{H}^{inc}$ is the incident field in the primary waveguide.
- **r** and **r'** are position vectors from the origin to the field point at (x, y, z) and the source point at (x', y', z') respectively.

Figure 3.1 illustrates the coordinate systems used in the formulation and defines the dimension and position variables.

Solving the electromagnetic problem of the waveguide coupler is not simple, but by making use of the field equivalence principles of Love and Schelkunoff [Collin 1991, Section 1.8], the problem can be divided into three separate regions each with its own boundary conditions, which can be solved more easily.

In accordance with the equivalence principle, the apertures in the waveguides are replaced by perfect electric conductors with equivalent sheets of magnetic current on them, so that the fields excited in the waveguides by the magnetic current sheets will be the same as those of the original problem. The same principle applies to the slot, where the two interfaces with the waveguides are replaced by perfect electrical conductors and sheets of magnetic current. The three regions of the equivalent problem are shown in Figure 3.2.

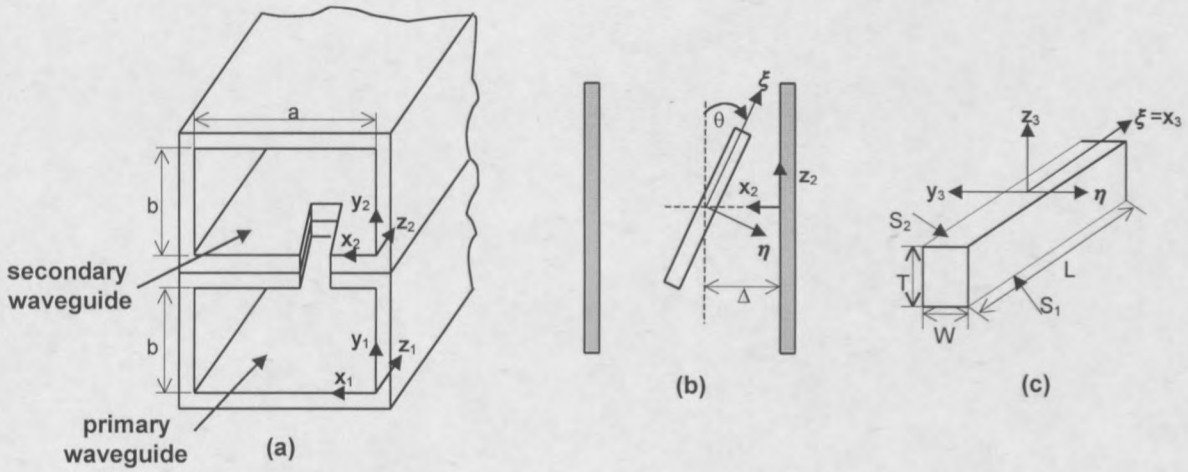

Figure 3.1: Problem coordinates and variables.

(a) Cross-section through the centre of the slot showing the two waveguide coordinate systems. (b) The slot viewed from above (in the plane y_2=0). (c) The slot and its coordinate system.

As indicated in Figure 3.2, the magnetic currents are assumed to have only a ξ component. This follows from the assumption that the slot is long and narrow enough so that the longitudinal E fields and transversal H fields in the slot will be negligible, or, equivalently, that only TE_{m0}-modes exist in the slot. The definition of 'narrowness' is quantified by Vu Khac and Carson as the condition that the length of the slot should be at least seven times its width [Vu Khac 1973].

After the application of the equivalence principle, there are two unknowns in the problem (the magnetic current magnitudes M_1 and M_2), and therefore two equations are required to solve the system. These will be obtained through application of the boundary conditions across the

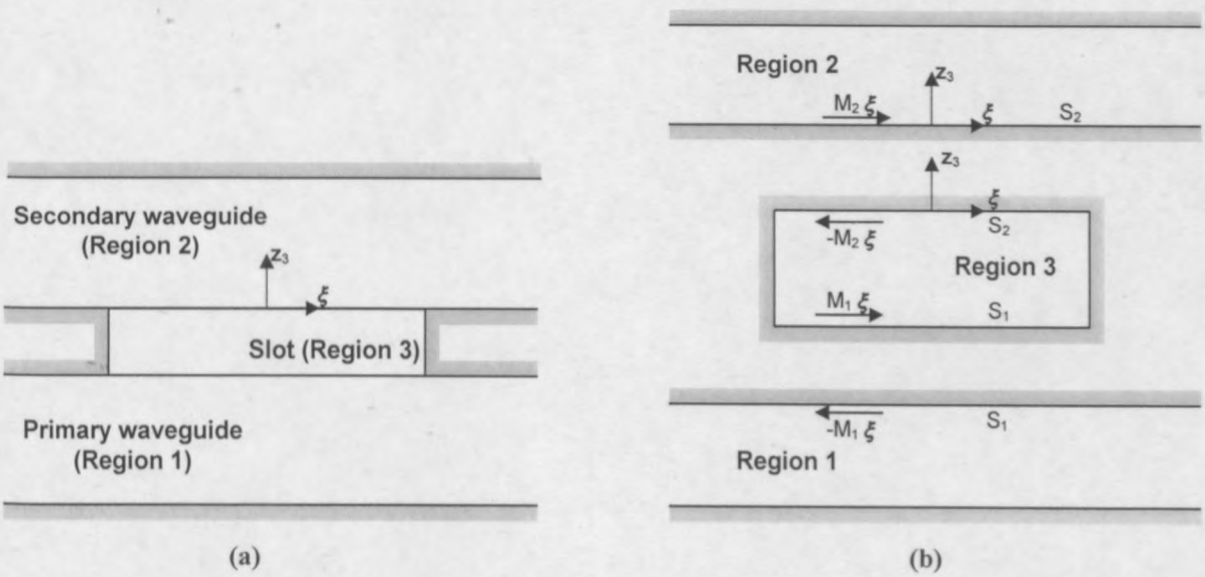

Figure 3.2: Cross-section through the length of the slot, showing the division of the structure into different regions by application of the equivalence principle. (a) shows the regions in relation to each other and (b) shows each region separately, indicating the equivalent magnetic currents.

interface surfaces S_1 and S_2.

The boundary conditions that need to be satisfied are as follows [Hildebrand 1996]:

1. The tangential **E** field must be continuous across S_1 and S_2. This condition has already been satisfied through proper choice of the magnetic currents on the surfaces.

2. The tangential **E** field must be zero on all perfect electrical conductors. This property will be incorporated in the various Green's Functions.

3. The tangential **H** field must be continuous across S_1 and S_2. This condition will lead to the integral equations that characterise the problem.

Applying boundary condition number 3 to the surfaces shown in Figure 3.2 leads to the following two equations:

On S_1:

$$\mathbf{H}_t^{inc} + \mathbf{H}_t^{(1)} = \mathbf{H}_t^{(3)}$$

$$\Rightarrow \mathbf{H}_t(-M_1\xi)^{(1)} - \mathbf{H}_t(M_1\xi)^{(3)} - \mathbf{H}_t(-M_2\xi)^{(3)} = -\mathbf{H}_t^{inc} \tag{3.6.1}$$

On S_2:

$$\mathbf{H}_t^{(2)} = \mathbf{H}_t^{(3)}$$

$$\Rightarrow \mathbf{H}_t(M_1\xi)^{(3)} + \mathbf{H}_t(-M_2\xi)^{(3)} - \mathbf{H}_t(M_2\xi)^{(2)} = 0 \tag{3.6.2}$$

Following the procedure outlined in Section 3.2, equation (3.6) can be converted to a matrix. The first step is to express the unknown quantities in terms of basis functions. Since the **E** field in the slot is approximately sinusoidal, especially when close to resonance, global sinusoidal basis functions have been found to give good results [Lyon 1981, Josefsson 1987, Datta 1995]. The Galerkin method has been used with success by the same authors. The unknown quantities are therefore expressed as:

$$\begin{aligned} \mathbf{M}_1(\mathbf{r}') &= \sum_{p=1}^{N} A_p \mathbf{f}_p(\mathbf{r}') \\ \mathbf{M}_2(\mathbf{r}') &= \sum_{p=1}^{N} B_p \mathbf{f}_p(\mathbf{r}'), \end{aligned} \tag{3.7.1}$$

where A_p and B_p are the unknown complex coefficients and the basis functions are given by

$$\mathbf{f}_p(\mathbf{r}') = \frac{1}{W} \mathrm{Sin}\left[\frac{p\pi}{L}\left(\xi' + \frac{L}{2}\right)\right]\xi. \tag{3.7.2}$$

The testing (weighting) functions are the same as the basis functions, namely

$$\mathbf{f}_q(\mathbf{r}) = \frac{1}{W}\,\mathrm{Sin}\left[\frac{q\pi}{L}\left(\xi + \frac{L}{2}\right)\right]\xi. \tag{3.7.3}$$

Leaving $\mathbf{M}_1$ and $\mathbf{M}_2$ in symbolic form for the time being, the inner product with the weighting functions can be applied to (3.6) to give, for q = 1..N,

On S_1:
$$\int_{S_1} \mathbf{f}_q(\mathbf{r})\cdot\left(\mathbf{H}_t(-M_1\xi)^{(1)} - \mathbf{H}_t(M_1\xi)^{(3)} - \mathbf{H}_t(-M_2\xi)^{(3)}\right)dS = -\int_{S_1}\mathbf{f}_q(\mathbf{r})\cdot\mathbf{H}_t^{inc}\,dS$$

$$\Rightarrow \int_{S_1}\mathbf{f}_q(\mathbf{r})\cdot\mathbf{H}_t(-M_1\xi)^{(1)}\,dS - \int_{S_1}\mathbf{f}_q(\mathbf{r})\cdot\mathbf{H}_t(M_1\xi)^{(3)}\,dS$$
$$-\int_{S_1}\mathbf{f}_q(\mathbf{r})\cdot\mathbf{H}_t(-M_2\xi)^{(3)}\,dS = -\int_{S_1}\mathbf{f}_q(\mathbf{r})\cdot\mathbf{H}_t^{inc}\,dS \tag{3.8.1}$$

On S_2:
$$\int_{S_2}\mathbf{f}_q(\mathbf{r})\cdot\left(\mathbf{H}_t(M_1\xi)^{(3)} + \mathbf{H}_t(-M_2\xi)^{(3)} - \mathbf{H}_t(M_2\xi)^{(2)}\right)dS = 0$$

$$\Rightarrow \int_{S_2}\mathbf{f}_q(\mathbf{r})\cdot\mathbf{H}_t(M_1\xi)^{(3)}\,dS + \int_{S_2}\mathbf{f}_q(\mathbf{r})\cdot\mathbf{H}_t(-M_2\xi)^{(3)}\,dS$$
$$-\int_{S_2}\mathbf{f}_q(\mathbf{r})\cdot\mathbf{H}_t(M_2\xi)^{(2)}\,dS = 0 \tag{3.8.2}$$

Equation (3.8) can be rewritten in matrix form as follows:

$$\begin{bmatrix} [Y_1^{11}]+[Y_1^{31}] & [Y_1^{32}] \\ [Y_2^{31}] & [Y_2^{32}]+[Y_2^{22}] \end{bmatrix}\begin{bmatrix}[A]\\[B]\end{bmatrix} = \begin{bmatrix}[H]\\[0]\end{bmatrix} \tag{3.9}$$

where the different components are given by the following equations for p,q = 1..N. Note that, because of the matrix notation, the summation symbol and the unknown coefficients were removed from the expressions for the magnetic currents.

$$[Y_1^{11}]_{qp} = \int_{S_1}\mathbf{f}_q(\mathbf{r})\cdot\mathbf{H}_t(-f_p(\mathbf{r}'))^{(1)}\,dS \tag{3.10.1}$$

$$[Y_1^{31}]_{qp} = -\int_{S_1}\mathbf{f}_q(\mathbf{r})\cdot\mathbf{H}_t(f_p(\mathbf{r}'))^{(3)}\,dS \tag{3.10.2}$$

$$[Y_1^{32}]_{qp} = -\int_{S_1}\mathbf{f}_q(\mathbf{r})\cdot\mathbf{H}_t(-f_p(\mathbf{r}'))^{(3)}\,dS \tag{3.10.3}$$

$$[Y_2^{31}]_{qp} = \int_{S_2}\mathbf{f}_q(\mathbf{r})\cdot\mathbf{H}_t(f_p(\mathbf{r}'))^{(3)}\,dS \tag{3.10.4}$$

$$[Y_2^{32}]_{qp} = \int_{S_2} \mathbf{f}_q(\mathbf{r}) \cdot \mathbf{H}_t(-f_p(\mathbf{r}'))^{(3)} \, dS \tag{3.10.5}$$

$$[Y_2^{22}]_{qp} = -\int_{S_2} \mathbf{f}_q(\mathbf{r}) \cdot \mathbf{H}_t(f_p(\mathbf{r}'))^{(2)} \, dS \tag{3.10.6}$$

$$[H]_q = -\int_{S_1} \mathbf{f}_q(\mathbf{r}) \cdot \mathbf{H}_t^{inc} \, dS \tag{3.10.7}$$

The notation for the matrix components is such that $\left[\mathbf{Y}_i^{ab}\right]$ refers to the field in region *a* that was excited by $\mathbf{M}_b$ and evaluated on S_i. $[A]_p$ and $[B]_p$ are the unknown coefficients.

Equation (3.9) gives the general formulation for the slot problem. The different matrix components specified in (3.10) can now be evaluated for a specific waveguide-and-slot configuration.

The amount of work involved can be reduced by noting that for the current problem several of the matrix components are equal. The Lorentz Reciprocity Theorem [Collin 1991, Section 1.10] can be used to show that the two components relating to the field on one surface of the slot excited by the current on the opposite surface of the slot are equal, i.e. $\left[\mathbf{Y}_1^{32}\right] = \left[\mathbf{Y}_2^{31}\right]$ (see Appendix B for the derivation). Because the slot is symmetric around the x_2z_2-plane at $y_2 = -\frac{t}{2}$, the components relating to the field on each surface of the slot excited by the current on that same surface, are equal, i.e. $\left[\mathbf{Y}_1^{31}\right] = \left[\mathbf{Y}_2^{32}\right]$. Finally, the two waveguides are identical and similarly oriented, and therefore the components relating to the fields excited in the waveguides by the currents on the slot surfaces are equal as well, i.e. $\left[\mathbf{Y}_1^{11}\right] = \left[\mathbf{Y}_2^{22}\right]$.

3.4 Solution of the matrix components for a general slot

In this section the matrix components defined in (3.10) will be solved in detail, starting with the definition of the incident field. Firstly, in Table 3.1 some variables are defined that will be used in the derivation, and in Table 3.2 equations for coordinate transformations are given. These comply with the coordinate systems shown in Figure 3.1.

Waveguide dimensions:	a, b
Slot dimensions:	L, W, T
Frequency:	$\omega = 2\pi f$
Permeability and permittivity of the waveguide medium:	$\mu,\ \epsilon$
Intrinsic impedance of the waveguide medium:	$Z_0 = \sqrt{\frac{\mu}{\epsilon}}$
Velocity of light in the waveguide medium:	$c = \frac{1}{\sqrt{\mu\epsilon}}$
Wavenumber:	$k = \frac{\omega}{c}$
Cut-off wavenumber in the waveguide:	$k_c = \sqrt{\left(\frac{m\pi}{a}\right)^2 + \left(\frac{n\pi}{b}\right)^2}$
Cut-off wavenumber in the slot:	$k_{cs} = \sqrt{\left(\frac{m\pi}{L}\right)^2 + \left(\frac{n\pi}{W}\right)^2}$
Different forms of the propagation constant:	$\Gamma_{mn} = \sqrt{k_c^2 - k^2} = j\beta_{mn}$ $k_g = \sqrt{k^2 - k_c^2} = \beta_{mn}^*$
Neumann constant:	$\epsilon_{0j} = \begin{cases} 1, & j = 0 \\ 2, & j > 0 \end{cases}$
Kronecker delta:	$\delta_{mn} = \begin{cases} 1, & m = n \\ 0, & m \neq n \end{cases}$
Trigonometrical shorthand:	$S_x = \mathrm{Sin}\left[\frac{m\pi}{a}x\right]$ $C_x = \mathrm{Cos}\left[\frac{m\pi}{a}x\right]$ $S_y = \mathrm{Sin}\left[\frac{n\pi}{b}y\right]$ $C_y = \mathrm{Cos}\left[\frac{n\pi}{b}y\right]$

Table 3.1: Definitions of variables used in this chapter.

Direction transformations (unit vectors)	Position coordinate transformations (scalars)
$\mathbf{x_1} = \mathbf{x_2} = -\mathrm{Sin}[\theta]\,\xi - \mathrm{Cos}[\theta]\,\eta$	$x_1 = x_2 = -\mathrm{Sin}[\theta]\,\xi - \mathrm{Cos}[\theta]\,\eta + \Delta$
$\mathbf{y_1} = \mathbf{y_2} = \mathbf{z_3}$	$y_1 = y_2 + b + T = z_3 + b + T$
$\mathbf{z_1} = \mathbf{z_2} = \mathrm{Cos}[\theta]\,\xi - \mathrm{Sin}[\theta]\,\eta$	$z_1 = z_2 = \mathrm{Cos}[\theta]\,\xi - \mathrm{Sin}[\theta]\,\eta$
$\xi = \mathbf{x_3} = -\mathrm{Sin}[\theta]\,\mathbf{x_1} + \mathrm{Cos}[\theta]\,\mathbf{z_1}$ $= -\mathrm{Sin}[\theta]\,\mathbf{x_2} + \mathrm{Cos}[\theta]\,\mathbf{z_2}$	$\xi = x_3 = -\mathrm{Sin}[\theta]\,(x_1 - \Delta) + \mathrm{Cos}[\theta]\,z_1$ $= -\mathrm{Sin}[\theta]\,(x_2 - \Delta) + \mathrm{Cos}[\theta]\,z_2$
$\eta = -\mathbf{y_3} = -\mathrm{Cos}[\theta]\,\mathbf{x_1} - \mathrm{Sin}[\theta]\,\mathbf{z_1}$ $= -\mathrm{Cos}[\theta]\,\mathbf{x_2} - \mathrm{Sin}[\theta]\,\mathbf{z_2}$	$\eta = -y_3 = -\mathrm{Cos}[\theta]\,(x_1 - \Delta) - \mathrm{Sin}[\theta]\,z_1$ $= -\mathrm{Cos}[\theta]\,(x_2 - \Delta) - \mathrm{Sin}[\theta]\,z_2$

Table 3.2: **Coordinate transformations for the general slot of Figure 3.1.**

3.4.1 The incident field component

The **H** fields in the waveguide are normalised so that the power in both TE and TM modes is unity. The equations for the normalised TE_{mn} and TM_{mn} modes are [Collin 1991, Sections 5.3-5.4 and Collin 1992, Section 3.17]:

$$\mathbf{H}_{TE} = -\sqrt{\frac{2k_c^2\,\epsilon_{0m}\,\epsilon_{0n}}{ab\,Z_0}}\sqrt{\frac{\beta_{mn}}{k}}\,\frac{1}{k_c^2} \times\left(\pm\frac{m\pi}{a}S_x C_y\,\mathbf{x} \pm \frac{n\pi}{b}C_x S_y\,\mathbf{y} - j\frac{k_c^2}{\beta_{mn}}C_x C_y\,\mathbf{z}\right)e^{\mp\Gamma_{mn}z} \qquad (3.11.1)$$

$$\mathbf{H}_{TM} = j\sqrt{\frac{2k_c^2\,\epsilon_{0m}\,\epsilon_{0n}}{ab\,Z_0}}\sqrt{\frac{k}{\beta_{mn}}}\,\frac{1}{k_c^2}\left(\frac{n\pi}{b}S_x C_y\,\mathbf{x} - \frac{m\pi}{a}C_x S_y\,\mathbf{y}\right)e^{\mp\Gamma_{mn}z}. \qquad (3.11.2)$$

In the above equations, the upper signs are for waves travelling in the positive z direction and the lower signs for waves travelling in the negative z direction. The equations are valid for all non-negative values of m and n, except the case m = n = 0.

The incident field is assumed to be the TE_{10} mode incident in the primary waveguide and travelling in the positive z direction. The reference plane is taken to be at $z_1 = z_i$ and should not coincide with the slot. Applying these assumptions to (3.11.1) yields

$$\mathbf{H}^{inc} = -2\sqrt{\frac{\beta_{10}}{abkZ_0}}\left(\mathrm{Sin}\left[\frac{\pi}{a}x_1\right]\mathbf{x_1} - j\frac{\pi}{a}\frac{1}{\beta_{10}}\mathrm{Cos}\left[\frac{\pi}{a}x_1\right]\mathbf{z_1}\right)e^{-\Gamma_{10}(z_1-z_i)}, \tag{3.12}$$

so that the components of the incident field are

$$H_{x_1}^{inc} = -2\sqrt{\frac{\beta_{10}}{abkZ_0}}\,\mathrm{Sin}\left[\frac{\pi}{a}x_1\right]e^{-\Gamma_{10}(z_1-z_i)} \tag{3.13.1}$$

$$H_{z_1}^{inc} = \frac{2j}{\beta_{10}}\frac{\pi}{a}\sqrt{\frac{\beta_{10}}{abkZ_0}}\,\mathrm{Cos}\left[\frac{\pi}{a}x_1\right]e^{-\Gamma_{10}(z_1-z_i)}. \tag{3.13.2}$$

To find the matrix component $[H]_q$, (3.12) is substituted into (3.10.7) and coordinate transformations from Table 3.2 are used:

$$[H]_q = 2\sqrt{\frac{\beta_{10}}{abkZ_0}}\,e^{\Gamma_{10}z_i}\int_{S_1} e^{-\Gamma_{10}z_1}\mathbf{f}_q(\mathbf{r})\cdot \left(\left(-\mathrm{Sin}[\theta]\,\mathrm{Sin}\left[\frac{\pi}{a}x_1\right] - j\frac{\pi}{a}\frac{1}{\beta_{10}}\mathrm{Cos}[\theta]\,\mathrm{Cos}\left[\frac{\pi}{a}x_1\right]\right)\xi + \left(-\mathrm{Cos}[\theta]\,\mathrm{Sin}\left[\frac{\pi}{a}x_1\right] + j\frac{\pi}{a}\frac{1}{\beta_{10}}\mathrm{Sin}[\theta]\,\mathrm{Cos}\left[\frac{\pi}{a}x_1\right]\right)\eta\right)dS \tag{3.14}$$

The weighting function is substituted from (3.7.3) and the limits of the integration over S_1 are specified:

$$[H]_q = \frac{2}{W}\sqrt{\frac{\beta_{10}}{abkZ_0}}\,e^{\Gamma_{10}z_i}\int_{-\frac{L}{2}}^{\frac{L}{2}}\int_{-\frac{W}{2}}^{\frac{W}{2}} e^{-\Gamma_{10}(\mathrm{Cos}[\theta]\xi - \mathrm{Sin}[\theta]\eta)}\,\mathrm{Sin}\left[\frac{q\pi}{L}\left(\xi+\frac{L}{2}\right)\right] \times\left(-\mathrm{Sin}[\theta]\,\mathrm{Sin}\left[\frac{\pi}{a}(-\mathrm{Sin}[\theta]\xi - \mathrm{Cos}[\theta]\eta + \Delta)\right] - j\frac{\pi}{a}\frac{1}{\beta_{10}}\mathrm{Cos}[\theta]\,\mathrm{Cos}\left[\frac{\pi}{a}(-\mathrm{Sin}[\theta]\xi - \mathrm{Cos}[\theta]\eta + \Delta)\right]\right)d\eta\,d\xi \tag{3.15}$$

This is the final expression for $[H]_q$. Although it is not difficult to analytically simplify the integral, the process is very tedious and time-consuming. All the integrals are therefore left to be computed numerically. When the special cases of the longitudinal and transverse slots are considered, simplifications will be made to make the analytical solution of the integrals more practical.

3.4.2 Green's Functions

In order to solve the remaining matrix components it is necessary to express the fields in the waveguides and slot in terms of the magnetic currents on S_1 and S_2. This is done by using the appropriate Green's Functions [Tai 1994].

3.4.2.1 Waveguide dyadic Green's Function

When the waveguide dyadic Green's Function is formulated, care must be taken not to overlook the singularity in the source region. Although it seems plausible to represent the complete field in the waveguide as a superposition of the TE and TM modes as was proposed in earlier works such as [Collin 1969, Chapter 14], it has been pointed out by several authors that this does not satisfy Maxwell's equations in the source region [Collin 1973, Lyon 1981].

Two approaches to finding the complete solution (i.e. one that is also valid in the source region) of the dyadic Green's Function in rectangular waveguide involve distribution theory and potential theory respectively. The principles of generalised functions (distribution theory) were used by Rahmat-Samii [Rahmat-Samii 1975] as well as Lee et al. [Lee 1980]. Stevenson as well as Lyon and Sangster [Stevenson 1948, Lyon 1981] made use of a potential Green's Function to find the complete solution in the source region.

The method of potentials is a well-known technique employed to solve electromagnetic boundary-value problems [Balanis 1989, Chapter 6]. A vector potential pair, **A** and **F**, is introduced in the process of solving for the **H** and **E** fields. These potentials can be written in terms of Green's Functions in exactly the same way as the fields. Therefore, starting with a potential Green's Function, the potential can be found and from the potential, the field. Following this 'detour' procedure gives the full solution for the fields everywhere, including the source region. The procedure can be set out by starting with Maxwell's equations in the MKSA system*. Assuming a time dependence of $e^{j\omega t}$, they are given by the following set of equations:

$$\nabla \times \mathbf{E} = -\mathbf{M} - j\omega\mu\mathbf{H} \tag{3.16}$$

$$\nabla \times \mathbf{H} = \mathbf{J} + j\omega\epsilon\mathbf{E} \tag{3.17}$$

$$\nabla \cdot \mathbf{E} = \frac{\rho_e}{\epsilon} \tag{3.18}$$

---

* Note that Stevenson did not use the MKSA system.

$$\nabla \cdot \mathbf{H} = \frac{\rho_m}{\mu} \tag{3.19}$$

For this problem, setting $\mathbf{J} = \rho_e = 0$ and introducing a vector potential $\mathbf{F}$ such that

$$\mathbf{E} = -\frac{1}{\epsilon} \nabla \times \mathbf{F}$$

leads to an equation for $\mathbf{H}$ in terms of $\mathbf{F}$:

$$\mathbf{H} = -j\omega\mathbf{F} - j\frac{1}{\omega\mu\epsilon} \nabla(\nabla \cdot \mathbf{F}), \tag{3.20}$$

and an expression for $\mathbf{F}$ in the form

$$\nabla^2 \mathbf{F} + k^2 \mathbf{F} = -\epsilon \mathbf{M}. \tag{3.21}$$

Equation (3.21) can be written in terms of a dyadic Green's Function as follows [Lyon 1981]:

$$\mathbf{F} = \epsilon \int_S \mathbf{M}(\mathbf{r}') \cdot \bar{\mathbf{G}}^{FM}(\mathbf{r}, \mathbf{r}')\, dS', \tag{3.22}$$

where the dyadic Green's Function is a solution to the boundary-value problem

$$\nabla^2 \bar{\mathbf{G}}^{FM}(\mathbf{r}, \mathbf{r}') + k^2 \bar{\mathbf{G}}^{FM}(\mathbf{r}, \mathbf{r}') = -\bar{\mathbf{I}}\delta(\mathbf{r} - \mathbf{r}') \tag{3.23.1}$$

with the boundary conditions

$$\mathbf{n} \times \nabla \times \bar{\mathbf{G}}^{FM}(\mathbf{r}, \mathbf{r}') = 0 \tag{3.23.2}$$

$$\mathbf{n} \cdot \bar{\mathbf{G}}^{FM}(\mathbf{r}, \mathbf{r}') = 0 \tag{3.23.3}$$

enforced on the waveguide walls. In the above equation $\bar{\mathbf{I}}$ is the dyadic idem factor ($\bar{\mathbf{I}} = \bar{\mathbf{xx}} + \bar{\mathbf{yy}} + \bar{\mathbf{zz}}$) and $\delta(\mathbf{r} - \mathbf{r}')$ is the Dirac delta function. (For an introduction to dyadic analysis, see [Collin 1991].)

The solution to (3.23) is given by Rahmat-Samii as [Rahmat-Samii 1975]:

$$\bar{\mathbf{G}}^{FM}(\mathbf{r}, \mathbf{r}') = \frac{1}{2ab} \sum_{m=0}^{\infty} \sum_{n=0}^{\infty} \frac{\epsilon_{0m}\epsilon_{0n}}{\Gamma_{mn}} e^{-\Gamma_{mn}|z-z'|} (S_x C_y S_x' C_y' \mathbf{xx} + C_x S_y C_x' S_y' \mathbf{yy} + C_x C_y C_x' C_y' \mathbf{zz}) \tag{3.24}$$

Thus the dyadic Green's Function given in (3.24) can be used together with (3.20) and (3.22) to solve for the $\mathbf{H}$ field in the waveguide excited by a magnetic current on the wall.

3.4.2.2 Cavity Green's Function

The slot region can be regarded as a rectangular cavity with dimensions L x W x T. Since there is no singularity in the cavity Green's Function [Rengarajan 1989-3], it can be written as a superposition of waveguide modes and computed without the need for an intermediate vector potential. In this case only the $\xi\xi$-component of the Green's Function is necessary, since this is the direction of both the magnetic current source and the resulting H field in the slot (because the slot is narrow). The equation for the **H** field and the necessary component of the magnetic dyadic Green's Function for the rectangular cavity is given by [Lyon 1981, note that the first bracket is misplaced]:

$$\mathbf{H}(\mathbf{r}) = \int_S \bar{\mathbf{G}}(\mathbf{r}, \mathbf{r}') \cdot \mathbf{M}_S(\mathbf{r}')\, dS' \tag{3.25}$$

$$G_{\xi\xi}^{cav}(\mathbf{r}, \mathbf{r}') = \frac{2jk}{WLZ_0} \sum_{m=1}^{\infty} \sum_{n=0}^{\infty} \epsilon_{0n} \frac{1 - \left(\frac{m\pi}{kL}\right)^2}{k_g \mathrm{Sin}[k_g T]}$$
$$\mathrm{Cos}\left[\frac{n\pi}{W}\left(-\eta + \frac{W}{2}\right)\right] \mathrm{Sin}\left[\frac{m\pi}{L}\left(\xi + \frac{L}{2}\right)\right] \mathrm{Cos}\left[k_g \begin{pmatrix} z_3 \\ z_3 + T \end{pmatrix}\right]$$
$$\mathrm{Cos}\left[\frac{n\pi}{W}\left(-\eta' + \frac{W}{2}\right)\right] \mathrm{Sin}\left[\frac{m\pi}{L}\left(\xi' + \frac{L}{2}\right)\right] \mathrm{Cos}\left[k_g \begin{pmatrix} z_3' + T \\ z_3' \end{pmatrix}\right], \; z_3 \gtrless z_3' \tag{3.26}$$

The upper and lower expressions in the last terms on the second and third lines correspond to the case $z_3 > z_3'$ and $z_3 < z_3'$ respectively, as indicated. The two cases converge to the same value when $z_3 = z_3'$. This kind of notation will be used in the rest of the derivation without further explanation.

3.4.3 Components relating to the fields in the slot

The four matrix components $\left[Y_1^{31}\right], \left[Y_1^{32}\right], \left[Y_2^{31}\right], \left[Y_2^{32}\right]$ relate to the fields in the slot excited by the magnetic currents on the two surfaces. It has already been shown in Section 3.3 that only two of these need to be computed because of symmetry and reciprocity.

The first component to be dealt with is $\left[Y_1^{31}\right]$, relating to the field in the slot excited by the current on S_1 and evaluated on S_1. Starting with the definition in (3.10.2) and substituting the weighting function from (3.7.3), gives:

$$\left[Y_1^{31}\right]_{qp} = -\frac{1}{W} \int_{S_1} \mathrm{Sin}\left[\frac{q\pi}{L}\left(\xi + \frac{L}{2}\right)\right] H_\xi\left(f_p(\mathbf{r}')\right)^{(3)}\, dS$$

Writing the **H** field in terms of the cavity Green's Function of (3.26) with the aid of (3.25) gives:

$$[Y_1^{31}]_{qp} = -\frac{2jk}{W^2 L Z_0}\int_{S_1} \mathrm{Sin}\left[\frac{q\pi}{L}\left(\xi+\frac{L}{2}\right)\right]\int_{S_1} f_p(\mathbf{r}')\sum_{m=1}^{\infty}\sum_{n=0}^{\infty}\epsilon_{0n}$$

$$\frac{1-\left(\frac{m\pi}{kL}\right)^2}{k_g \mathrm{Sin}[k_g T]}\mathrm{Cos}\left[\frac{n\pi}{W}\left(-\eta+\frac{W}{2}\right)\right]\mathrm{Sin}\left[\frac{m\pi}{L}\left(\xi+\frac{L}{2}\right)\right]\mathrm{Cos}\left[k_g\begin{pmatrix} z_3 \\ z_3+T\end{pmatrix}\right] \qquad (3.27)$$

$$\mathrm{Cos}\left[\frac{n\pi}{W}\left(-\eta'+\frac{W}{2}\right)\right]\mathrm{Sin}\left[\frac{m\pi}{L}\left(\xi'+\frac{L}{2}\right)\right]\mathrm{Cos}\left[k_g\begin{pmatrix} z_3'+T \\ z_3'\end{pmatrix}\right] d\mathrm{S}'\, d\mathrm{S},\ z_3 \gtrless z_3'.$$

The summations and integrations can be interchanged and the f_p substituted from (3.7). Also, since integration over both the primed and unprimed variables takes place on S_1,

$$z_3 = z_3' = -T$$

which makes it possible to replace the upper and lower expressions with only one expression:

$$\mathrm{Cos}\left[k_g\begin{pmatrix} z_3 \\ z_3+T\end{pmatrix}\right]\mathrm{Cos}\left[k_g\begin{pmatrix} z_3'+T \\ z_3'\end{pmatrix}\right] = \mathrm{Cos}\begin{pmatrix} -k_g T \\ 0\end{pmatrix}\mathrm{Cos}\begin{pmatrix} 0 \\ -k_g T\end{pmatrix} = \mathrm{Cos}[k_g T].$$

Remembering that n = 0 in the slot further simplifies (3.27) to:

$$[Y_1^{31}]_{qp} = -\frac{2jk}{W^3 L Z_0}\sum_{m=1}^{\infty}\left(1-\left(\frac{m\pi}{kL}\right)^2\right)\frac{\mathrm{Cos}[k_{g0}T]}{k_{g0}\mathrm{Sin}[k_{g0}T]}\int_{S_1}\mathrm{Sin}\left[\frac{q\pi}{L}\left(\xi+\frac{L}{2}\right)\right]$$

$$\mathrm{Sin}\left[\frac{m\pi}{L}\left(\xi+\frac{L}{2}\right)\right]d\mathrm{S}\int_{S_1}\mathrm{Sin}\left[\frac{p\pi}{L}\left(\xi'+\frac{L}{2}\right)\right]\mathrm{Sin}\left[\frac{m\pi}{L}\left(\xi'+\frac{L}{2}\right)\right]d\mathrm{S}'$$

where $k_{g0} = \sqrt{k^2-\left(\frac{m\pi}{L}\right)^2}$.

Substituting the integration limits and simplifying the integrals lead to:

$$[Y_1^{31}]_{qp} = -\frac{2jk}{WLZ_0}\sum_{m=1}^{\infty}\left(1-\left(\frac{m\pi}{kL}\right)^2\right)\frac{\mathrm{Cos}[k_{g0}T]}{k_{g0}\mathrm{Sin}[k_{g0}T]}\frac{L^2}{4}\delta_{mp}\delta_{mq}$$

$$= -\frac{jkL}{2WZ_0}\left(1-\left(\frac{p\pi}{kL}\right)^2\right)\frac{\mathrm{Cos}[k_{zp}T]}{k_{zp}\mathrm{Sin}[k_{zp}T]}\delta_{pq} \qquad (3.28.1)$$

where $k_{zp} = \sqrt{k^2-\left(\frac{p\pi}{L}\right)^2}$. (3.28.2)

This completes the derivation for $\left[\mathbf{Y_1^{31}}\right] = \left[\mathbf{Y_2^{32}}\right]$.

The two components $\left[\mathbf{Y}_1^{32}\right]$ and $\left[\mathbf{Y}_2^{31}\right]$ are solved by following a similar procedure. The equation is:

$$[Y_1^{32}]_{qp} = [Y_2^{31}]_{qp} = \frac{jkL}{2WZ_0}\left(1-\left(\frac{p\pi}{kL}\right)^2\right)\frac{1}{k_{zp}\,\mathrm{Sin}[k_{zp}T]}\,\delta_{pq} \tag{3.29}$$

3.4.4 Components relating to the fields in the waveguides

The last two components, $\left[\mathbf{Y}_1^{11}\right]$ and $\left[\mathbf{Y}_2^{22}\right]$, are more complicated since they involve more than one Green's function component, but the procedure is basically the same. The equation for the components of $\left[\mathbf{Y}_1^{11}\right]$ is repeated here from (3.10.1):

$$[Y_1^{11}]_{qp} = \int_{S_1} \mathbf{f}_q(\mathbf{r})\cdot\mathbf{H}_t(-f_p(\mathbf{r}'))^{(1)}\,dS \tag{3.30}$$

Since only the ξ-component of $\mathbf{H}$ is required, coordinate transformations from Table 3.2 can be used to write

$$\begin{aligned} H_\xi &= -\mathrm{Sin}[\theta]\,H_x + \mathrm{Cos}[\theta]\,H_z \\ \Rightarrow H_\xi &= [-\mathrm{Sin}[\theta]\ \ \mathrm{Cos}[\theta]]\begin{bmatrix} H_x \\ H_z \end{bmatrix}. \end{aligned} \tag{3.31}$$

The components of $\mathbf{H}$ on the right-hand side of (3.31) can be expanded using (3.20), noting that since the magnetic current $\mathbf{M}$ does not have a **y**-component, F_y can be set to zero.

$$\mathbf{H}(\mathbf{M}) = -j\omega\mathbf{F}(\mathbf{M}) - \frac{j}{\omega\mu\epsilon}\nabla(\nabla\cdot\mathbf{F}(\mathbf{M}))$$

$$\Rightarrow H_x(\mathbf{M}) = -\frac{j}{\omega\mu\epsilon}\frac{\partial^2 F_z(\mathbf{M})}{\partial z\,\partial x} - \frac{j}{\omega\mu\epsilon}\frac{\partial^2 F_x(\mathbf{M})}{\partial x^2} - j\omega F_x(\mathbf{M}) \tag{3.32}$$

$$\text{and } H_z(\mathbf{M}) = -\frac{j}{\omega\mu\epsilon}\frac{\partial^2 F_z(\mathbf{M})}{\partial z^2} - j\omega F_z(\mathbf{M}) - \frac{j}{\omega\mu\epsilon}\frac{\partial^2 F_x(\mathbf{M})}{\partial z\,\partial x} \tag{3.33}$$

This can be written in matrix form as

$$\begin{bmatrix} H_x(M_\xi\xi(\mathbf{r}')) \\ H_y(M_\xi\xi(\mathbf{r}')) \end{bmatrix} = -\frac{j}{\omega\mu\epsilon}\begin{bmatrix} \frac{\partial^2}{\partial x^2}+k^2 & \frac{\partial^2}{\partial z\,\partial x} \\ \frac{\partial^2}{\partial z\,\partial x} & \frac{\partial^2}{\partial z^2}+k^2 \end{bmatrix}\begin{bmatrix} F_x(M_\xi\xi(\mathbf{r}')) \\ F_z(M_\xi\xi(\mathbf{r}')) \end{bmatrix} \tag{3.34}$$

and again the right-hand side components can be expanded, using (3.22) as well as coordinate transformations from Table 3.2:

$$\mathbf{F}(M_\xi \xi(\mathbf{r'})) = \epsilon \int_S M_\xi(\mathbf{r'})\,\xi \cdot \mathbf{G}^{FM}(\mathbf{r}, \mathbf{r'})\, dS'$$

$$= \epsilon \int_S M_\xi(\mathbf{r'})\,(-\mathrm{Sin}[\theta]\,\mathbf{x} + \mathrm{Cos}[\theta]\,\mathbf{z}) \cdot \left(G_{xx}^{FM}(\mathbf{r}, \mathbf{r'})\,\mathbf{xx} + G_{yy}^{FM}(\mathbf{r}, \mathbf{r'})\,\mathbf{yy} + G_{zz}^{FM}(\mathbf{r}, \mathbf{r'})\,\mathbf{zz}\right) dS'$$

$$\Rightarrow F_x(M_\xi \xi(\mathbf{r'})) = -\epsilon\,\mathrm{Sin}[\theta] \int_S M_\xi(\mathbf{r'})\, G_{xx}^{FM}(\mathbf{r}, \mathbf{r'})\, dS'$$

$$\text{and } F_z(M_\xi \xi(\mathbf{r'})) = \epsilon\,\mathrm{Cos}[\theta] \int_S M_\xi(\mathbf{r'})\, G_{zz}^{FM}(\mathbf{r}, \mathbf{r'})\, dS' \tag{3.35}$$

Substituting the results from (3.35) into (3.34) and then back into (3.31) leads to a compact expression for H_ξ:

$$H_\xi(M_\xi \xi(\mathbf{r'})) = \frac{j}{\omega\mu}[-\mathrm{Sin}[\theta]\ \mathrm{Cos}[\theta]] \begin{bmatrix} \frac{\partial^2}{\partial x^2} + k^2 & \frac{\partial^2}{\partial z\,\partial x} \\ \frac{\partial^2}{\partial z\,\partial x} & \frac{\partial^2}{\partial z^2} + k^2 \end{bmatrix} \begin{bmatrix} \mathrm{Sin}[\theta] \int_S M_\xi(\mathbf{r'})\, G_{xx}^{FM}(\mathbf{r}, \mathbf{r'})\, dS' \\ -\mathrm{Cos}[\theta] \int_S M_\xi(\mathbf{r'})\, G_{zz}^{FM}(\mathbf{r}, \mathbf{r'})\, dS' \end{bmatrix}$$

$$\Rightarrow H_\xi(-\mathbf{f}_p(\mathbf{r'})) = \frac{j}{\omega\mu}[-\mathrm{Sin}[\theta]\ \mathrm{Cos}[\theta]] \begin{bmatrix} \frac{\partial^2}{\partial x^2} + k^2 & \frac{\partial^2}{\partial z\,\partial x} \\ \frac{\partial^2}{\partial z\,\partial x} & \frac{\partial^2}{\partial z^2} + k^2 \end{bmatrix} \begin{bmatrix} -\mathrm{Sin}[\theta] \int_S f_p(\mathbf{r'})\, G_{xx}^{FM}(\mathbf{r}, \mathbf{r'})\, dS' \\ \mathrm{Cos}[\theta] \int_S f_p(\mathbf{r'})\, G_{zz}^{FM}(\mathbf{r}, \mathbf{r'})\, dS' \end{bmatrix}$$

(3.36)

Substituting (3.36) into (3.10.1) gives:

$$[Y_1^{11}]_{qp} = \frac{1}{W} \frac{j}{\omega\mu} \int_{S_1} \mathrm{Sin}\left[\frac{q\pi}{L}\left(\xi + \frac{L}{2}\right)\right][-\mathrm{Sin}[\theta]\ \mathrm{Cos}[\theta]]$$

$$* \begin{bmatrix} \frac{\partial^2}{\partial x^2} + k^2 & \frac{\partial^2}{\partial z\,\partial x} \\ \frac{\partial^2}{\partial z\,\partial x} & \frac{\partial^2}{\partial z^2} + k^2 \end{bmatrix} \begin{bmatrix} -\mathrm{Sin}[\theta] \int_{S_1} f_p(\mathbf{r'})\, G_{xx}^{FM}(\mathbf{r}, \mathbf{r'})\, dS' \\ \mathrm{Cos}[\theta] \int_{S_1} f_p(\mathbf{r'})\, G_{zz}^{FM}(\mathbf{r}, \mathbf{r'})\, dS' \end{bmatrix} dS \tag{3.37}$$

Substituting the magnetic current basis function from (3.7) and the Green's Function components from (3.24), setting $y_1 = b$ on S_1, leads to

$$[Y_1^{11}]_{qp} = \frac{j}{2W^2 ab\omega\mu} \sum_{m=0}^{\infty} \sum_{n=0}^{\infty} \frac{\epsilon_{0m}\epsilon_{0n}}{\Gamma_{mn}} \int_{S_1} \mathrm{Sin}\left[\frac{q\pi}{L}\left(\xi + \frac{L}{2}\right)\right][-\mathrm{Sin}[\theta]\ \mathrm{Cos}[\theta]]$$

$$* \begin{bmatrix} \frac{\partial^2}{\partial x^2} + k^2 & \frac{\partial^2}{\partial z\,\partial x} \\ \frac{\partial^2}{\partial z\,\partial x} & \frac{\partial^2}{\partial z^2} + k^2 \end{bmatrix} \begin{bmatrix} -\mathrm{Sin}[\theta]\, S_x \int_{S_1} \mathrm{Sin}\left[\frac{p\pi}{L}\left(\xi' + \frac{L}{2}\right)\right] e^{-\Gamma_{mn}|z-z'|}\, S_x'\, dS' \\ \mathrm{Cos}[\theta]\, C_x \int_{S_1} \mathrm{Sin}\left[\frac{p\pi}{L}\left(\xi' + \frac{L}{2}\right)\right] e^{-\Gamma_{mn}|z-z'|}\, C_x'\, dS' \end{bmatrix} dS \tag{3.38}$$

which is the final expression for $\left[\mathbf{Y}_1^{11}\right]$.

The results of this section are summarised in equation (3.40) below. It is worth emphasising here that these equations enable us to solve (3.40.1) for the A_p and B_p. They are the unknown coefficients for the magnetic currents on the aperture surfaces of a general inclined slot in the common broad wall of two parallel waveguides. If these currents are known, it is possible to find the fields anywhere in the waveguides by making use of Green's Functions. Knowing the fields enables us to compute the scattering parameters of the system, and these s-parameters provide the data necessary to train a neural network that can solve for the s-parameters of different structures, once properly trained.

(3.9):
$$\begin{bmatrix} [Y_1^{11}]+[Y_1^{31}] & [Y_1^{32}] \\ [Y_2^{31}] & [Y_2^{32}]+[Y_2^{22}] \end{bmatrix} \begin{bmatrix} [A] \\ [B] \end{bmatrix} = \begin{bmatrix} [H] \\ [0] \end{bmatrix} \tag{3.40.1}$$

(3.15):
$$[H]_q = \frac{2}{W}\sqrt{\frac{\beta_{10}}{abkZ_0}}\, e^{\Gamma_{10} z_i} \int_{-\frac{L}{2}}^{\frac{L}{2}} \int_{-\frac{W}{2}}^{\frac{W}{2}} e^{-\Gamma_{10}(\mathrm{Cos}[\theta]\,\xi - \mathrm{Sin}[\theta]\,\eta)} \mathrm{Sin}\left[\frac{q\pi}{L}\left(\xi + \frac{L}{2}\right)\right] \times \left\{ -\mathrm{Sin}[\theta]\,\mathrm{Sin}\left[\frac{\pi}{a}(-\mathrm{Sin}[\theta]\,\xi - \mathrm{Cos}[\theta]\,\eta + \Delta)\right] - j\frac{\pi}{a}\frac{1}{\beta_{10}}\mathrm{Cos}[\theta]\,\mathrm{Cos}\left[\frac{\pi}{a}(-\mathrm{Sin}[\theta]\,\xi - \mathrm{Cos}[\theta]\,\eta + \Delta)\right] \right\} d\eta\, d\xi \tag{3.40.2}$$

(3.28.1):
$$[Y_2^{32}]_{qp} = [Y_1^{31}]_{qp} = -\frac{jkL}{2WZ_0}\left(1 - \left(\frac{p\pi}{kL}\right)^2\right)\frac{\mathrm{Cos}[k_{zp}T]}{k_{zp}\,\mathrm{Sin}[k_{zp}T]}\,\delta_{pq} \tag{3.40.3}$$

(3.29):
$$[Y_1^{32}]_{qp} = [Y_2^{31}]_{qp} = \frac{jkL}{2WZ_0}\left(1 - \left(\frac{p\pi}{kL}\right)^2\right)\frac{1}{k_{zp}\,\mathrm{Sin}[k_{zp}T]}\,\delta_{pq} \tag{3.40.4}$$

(3.38):

$$[Y_1^{11}]_{qp} = [Y_2^{22}]_{qp} = \frac{j}{2W^2 ab\omega\mu}\sum_{m=0}^{\infty}\sum_{n=0}^{\infty}\frac{\epsilon_{0m}\epsilon_{0n}}{\Gamma_{mn}}\int_S \mathrm{Sin}\left[\frac{q\pi}{L}\left(\xi + \frac{L}{2}\right)\right][-\mathrm{Sin}[\theta]\ \mathrm{Cos}[\theta]] * \begin{bmatrix} \frac{\partial^2}{\partial x^2}+k^2 & \frac{\partial^2}{\partial z\,\partial x} \\ \frac{\partial^2}{\partial z\,\partial x} & \frac{\partial^2}{\partial z^2}+k^2 \end{bmatrix} \begin{bmatrix} -\mathrm{Sin}[\theta]\,S_x \int_S \mathrm{Sin}\left[\frac{p\pi}{L}\left(\xi' + \frac{L}{2}\right)\right] e^{-\Gamma_{mn}|z-z'|} S_x'\, dS' \\ \mathrm{Cos}[\theta]\,C_x \int_S \mathrm{Sin}\left[\frac{p\pi}{L}\left(\xi' + \frac{L}{2}\right)\right] e^{-\Gamma_{mn}|z-z'|} C_x'\, dS' \end{bmatrix} dS \tag{3.40.5}$$

3.5 Calculating the scattering parameters for the general slot

The four-port coupler has 16 scattering parameters in its complete S matrix:

$$\begin{bmatrix} S_{11} & S_{12} & S_{13} & S_{14} \\ S_{21} & S_{22} & S_{23} & S_{24} \\ S_{31} & S_{32} & S_{33} & S_{34} \\ S_{41} & S_{42} & S_{43} & S_{44} \end{bmatrix}$$

If the ports are defined as shown in Figure 3.3, then the symmetry of the structure leads to the following equations:

$$S_{11} = S_{22} = S_{33} = S_{44}$$
$$S_{12} = S_{21} = S_{34} = S_{43}$$
$$S_{13} = S_{31} = S_{24} = S_{42}$$
$$S_{14} = S_{41} = S_{23} = S_{32}$$

It is therefore only necessary to model s_{11}, s_{21}, s_{31} and s_{41}. As can be seen from equations (1.1) to (1.3), all the characteristic properties of the coupler can be described in terms of these four scattering parameters.

Each of these parameters is the ratio of the outgoing dominant mode field at a port to the incident field at port 1. It was decided to use the H_x field components to compute the s-parameters. Then the four equations are:

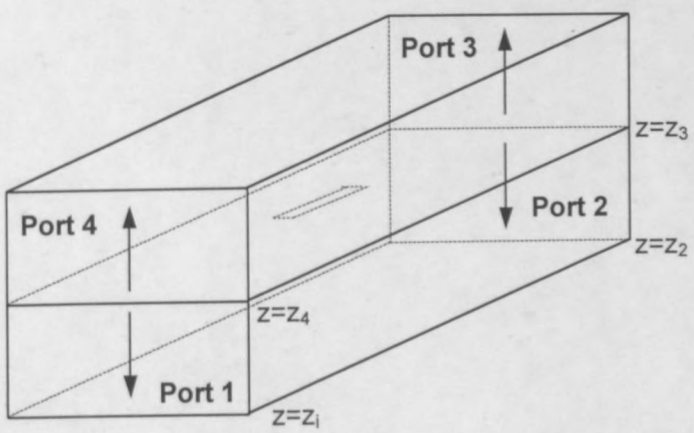

Figure 3.3: The port numbers and field directions for the coupler configuration.

$$S_{11} = \frac{\left(H_x^{reflected}\right)_{z=z_i}}{\left(H_x^{inc}\right)_{z=z_i}} \tag{3.41.1}$$

$$S_{21} = \frac{\left(H_x^{reflected}\right)_{z=z_2} + \left(H_x^{inc}\right)_{z=z_2}}{\left(H_x^{inc}\right)_{z=z_i}} \tag{3.41.2}$$

$$S_{31} = \frac{\left(H_x^{reflected}\right)_{z=z_3}}{\left(H_x^{inc}\right)_{z=z_i}} \tag{3.41.3}$$

$$S_{41} = \frac{\left(H_x^{reflected}\right)_{z=z_4}}{\left(H_x^{inc}\right)_{z=z_i}} \tag{3.41.4}$$

The denominator, which is common to all four equations, is given by (3.13.1) evaluated at $z = z_i$ and is equal to

$$\left(H_{x_1}^{inc}\right)_{z=z_i} = -2\sqrt{\frac{\beta_{10}}{a\,b\,k\,Z_0}}\,\mathrm{Sin}\left[\frac{\pi}{a}x_1\right] \tag{3.42}$$

The numerators can be determined by extracting H_x from (3.34):

$$H_x^{reflected}(M_\xi \xi(\mathbf{r}')) = -\frac{j}{\omega\mu\epsilon}\left(\left(\frac{\partial^2}{\partial x^2} + k^2\right)F_x(M_\xi \xi(\mathbf{r}')) + \frac{\partial^2}{\partial z\,\partial x}F_z(M_\xi \xi(\mathbf{r}'))\right)$$

Substituting F_x and F_z from (3.35) gives:

$$H_x^{reflected}(M_\xi \xi(\mathbf{r}')) = -\frac{j}{\omega\mu\epsilon}\left(\left(\frac{\partial^2}{\partial x^2} + k^2\right)\left(-\epsilon\,\mathrm{Sin}[\theta]\int_S M_\xi(\mathbf{r}')\,G_{xx}^{FM}(\mathbf{r},\mathbf{r}')\,dS'\right) + \frac{\partial^2}{\partial z\,\partial x}\left(\epsilon\,\mathrm{Cos}[\theta]\int_S M_\xi(\mathbf{r}')\,G_{zz}^{FM}(\mathbf{r},\mathbf{r}')\,dS'\right)\right)$$

Substituting the Green's Function components from (3.24) gives:

$$H_x^{reflected}(M_\xi \xi(\mathbf{r}')) = -\frac{j}{\omega\mu}\,\frac{1}{2ab}\sum_{m=0}^{\infty}\sum_{n=0}^{\infty}\frac{\epsilon_{0m}\epsilon_{0n}}{\Gamma_{mn}}C_y\,C_y' * \left(-\mathrm{Sin}[\theta]\left(\frac{\partial^2}{\partial x^2} + k^2\right)S_x\int_S M_\xi(\mathbf{r}')\,e^{-\Gamma_{mn}|z-z'|}S_x'\,dS' + \mathrm{Cos}[\theta]\,\frac{\partial^2}{\partial z\,\partial x}C_x\int_S M_\xi(\mathbf{r}')\,e^{-\Gamma_{mn}|z-z'|}C_x'\,dS'\right) \tag{3.43}$$

The magnetic current is substituted in such a way that it can represent the magnetic current either on S_1 or on S_2. The specific case will be dealt with for each s-parameter separately. Let

$$M_\xi \xi(\mathbf{r}') = \frac{1}{W}\sum_{p=1}^{N} K_p \operatorname{Sin}\left[\frac{p\pi}{L}\left(\xi + \frac{L}{2}\right)\right]$$

where:

$$K_p = -A_p \quad \text{on } S_1$$
$$K_p = B_p \quad \text{on } S_2$$

Then (3.43) becomes:

$$H_x^{\text{reflected}}(M_\xi \xi(\mathbf{r}')) = -\frac{j}{2Wab\omega\mu}\sum_{p=1}^{N} K_p \sum_{m=0}^{\infty}\sum_{n=0}^{\infty}\frac{\epsilon_{0m}\epsilon_{0n}}{\Gamma_{mn}}\operatorname{Cos}\left[\frac{n\pi}{b}y\right]\operatorname{Cos}\left[\frac{n\pi}{b}y'\right]$$
$$\left(-\operatorname{Sin}[\theta]\left(\frac{\partial^2}{\partial x^2}+k^2\right)\operatorname{Sin}\left[\frac{m\pi}{a}x\right]\int_S \operatorname{Sin}\left[\frac{p\pi}{L}\left(\xi+\frac{L}{2}\right)\right]e^{-\Gamma_{mn}|z-z'|}\operatorname{Sin}\left[\frac{m\pi}{a}x'\right]dS'\right.$$
$$\left.+\operatorname{Cos}[\theta]\frac{\partial^2}{\partial z\partial x}\operatorname{Cos}\left[\frac{m\pi}{a}x\right]\int_S \operatorname{Sin}\left[\frac{p\pi}{L}\left(\xi+\frac{L}{2}\right)\right]e^{-\Gamma_{mn}|z-z'|}\operatorname{Cos}\left[\frac{m\pi}{a}x'\right]dS'\right) \qquad (3.44)$$

Since only the dominant TE_{10} mode is considered for the s-parameters, (3.44) can be simplified to:

$$H_{x,TE_{10}}^{\text{reflected}}(M_\xi \xi(\mathbf{r}')) = \frac{j\operatorname{Sin}[\theta]}{Wab\omega\mu}\frac{1}{\Gamma_{10}}\sum_{p=1}^{N} K_p\left(\frac{\partial^2}{\partial x^2}+k^2\right)\left(\operatorname{Sin}\left[\frac{\pi}{a}x\right]\right.$$
$$\left.*\int_S \operatorname{Sin}\left[\frac{p\pi}{L}\left(\xi+\frac{L}{2}\right)\right]e^{-\Gamma_{10}|z-z'|}\operatorname{Sin}\left[\frac{\pi}{a}x'\right]dS'\right)$$
$$-\frac{j\operatorname{Cos}[\theta]}{Wab\omega\mu}\frac{1}{\Gamma_{10}}\sum_{p=1}^{N} K_p\frac{\partial^2}{\partial z\partial x}\left(\operatorname{Cos}\left[\frac{\pi}{a}x\right]\right.$$
$$\left.*\int_S \operatorname{Sin}\left[\frac{p\pi}{L}\left(\xi+\frac{L}{2}\right)\right]e^{-\Gamma_{10}|z-z'|}\operatorname{Cos}\left[\frac{\pi}{a}x'\right]dS'\right)$$

Now for the two cases $z > z'$ (at ports 2 and 3) and $z < z'$ (at ports 1 and 4), the differentiation can be performed and the fields written as

$$\left(H_x^{reflected}\right)_{z<z'} = \frac{j\,Sin[\theta]}{W\,a\,b\,\omega\,\mu}\,\frac{1}{\Gamma_{10}}\,e^{\Gamma_{10}\,z}\left(k^2-\left(\frac{\pi}{a}\right)^2\right)Sin\left[\frac{\pi}{a}x\right]\sum_{p=1}^{N}K_p$$

$$*\int_{-\frac{L}{2}}^{\frac{L}{2}}Sin\left[\frac{p\,\pi}{L}\left(\xi'+\frac{L}{2}\right)\right]\int_{-\frac{W}{2}}^{\frac{W}{2}}e^{-\Gamma_{10}\,z'}\,Sin\left[\frac{\pi}{a}x'\right]d\eta'\,d\xi'$$

$$+\frac{j\,Cos[\theta]\,\pi}{W\,a^2\,b\,\omega\,\mu}\,e^{\Gamma_{10}\,z}\,Sin\left[\frac{\pi}{a}x\right]\sum_{p=1}^{N}K_p$$

$$*\int_{-\frac{L}{2}}^{\frac{L}{2}}Sin\left[\frac{p\,\pi}{L}\left(\xi'+\frac{L}{2}\right)\right]\int_{-\frac{W}{2}}^{\frac{W}{2}}e^{-\Gamma_{10}\,z'}\,Cos\left[\frac{\pi}{a}x'\right]d\eta'\,d\xi' \qquad (3.45.1)$$

$$\left(H_x^{reflected}\right)_{z>z'} = -\frac{j\,Sin[\theta]}{W\,a\,b\,\omega\,\mu}\,\frac{1}{\Gamma_{10}}\,e^{-\Gamma_{10}\,z}\left(k^2-\left(\frac{\pi}{a}\right)^2\right)Sin\left[\frac{\pi}{a}x\right]\sum_{p=1}^{N}K_p$$

$$*\int_{-\frac{L}{2}}^{\frac{L}{2}}Sin\left[\frac{p\,\pi}{L}\left(\xi'+\frac{L}{2}\right)\right]\int_{-\frac{W}{2}}^{\frac{W}{2}}e^{\Gamma_{10}\,z'}\,Sin\left[\frac{\pi}{a}x'\right]d\eta'\,d\xi'$$

$$-\frac{j\,Cos[\theta]\,\pi}{W\,a^2\,b\,\omega\,\mu}\,Sin\left[\frac{\pi}{a}x\right]e^{-\Gamma_{10}\,z}\sum_{p=1}^{N}K_p$$

$$*\int_{-\frac{L}{2}}^{\frac{L}{2}}Sin\left[\frac{p\,\pi}{L}\left(\xi'+\frac{L}{2}\right)\right]\int_{-\frac{W}{2}}^{\frac{W}{2}}e^{\Gamma_{10}\,z'}\,Cos\left[\frac{\pi}{a}x'\right]d\eta'\,d\xi' \qquad (3.45.2)$$

The reflected field at each port can be determined using (3.45.1) and (3.45.2) under the following conditions:

$$\begin{aligned}
&\text{At port 1}: \quad K_p = -A_p, \quad z<z', \quad z=z_1\\
&\text{At port 2}: \quad K_p = -A_p, \quad z>z', \quad z=z_2\\
&\text{At port 3}: \quad K_p = B_p, \quad z>z', \quad z=z_3\\
&\text{At port 4}: \quad K_p = B_p, \quad z<z', \quad z=z_4
\end{aligned}$$

The results are:

$$\left(H_x^{reflected}\right)_{z=z_i} = -\frac{j}{W\,a\,b\,\omega\,\mu}\,\frac{1}{\Gamma_{10}}\,Sin\left[\frac{\pi}{a}x_1\right]e^{\Gamma_{10}\,z_i}\sum_{p=1}^{N}A_p\Bigg($$

$$Cos[\theta]\,\frac{\pi}{a}\,\Gamma_{10}\int_{-\frac{L}{2}}^{\frac{L}{2}}Sin\left[\frac{p\,\pi}{L}\left(\xi'+\frac{L}{2}\right)\right]\int_{-\frac{W}{2}}^{\frac{W}{2}}Cos\left[\frac{\pi}{a}x_1'\right]e^{-\Gamma_{10}\,z_1'}\,d\eta'\,d\xi'$$

$$+\,Sin[\theta]\left(k^2-\left(\frac{\pi}{a}\right)^2\right)\int_{-\frac{L}{2}}^{\frac{L}{2}}Sin\left[\frac{p\,\pi}{L}\left(\xi'+\frac{L}{2}\right)\right]\int_{-\frac{W}{2}}^{\frac{W}{2}}Sin\left[\frac{\pi}{a}x_1'\right]e^{-\Gamma_{10}\,z_1'}\,d\eta'\,d\xi'\Bigg) \qquad (3.46.1)$$

$$\left(H_x^{reflected}\right)_{z=z_2} = \frac{j}{W\,a\,b\,\omega\mu}\,\frac{1}{\Gamma_{10}}\,\mathrm{Sin}\left[\frac{\pi}{a}x\right]e^{-\Gamma_{10}z_2}\sum_{p=1}^{N}A_p\Bigg($$

$$+\mathrm{Cos}[\theta]\,\frac{\pi}{a}\,\Gamma_{10}\int_{-\frac{L}{2}}^{\frac{L}{2}}\mathrm{Sin}\left[\frac{p\pi}{L}\left(\xi'+\frac{L}{2}\right)\right]\int_{-\frac{W}{2}}^{\frac{W}{2}}\mathrm{Cos}\left[\frac{\pi}{a}x'\right]e^{\Gamma_{10}z'}\,d\eta'\,d\xi'$$

$$+\mathrm{Sin}[\theta]\left(k^2-\left(\frac{\pi}{a}\right)^2\right)\int_{-\frac{L}{2}}^{\frac{L}{2}}\mathrm{Sin}\left[\frac{p\pi}{L}\left(\xi'+\frac{L}{2}\right)\right]\int_{-\frac{W}{2}}^{\frac{W}{2}}\mathrm{Sin}\left[\frac{\pi}{a}x'\right]e^{\Gamma_{10}z'}\,d\eta'\,d\xi'\Bigg) \qquad (3.46.2)$$

$$\left(H_x^{reflected}\right)_{z=z_3} = -\frac{j}{W\,a\,b\,\omega\mu}\,\frac{1}{\Gamma_{10}}\,\mathrm{Sin}\left[\frac{\pi}{a}x\right]e^{-\Gamma_{10}z_3}\sum_{p=1}^{N}B_p\Bigg($$

$$+\mathrm{Cos}[\theta]\,\frac{\pi}{a}\,\Gamma_{10}\int_{-\frac{L}{2}}^{\frac{L}{2}}\mathrm{Sin}\left[\frac{p\pi}{L}\left(\xi'+\frac{L}{2}\right)\right]\int_{-\frac{W}{2}}^{\frac{W}{2}}\mathrm{Cos}\left[\frac{\pi}{a}x'\right]e^{\Gamma_{10}z'}\,d\eta'\,d\xi'$$

$$+\mathrm{Sin}[\theta]\left(k^2-\left(\frac{\pi}{a}\right)^2\right)\int_{-\frac{L}{2}}^{\frac{L}{2}}\mathrm{Sin}\left[\frac{p\pi}{L}\left(\xi'+\frac{L}{2}\right)\right]\int_{-\frac{W}{2}}^{\frac{W}{2}}\mathrm{Sin}\left[\frac{\pi}{a}x'\right]e^{\Gamma_{10}z'}\,d\eta'\,d\xi'\Bigg) \qquad (3.46.3)$$

$$\left(H_x^{reflected}\right)_{z=z_4} = \frac{j}{W\,a\,b\,\omega\mu}\,\frac{1}{\Gamma_{10}}\,\mathrm{Sin}\left[\frac{\pi}{a}x_1\right]e^{\Gamma_{10}z_4}\sum_{p=1}^{N}B_p\Bigg($$

$$\mathrm{Cos}[\theta]\,\frac{\pi}{a}\,\Gamma_{10}\int_{-\frac{L}{2}}^{\frac{L}{2}}\mathrm{Sin}\left[\frac{p\pi}{L}\left(\xi'+\frac{L}{2}\right)\right]\int_{-\frac{W}{2}}^{\frac{W}{2}}\mathrm{Cos}\left[\frac{\pi}{a}x_1'\right]e^{-\Gamma_{10}z_1'}\,d\eta'\,d\xi'$$

$$+\mathrm{Sin}[\theta]\left(k^2-\left(\frac{\pi}{a}\right)^2\right)\int_{-\frac{L}{2}}^{\frac{L}{2}}\mathrm{Sin}\left[\frac{p\pi}{L}\left(\xi'+\frac{L}{2}\right)\right]\int_{-\frac{W}{2}}^{\frac{W}{2}}\mathrm{Sin}\left[\frac{\pi}{a}x_1'\right]e^{-\Gamma_{10}z_1'}\,d\eta'\,d\xi'\Bigg) \qquad (3.46.4)$$

Now, using (3.42) and (3.46) in (3.41), the final equations for the scattering parameters are determined:

$$S_{11} = \frac{j}{2W\sqrt{a\,b\,k\,Z_0\,\beta_{10}}}\,e^{\Gamma_{10}z_i}\sum_{p=1}^{N}A_p\Bigg($$

$$\mathrm{Cos}[\theta]\,\frac{\pi}{a}\int_{-\frac{L}{2}}^{\frac{L}{2}}\mathrm{Sin}\left[\frac{p\pi}{L}\left(\xi'+\frac{L}{2}\right)\right]\int_{-\frac{W}{2}}^{\frac{W}{2}}\mathrm{Cos}\left[\frac{\pi}{a}x_1'\right]e^{-\Gamma_{10}z_1'}\,d\eta'\,d\xi'$$

$$+\mathrm{Sin}[\theta]\,\frac{1}{\Gamma_{10}}\left(k^2-\left(\frac{\pi}{a}\right)^2\right)\int_{-\frac{L}{2}}^{\frac{L}{2}}\mathrm{Sin}\left[\frac{p\pi}{L}\left(\xi'+\frac{L}{2}\right)\right]\int_{-\frac{W}{2}}^{\frac{W}{2}}\mathrm{Sin}\left[\frac{\pi}{a}x_1'\right]e^{-\Gamma_{10}z_1'}\,d\eta'\,d\xi'\Bigg) \qquad (3.47.1)$$

$$S_{21} = e^{-\Gamma_{10}(z_2 - z_i)} - \frac{j}{2W\sqrt{abkZ_0\beta_{10}}} e^{-\Gamma_{10} z_2} \sum_{p=1}^{N} A_p \Bigg(\\ + \mathrm{Cos}[\theta] \frac{\pi}{a} \int_{-\frac{L}{2}}^{\frac{L}{2}} \mathrm{Sin}\left[\frac{p\pi}{L}\left(\xi' + \frac{L}{2}\right)\right] \int_{-\frac{W}{2}}^{\frac{W}{2}} \mathrm{Cos}\left[\frac{\pi}{a} x'\right] e^{\Gamma_{10} z'} \, d\eta' \, d\xi' \\ + \mathrm{Sin}[\theta] \frac{1}{\Gamma_{10}} \left(k^2 - \left(\frac{\pi}{a}\right)^2\right) \int_{-\frac{L}{2}}^{\frac{L}{2}} \mathrm{Sin}\left[\frac{p\pi}{L}\left(\xi' + \frac{L}{2}\right)\right] \int_{-\frac{W}{2}}^{\frac{W}{2}} \mathrm{Sin}\left[\frac{\pi}{a} x'\right] e^{\Gamma_{10} z'} \, d\eta' \, d\xi' \Bigg) \qquad (3.47.2)$$

$$S_{31} = \frac{j}{2W\sqrt{abkZ_0\beta_{10}}} e^{-\Gamma_{10} z_3} \sum_{p=1}^{N} B_p \Bigg(\\ + \mathrm{Cos}[\theta] \frac{\pi}{a} \int_{-\frac{L}{2}}^{\frac{L}{2}} \mathrm{Sin}\left[\frac{p\pi}{L}\left(\xi' + \frac{L}{2}\right)\right] \int_{-\frac{W}{2}}^{\frac{W}{2}} \mathrm{Cos}\left[\frac{\pi}{a} x'\right] e^{\Gamma_{10} z'} \, d\eta' \, d\xi' \\ + \mathrm{Sin}[\theta] \frac{1}{\Gamma_{10}} \left(k^2 - \left(\frac{\pi}{a}\right)^2\right) \int_{-\frac{L}{2}}^{\frac{L}{2}} \mathrm{Sin}\left[\frac{p\pi}{L}\left(\xi' + \frac{L}{2}\right)\right] \int_{-\frac{W}{2}}^{\frac{W}{2}} \mathrm{Sin}\left[\frac{\pi}{a} x'\right] e^{\Gamma_{10} z'} \, d\eta' \, d\xi' \Bigg) \qquad (3.47.3)$$

$$S_{41} = -\frac{j}{2W\sqrt{abkZ_0\beta_{10}}} e^{\Gamma_{10} z_4} \sum_{p=1}^{N} B_p \Bigg(\\ \mathrm{Cos}[\theta] \frac{\pi}{a} \int_{-\frac{L}{2}}^{\frac{L}{2}} \mathrm{Sin}\left[\frac{p\pi}{L}\left(\xi' + \frac{L}{2}\right)\right] \int_{-\frac{W}{2}}^{\frac{W}{2}} \mathrm{Cos}\left[\frac{\pi}{a} x_1'\right] e^{-\Gamma_{10} z_1'} \, d\eta' \, d\xi' \\ + \mathrm{Sin}[\theta] \frac{1}{\Gamma_{10}} \left(k^2 - \left(\frac{\pi}{a}\right)^2\right) \int_{-\frac{L}{2}}^{\frac{L}{2}} \mathrm{Sin}\left[\frac{p\pi}{L}\left(\xi' + \frac{L}{2}\right)\right] \int_{-\frac{W}{2}}^{\frac{W}{2}} \mathrm{Sin}\left[\frac{\pi}{a} x_1'\right] e^{-\Gamma_{10} z_1'} \, d\eta' \, d\xi' \Bigg) \qquad (3.47.4)$$

This concludes the derivation of the general expressions for the s-parameters.

All the equations necessary for the complete solution of a general inclined slot have now been derived. The numerical solution can be computed in Mathematica or Matlab, but is very computer time and memory expensive. Instead, to confirm the validity of the equations and to implement the data in a neural network, simplifications have been made from a general inclined slot to a longitudinal and a transverse slot. The equations for these two special cases are given in the next two sections.

3.6 Solution for a longitudinal slot

The derivation of the matrix equation (3.9) was completely general and it can also be used for the case of the longitudinal slot shown in Figure 3.4. The definitions of the matrix components stay the same and the expressions in equations (3.40.2) - (3.40.5) can be used with $\theta = 0°$. The computations are set out in Appendix C and only the results are presented here. The complete set of simplified matrix components is:

$$[H]_q = -\frac{j4\pi q L}{W}\frac{e^{\Gamma_{10} z_i}}{\sqrt{a b k Z_0 \beta_{10}}}\mathrm{Cos}\left[\frac{\pi\Delta}{a}\right]\mathrm{Sin}\left[\frac{\pi W}{2a}\right]\frac{e^{\Gamma_{10}\frac{L}{2}} - (-1)^q e^{-\Gamma_{10}\frac{L}{2}}}{\pi^2 q^2 + L^2\Gamma_{10}^2} \tag{3.48.1}$$

$$[Y_2^{32}]_{qp} = [Y_1^{31}]_{qp} = -\frac{jkL}{2WZ_0}\left(1 - \left(\frac{p\pi}{kL}\right)^2\right)\frac{\mathrm{Cos}[k_{zp}T]}{k_{zp}\,\mathrm{Sin}[k_{zp}T]}\delta_{pq} \tag{3.48.2}$$

$$[Y_1^{32}]_{qp} = [Y_2^{31}]_{qp} = \frac{jkL}{2WZ_0}\left(1 - \left(\frac{p\pi}{kL}\right)^2\right)\frac{1}{k_{zp}\,\mathrm{Sin}[k_{zp}T]}\delta_{pq} \tag{3.48.3}$$

$$\begin{aligned}[Y_1^{11}]_{qp} = [Y_2^{22}]_{qp} = {} & \frac{j4aL^2}{W^2 b\pi^2\omega\mu}\sum_{m=1}^{\infty}\sum_{n=0}^{\infty}\frac{\epsilon_{0n}}{m^2\Gamma_{mn}}\mathrm{Cos}^2\left[\frac{m\pi\Delta}{a}\right]\mathrm{Sin}^2\left[\frac{m\pi W}{2a}\right] \\ & * \frac{1}{p^2\pi^2 + L^2\Gamma_{mn}^2}\left\{\Gamma_{mn}L\left(k^2 - \left(\frac{p\pi}{L}\right)^2\right)\delta_{pq}\right. \\ & \left. + pq\pi^2\frac{\Gamma_{mn}^2 + k^2}{\pi^2 q^2 + L^2\Gamma_{mn}^2}\left(1 - ((-1)^q + (-1)^p)e^{-\Gamma_{mn}L} + (-1)^{p+q}\right)\right\} \\ & + \frac{jL^2}{2ab\omega\mu}\sum_{n=0}^{\infty}\frac{\epsilon_{0n}}{\Gamma_{0n}}\frac{1}{p^2\pi^2 + L^2\Gamma_{0n}^2}\left\{\Gamma_{0n}L\left(k^2 - \left(\frac{p\pi}{L}\right)^2\right)\delta_{pq}\right. \\ & \left. + pq\pi^2\frac{\Gamma_{0n}^2 + k^2}{\pi^2 q^2 + L^2\Gamma_{0n}^2}\left(1 - ((-1)^q + (-1)^p)e^{-\Gamma_{0n}L} + (-1)^{p+q}\right)\right\}\end{aligned} \tag{3.48.4}$$

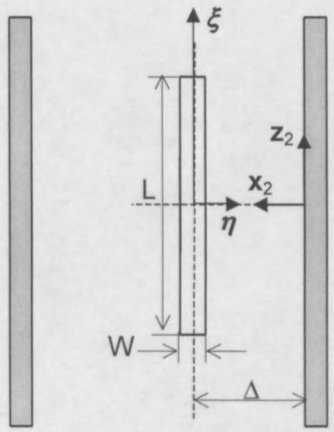

Figure 3.4: Top view of the longitudinal slot.

The s-parameters for the longitudinal slot can be obtained by substituting

$$\theta = 0°$$
$$x = \Delta - \eta$$
$$z = \xi$$

into (3.47) which are the equations for the scattering parameters for the general slot. Only the final equations are given here:

$$S_{11} = \frac{j}{W\sqrt{abkZ_0\beta_{10}}}\cos\left[\frac{\pi\Delta}{a}\right]\sin\left[\frac{\pi W}{2a}\right]e^{\Gamma_{10}z_i} * \sum_{p=1}^{N} A_p \frac{\pi p L}{\pi^2 p^2 + L^2\Gamma_{10}^2}\left(e^{\frac{L}{2}\Gamma_{10}} - (-1)^p e^{-\frac{L}{2}\Gamma_{10}}\right) \tag{3.49.1}$$

$$S_{21} = e^{-\Gamma_{10}(z_2 - z_i)} - \frac{j}{W\sqrt{abkZ_0\beta_{10}}}\cos\left[\frac{\pi\Delta}{a}\right]\sin\left[\frac{\pi W}{2a}\right]e^{-\Gamma_{10}z_2} * \sum_{p=1}^{N} A_p \frac{L\pi p}{\pi^2 p^2 + L^2\Gamma_{10}^2}\left(e^{-\frac{L}{2}\Gamma_{10}} - (-1)^p e^{\frac{L}{2}\Gamma_{10}}\right) \tag{3.49.2}$$

$$S_{31} = \frac{j}{W\sqrt{abkZ_0\beta_{10}}}\cos\left[\frac{\pi\Delta}{a}\right]\sin\left[\frac{\pi W}{2a}\right]e^{-\Gamma_{10}z_3} * \sum_{p=1}^{N} B_p \frac{L\pi p}{\pi^2 p^2 + L^2\Gamma_{10}^2}\left(e^{-\frac{L}{2}\Gamma_{10}} - (-1)^p e^{\frac{L}{2}\Gamma_{10}}\right) \tag{3.49.3}$$

$$S_{41} = -\frac{j}{W\sqrt{abkZ_0\beta_{10}}}\,\mathrm{Cos}\left[\frac{\pi\Delta}{a}\right]\mathrm{Sin}\left[\frac{\pi W}{2a}\right]e^{\Gamma_{10}z_4}$$
$$*\sum_{p=1}^{N} B_p \frac{\pi p L}{\pi^2 p^2 + L^2\Gamma_{10}^2}\left\{e^{\frac{L}{2}\Gamma_{10}} - (-1)^p e^{-\frac{L}{2}\Gamma_{10}}\right\} \qquad (3.49.4)$$

The equations for the longitudinal slot were implemented in Matlab. To verify that they are correct, two comparisons were carried out, the details of which are summarised in Table 3.3.

Slot 1 was simulated using Maxwell Eminence by Ansoft, a commercial Finite Element Method software package. The comparison between the Maxwell and Matlab simulations are shown in Figure 3.5. For Slot 2 the magnitude of S_{31} was compared with a published result [Sinha 1987, Figure 4] as shown in Figure 3.6. In both the Matlab implementations 10 basis functions were used to approximate the magnetic current and the double infinite sums were truncated to 3192 *mn*-modes. (The reasons for these choices are discussed in Section 3.8.)

Parameter	Symbol	Slot 1	Slot 2
Waveguide width	a	22.86 mm	22.86 mm
Waveguide height	b	10.16 mm	10.16 mm
Slot offset	Δ	2.5 mm	1.4224 mm
Slot length	L	13 mm	4 – 48 mm
Slot width	W	0.5 mm	1.5875 mm
Slot thickness	T	2.54 mm	1.58 mm
Distance from slot centre to ports	$-z_1$, z_2, z_3, $-z_4$	50 mm	50 mm
Frequency	f	8 – 12 GHz	9.26 GHz

Table 3.3: Waveguide and slot dimensions of the longitudinal test slots used for comparison between the Matlab code, a Maxwell simulation and a published result.

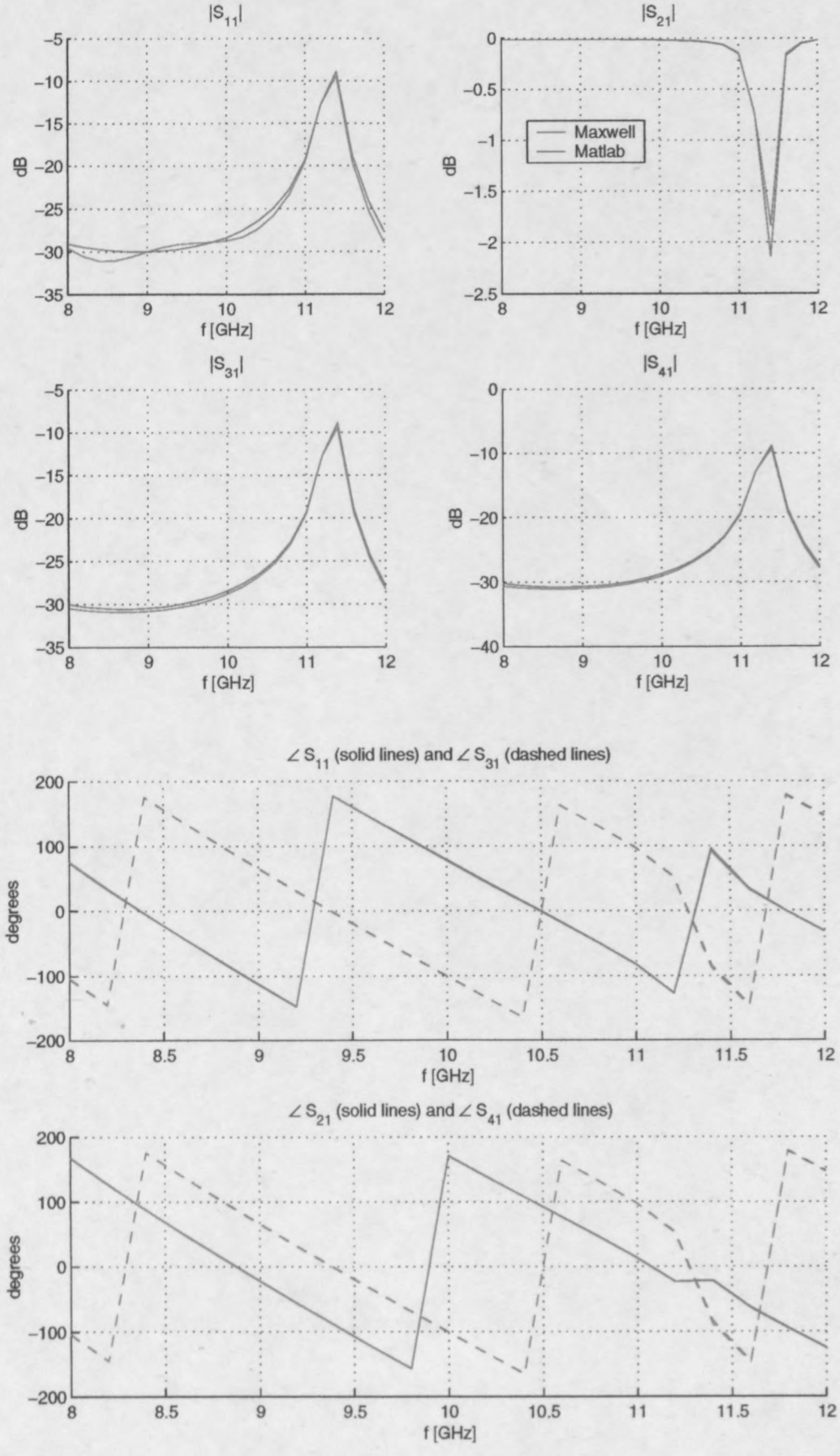

Figure 3.5: Scattering parameters for Slot 1 with dimensions L = 13 mm, W = 0.5 mm, Δ = 2.5 mm and T = 2.54 mm. The blue lines represent the Matlab simulation based on the equations derived in this chapter, and the red lines represent the Maxwell simulation.

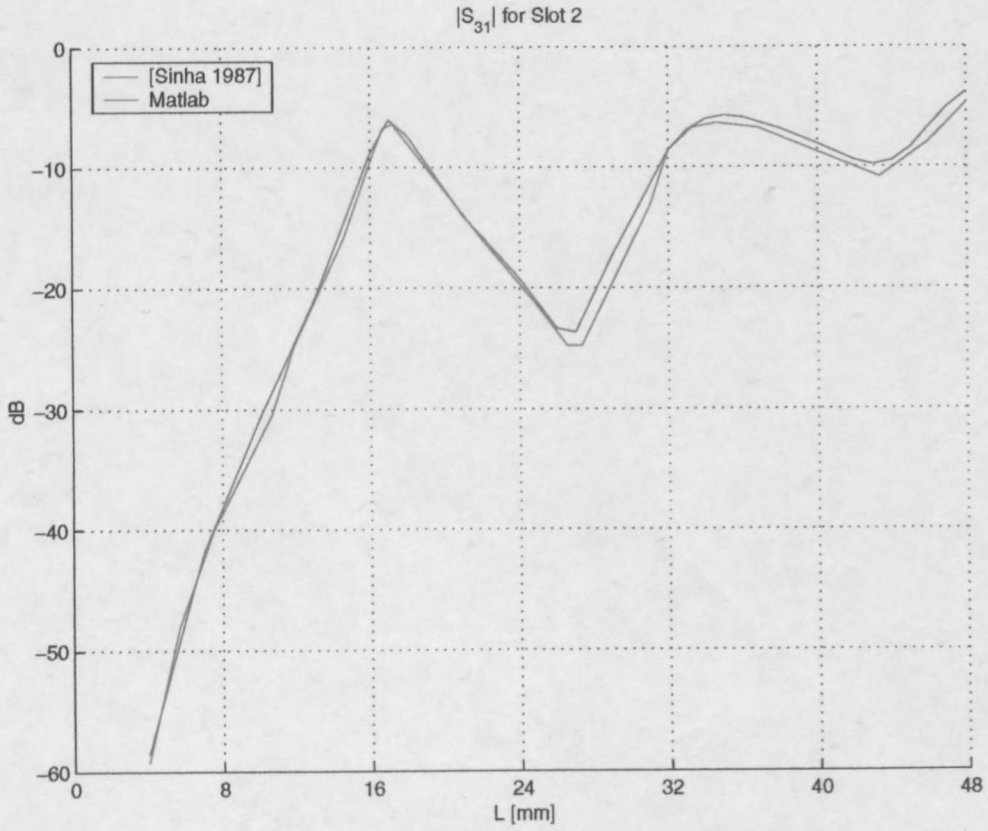

Figure 3.6: The magnitude of S_{31} for a longitudinal slot with W = 1.5875 mm, Δ = 1.4224 mm, T = 1.58 mm and f = 9.26 GHz. The result of the Matlab simulation is compared with Figure 4 from [Sinha 1987].

3.7 Solution for a transverse slot

To solve the matrix elements for the transverse slot shown in Figure 3.7, it was necessary to set $\theta = 90°$ in the equations for the general slot. The calculations are carried out in Appendix D. The matrix components for the transverse slot are:

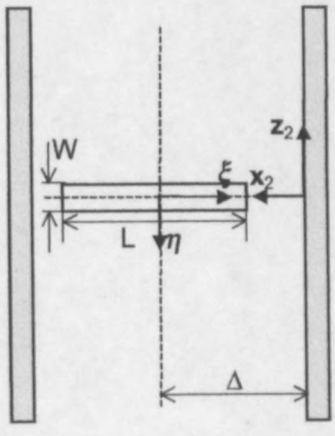

Figure 3.7: Top view of the transverse slot.

$$[H]_q = \frac{4}{\Gamma_{10}} \frac{L}{W} \sqrt{\frac{\beta_{10}}{abkZ_0}} \, \text{Sinh}\left[\frac{W}{2}\Gamma_{10}\right] e^{\Gamma_{10} z_i}$$

$$* \begin{cases} \frac{a}{\pi(a^2 q^2 - L^2)} \left((L + aq)\,\text{Cos}\left[\frac{\pi q}{2} + \frac{\pi \Delta}{a}\right] \text{Sin}\left[\frac{\pi q}{2} - \frac{\pi L}{2a}\right] \right. \\ \qquad \left. + (L - aq)\,\text{Cos}\left[\frac{\pi q}{2} - \frac{\pi \Delta}{a}\right] \text{Sin}\left[\frac{\pi q}{2} + \frac{\pi L}{2a}\right] \right), & L \neq aq \\ \frac{1}{2}\,\text{Cos}\left[\frac{q\pi}{2} + \frac{\pi \Delta}{a}\right], & L = aq \end{cases} \tag{3.50.1}$$

$$[Y_2^{32}]_{qp} = [Y_1^{31}]_{qp} = -\frac{jkL}{2WZ_0}\left(1 - \left(\frac{p\pi}{kL}\right)^2\right) \frac{\text{Cos}[k_{zp} T]}{k_{zp}\,\text{Sin}[k_{zp} T]} \delta_{pq} \tag{3.50.2}$$

$$[Y_1^{32}]_{qp} = [Y_2^{31}]_{qp} = \frac{jkL}{2WZ_0}\left(1 - \left(\frac{p\pi}{kL}\right)^2\right) \frac{1}{k_{zp}\,\text{Sin}[k_{zp} T]} \delta_{pq} \tag{3.50.3}$$

$$[Y_1^{11}]_{qp} = [Y_2^{22}]_{qp} = \frac{jL^2}{W^2 ab\omega\mu} \sum_{m=0}^{\infty} \sum_{n=0}^{\infty} \frac{\epsilon_{0m}\epsilon_{0n}}{\Gamma_{mn}^2} \left(k^2 - \left(\frac{m\pi}{a}\right)^2\right) \sigma(p)\,\sigma(q)$$

$$* \left\{ W - \frac{2}{\Gamma_{mn}} e^{-\frac{W}{2}\Gamma_{mn}} \text{Sinh}\left[\frac{W}{2}\Gamma_{mn}\right] \right\} \tag{3.50.4}$$

where:

$$\sigma(p) = \begin{cases} \frac{a}{\pi(a^2 p^2 - L^2 m^2)} \left((Lm + ap)\,\text{Cos}\left[\frac{\pi p}{2} + \frac{m\pi\Delta}{a}\right] \text{Sin}\left[\frac{\pi p}{2} - \frac{m\pi L}{2a}\right] \right. \\ \qquad \left. + (Lm - ap)\,\text{Cos}\left[\frac{\pi p}{2} - \frac{m\pi\Delta}{a}\right] \text{Sin}\left[\frac{\pi p}{2} + \frac{m\pi L}{2a}\right] \right), & Lm \neq ap \\ \frac{1}{2}\,\text{Cos}\left[\frac{p\pi}{2} + \frac{m\pi\Delta}{a}\right], & Lm = ap \end{cases}$$

The s-parameters for the transverse slot can be obtained by substituting

$$\theta = 90°$$
$$x = \Delta - \xi$$
$$z = -\eta$$

into (3.47) which are the equations for the scattering parameters for the general slot. The resulting equations are:

$$S_{11} = -\frac{jL}{W\sqrt{abkZ_0\beta_{10}}} \, \text{Sinh}\left[\frac{W}{2}\Gamma_{10}\right] e^{\Gamma_{10} z_i}$$

$$* \sum_{p=1}^{N} A_p \begin{cases} \frac{a}{\pi(ap - L)(ap + L)} \left((ap + L)\,\text{Cos}\left[\frac{p\pi}{2} + \frac{\pi\Delta}{a}\right] \text{Sin}\left[\frac{p\pi}{2} - \frac{L\pi}{2a}\right] \right. \\ \qquad \left. - (ap - L)\,\text{Cos}\left[\frac{p\pi}{2} - \frac{\pi\Delta}{a}\right] \text{Sin}\left[\frac{p\pi}{2} + \frac{L\pi}{2a}\right] \right), & L \neq ap \\ \frac{1}{2}\,\text{Cos}\left[\frac{p\pi}{2} + \frac{\pi\Delta}{a}\right], & L = ap \end{cases} \tag{3.51.1}$$

$$S_{21} = e^{-\Gamma_{10}(z_2 - z_i)} + \frac{jL}{W\sqrt{abkZ_0\beta_{10}}}\,\mathrm{Sinh}\left[\frac{W}{2}\Gamma_{10}\right]e^{-\Gamma_{10}z_2}$$

$$* \sum_{p=1}^{N} A_p \begin{cases} \dfrac{a}{\pi(ap-L)(ap+L)}\left((ap+L)\,\mathrm{Cos}\left[\dfrac{p\pi}{2}+\dfrac{\pi\Delta}{a}\right]\mathrm{Sin}\left[\dfrac{p\pi}{2}-\dfrac{L\pi}{2a}\right]\right. \\ \qquad \left. -(ap-L)\,\mathrm{Cos}\left[\dfrac{p\pi}{2}-\dfrac{\pi\Delta}{a}\right]\mathrm{Sin}\left[\dfrac{p\pi}{2}+\dfrac{L\pi}{2a}\right]\right), & L \neq ap \\ \dfrac{1}{2}\,\mathrm{Cos}\left[\dfrac{p\pi}{2}+\dfrac{\pi\Delta}{a}\right], & L = ap \end{cases} \qquad (3.51.2)$$

$$S_{31} = -\frac{jL}{W\sqrt{abkZ_0\beta_{10}}}\,\mathrm{Sinh}\left[\frac{W}{2}\Gamma_{10}\right]e^{-\Gamma_{10}z_3}$$

$$* \sum_{p=1}^{N} B_p \begin{cases} \dfrac{a}{\pi(ap-L)(ap+L)}\left((ap+L)\,\mathrm{Cos}\left[\dfrac{p\pi}{2}+\dfrac{\pi\Delta}{a}\right]\mathrm{Sin}\left[\dfrac{p\pi}{2}-\dfrac{L\pi}{2a}\right]\right. \\ \qquad \left. -(ap-L)\,\mathrm{Cos}\left[\dfrac{p\pi}{2}-\dfrac{\pi\Delta}{a}\right]\mathrm{Sin}\left[\dfrac{p\pi}{2}+\dfrac{L\pi}{2a}\right]\right), & L \neq ap \\ \dfrac{1}{2}\,\mathrm{Cos}\left[\dfrac{p\pi}{2}+\dfrac{\pi\Delta}{a}\right], & L = ap \end{cases} \qquad (3.51.3)$$

$$S_{41} = \frac{jL}{W\sqrt{abkZ_0\beta_{10}}}\,\mathrm{Sinh}\left[\frac{W}{2}\Gamma_{10}\right]e^{\Gamma_{10}z_4}$$

$$* \sum_{p=1}^{N} B_p \begin{cases} \dfrac{a}{\pi(ap-L)(ap+L)}\left((ap+L)\,\mathrm{Cos}\left[\dfrac{p\pi}{2}+\dfrac{\pi\Delta}{a}\right]\mathrm{Sin}\left[\dfrac{p\pi}{2}-\dfrac{L\pi}{2a}\right]\right. \\ \qquad \left. -(ap-L)\,\mathrm{Cos}\left[\dfrac{p\pi}{2}-\dfrac{\pi\Delta}{a}\right]\mathrm{Sin}\left[\dfrac{p\pi}{2}+\dfrac{L\pi}{2a}\right]\right), & L \neq ap \\ \dfrac{1}{2}\,\mathrm{Cos}\left[\dfrac{p\pi}{2}+\dfrac{\pi\Delta}{a}\right], & L = ap \end{cases} \qquad (3.51.4)$$

As in the case of the longitudinal slot, the equations for the transverse slot were implemented in Matlab and compared with results from Maxwell and from a published paper. The details of the two comparisons are given in Table 3.4. Figure 3.8 shows the comparison between Matlab and Maxwell for Slot 1, and Figure 3.9 shows the comparison of the Matlab results for Slot 2 with Figure 2(b) from [Datta 1995]. Again, 10 basis functions were used to approximate the magnetic current and the double infinite sums were truncated to 3192 *mn*-modes.

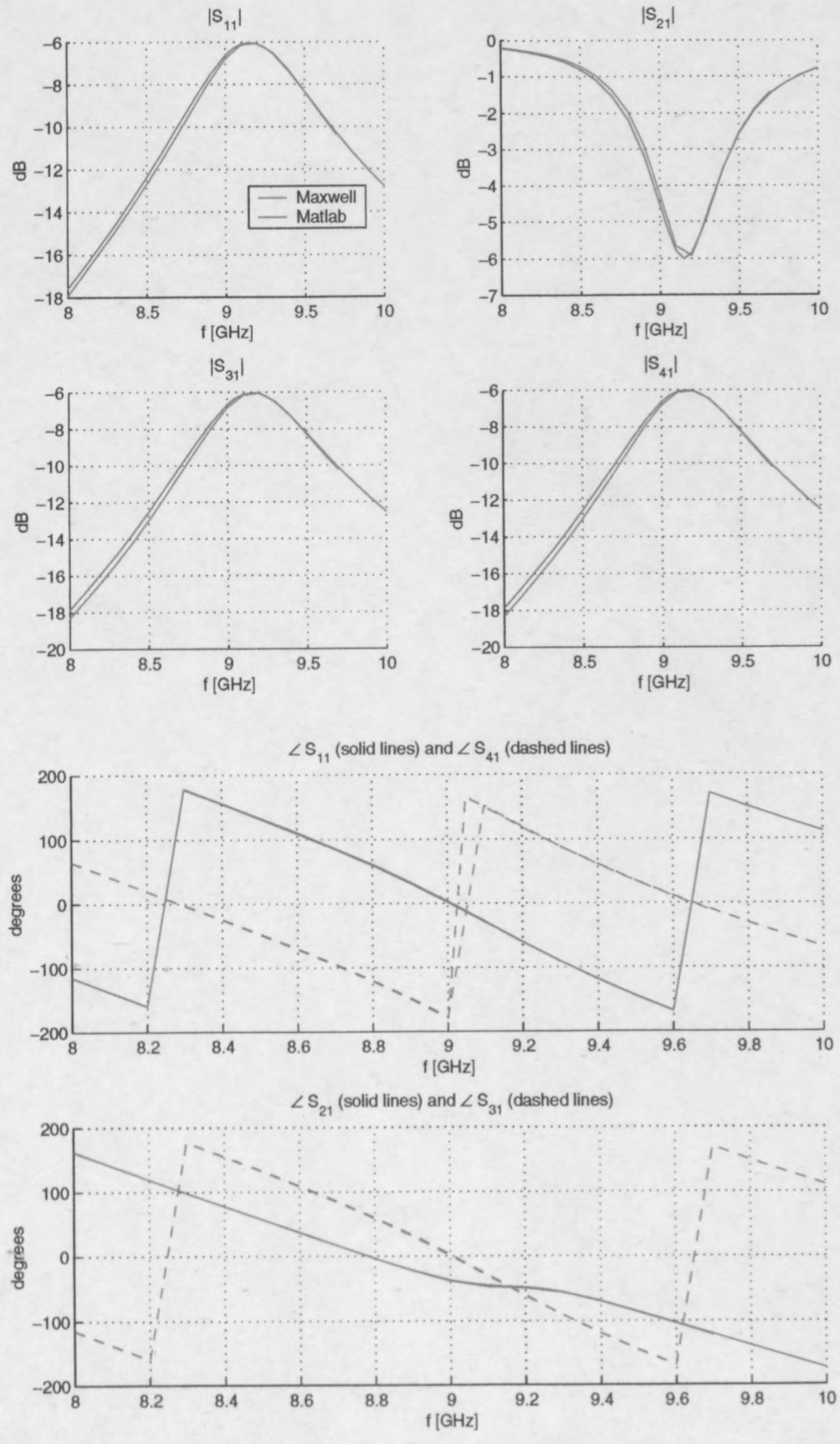

Figure 3.8: Scattering parameters for Slot 1 which is a centred transverse slot with dimensions L = 16 mm, W = 1 mm and T = 2 mm. The blue lines represent the Matlab simulation and the red lines the Maxwell simulation.

Parameter	Symbol	Slot 1	Slot 2
Waveguide width	a	22.86 mm	22.86 mm
Waveguide height	b	10.16 mm	10.16 mm
Slot offset	Δ	11.43 mm	11.43 mm
Slot length	L	16 mm	4–22 mm
Slot width	W	1 mm	1.5875 mm
Slot thickness	T	2 mm	1.58 mm
Distance from slot centre to ports	$-z_i$, z_2, z_3, $-z_4$	50 mm	50 mm
Frequency	f	8-10 GHz	9.375 GHz

Table 3.4: Waveguide and slot dimensions of the transverse test slots used for comparison between the Matlab code, a Maxwell simulation and a published result.

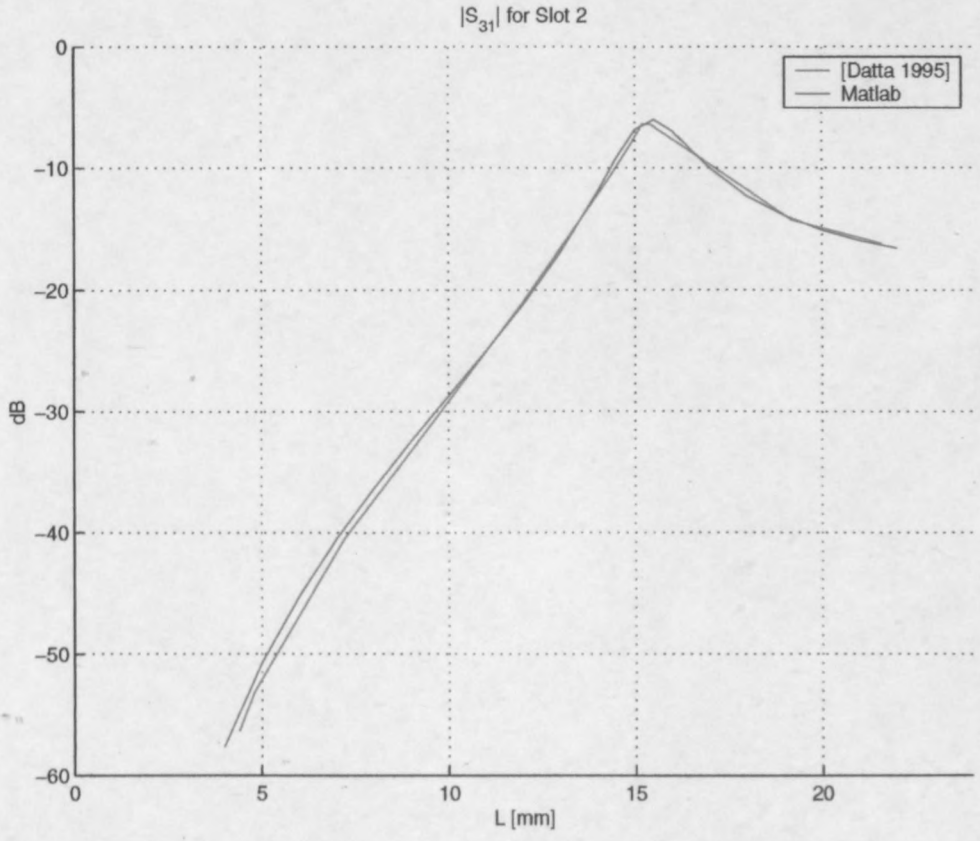

Figure 3.9: The magnitude of S_{31} for a centred transverse slot with W = 1.5875 mm, T = 1.58 mm and f = 9.375 GHz. The result of the Matlab simulation is compared with Figure 2(b) from [Datta 1995].

3.8 Implementation issues

The equations derived in Section 3.6 for the longitudinal slot were implemented in Matlab to generate training data for the neural networks. Two approximations arose from the numerical implementation. They are a consequence of the limited number of basis functions and the truncation of the infinite summations.

The number of basis functions N determines the accuracy of the field approximation. Large values of N, however, lead to large matrices. In the literature as little as one global sinusoidal basis function has been used for a radiating slot [Lyon 1981]. Datta et al. [Datta 1995] used three basis functions for waveguide coupling and Rengarajan used ten [Rengarajan 1989-2], the last shown to be accurate to within manufacturing tolerances. Therefore ten basis functions were considered to ensure accuracy without being too time-consuming.

The double infinite summations in the equations had to be truncated for the computer implementation. The double summations over the modes are slowly convergent and have been expressed in terms of rapidly converging series based on their asymptotic behaviour by some authors [Rengarajan 1989-2]. According to Lyon and Sangster, at least 2500 modes are necessary for the waveguide Green's function to converge [Lyon 1981]. Datta et al. also used 2500 modes (50 m-modes and 50 n-modes) [Datta 1995]. For this implementation, 3192 modes were used. Truncating the summation over m at $m = 83$ and the summation over n at $n = 37$ includes at least the first 2500 waveguide modes, as well as a few higher modes. It was confirmed that the solution converged sufficiently at this point and these values were used for all the simulations.

Further implementation details are discussed in the next chapter.

3.9 Extending the solution to crossed waveguides

Although not specifically relevant to the current application, the formulation can be extended to inclined waveguides with little effort. A short summary is presented here for the sake of completeness. For a crossed waveguide coupler like that shown in Figure 3.10, the only change in the equations is the coordinate system of the secondary waveguide. The new coordinate transformations are shown in Table 3.5.

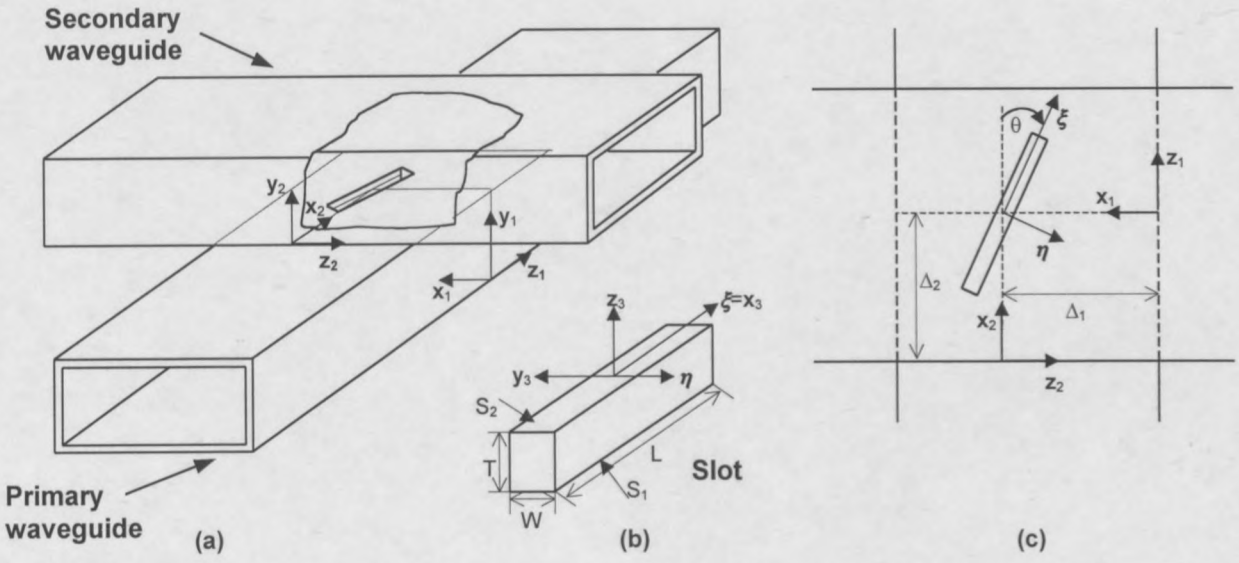

Figure 3.10: Crossed waveguides coupled by a single inclined slot. (a) Cut-away view of the waveguide intersection. (b) The slot coordinate system and dimensions. (c) Top view of the common waveguide wall .

The incident field component and $\left[\mathbf{Y}_1^{11}\right]$ remain unchanged, because they involve only the primary waveguide, and the components relating to coupling through the slot remain unchanged because they involve only the coordinates of the slot. The only component that will be different, is $\left[\mathbf{Y}_2^{22}\right]$. The equation for $\left[\mathbf{Y}_2^{22}\right]$ is given in (3.10.6):

$$[Y_2^{22}]_{qp} = -\int_{S_2} \mathbf{f}_q(\mathbf{r}) \cdot \mathbf{H}_t(f_p(\mathbf{r}'))^{(2)} \, dS \tag{3.52}$$

Once again only the ξ-component of $\mathbf{H}$ is required, and this time coordinate transformations from Table 3.5 give:

$$\begin{aligned} H_\xi(M_\xi \xi(\mathbf{r}')) &= \mathrm{Cos}[\theta] H_{x_2}(M_\xi \xi(\mathbf{r}')) + \mathrm{Sin}[\theta] H_{z_2}(M_\xi \xi(\mathbf{r}')) \\ \Rightarrow H_\xi(M_\xi \xi(\mathbf{r}')) &= [\mathrm{Cos}[\theta] \quad \mathrm{Sin}[\theta]] \begin{bmatrix} H_{x_2}(M_\xi \xi(\mathbf{r}')) \\ H_{z_2}(M_\xi \xi(\mathbf{r}')) \end{bmatrix} \end{aligned} \tag{3.53}$$

The components of $\mathbf{H}$ on the right-hand side of (3.53) can again be expanded using (3.20). The result is the same as that found previously in (3.34), if all coordinate variables are taken to refer to the secondary waveguide coordinate system. Thus:

$$\begin{bmatrix} H_{x_2}(M_\xi \xi(\mathbf{r}')) \\ H_{y_2}(M_\xi \xi(\mathbf{r}')) \end{bmatrix} = -\frac{j}{\omega \mu \epsilon} \begin{bmatrix} \frac{\partial^2}{\partial x_2^2} + k^2 & \frac{\partial^2}{\partial z_2 \partial x_2} \\ \frac{\partial^2}{\partial z_2 \partial x_2} & \frac{\partial^2}{\partial z_2^2} + k^2 \end{bmatrix} \begin{bmatrix} F_{x_2}(M_\xi \xi(\mathbf{r}')) \\ F_{z_2}(M_\xi \xi(\mathbf{r}')) \end{bmatrix} \tag{3.54}$$

Direction transformations (unit vectors)	Position coordinate transformations (scalars)
$\mathbf{x_1} = -\mathbf{z_2} = -\mathrm{Sin}[\theta]\,\xi - \mathrm{Cos}[\theta]\,\eta$	$x_1 = -\mathrm{Sin}[\theta]\,\xi - \mathrm{Cos}[\theta]\,\eta + \Delta_1$ $x_2 = \mathrm{Cos}[\theta]\,\xi - \mathrm{Sin}[\theta]\,\eta + \Delta_2$
$\mathbf{y_1} = \mathbf{y_2} = \mathbf{z_3}$	$y_1 = y_2 + b + T = z_3 + b + T$
$\mathbf{z_1} = \mathbf{x_2} = \mathrm{Cos}[\theta]\,\xi - \mathrm{Sin}[\theta]\,\eta$	$z_1 = \mathrm{Cos}[\theta]\,\xi - \mathrm{Sin}[\theta]\,\eta$ $z_2 = \mathrm{Sin}[\theta]\,\xi + \mathrm{Cos}[\theta]\,\eta$
$\xi = \mathbf{x_3} = -\mathrm{Sin}[\theta]\,\mathbf{x_1} + \mathrm{Cos}[\theta]\,\mathbf{z_1}$ $= \mathrm{Cos}[\theta]\,\mathbf{x_2} + \mathrm{Sin}[\theta]\,\mathbf{z_2}$	$\xi = x_3 = -\mathrm{Sin}[\theta]\,(x_1 - \Delta_1) + \mathrm{Cos}[\theta]\,z_1$ $= \mathrm{Cos}[\theta]\,(x_2 - \Delta_2) + \mathrm{Sin}[\theta]\,z_2$
$\eta = -\mathbf{y_3} = -\mathrm{Cos}[\theta]\,\mathbf{x_1} - \mathrm{Sin}[\theta]\,\mathbf{z_1}$ $= -\mathrm{Sin}[\theta]\,\mathbf{x_2} + \mathrm{Cos}[\theta]\,\mathbf{z_2}$	$\eta = -y_3 = -\mathrm{Cos}[\theta]\,(x_1 - \Delta_1) - \mathrm{Sin}[\theta]\,z_1$ $= -\mathrm{Sin}[\theta]\,(x_2 - \Delta_2) + \mathrm{Cos}[\theta]\,z_2$

Table 3.5: Coordinate relationships for the crossed waveguide coupler of Figure 3.10.

Again the right-hand side components can be expanded, using (3.22) as well as coordinate transformations from Table 3.5:

$$\begin{aligned}\mathbf{F}(M_\xi \xi(\mathbf{r}')) &= \epsilon \int_S M_\xi(\mathbf{r}')\,\xi \cdot \mathbf{G}^{FM}(\mathbf{r}, \mathbf{r}')\,dS' \\ &= \epsilon \int_S M_\xi(\mathbf{r}')\,(\mathrm{Cos}[\theta]\,\mathbf{x}_2 + \mathrm{Sin}[\theta]\,\mathbf{z}_2) \cdot \left(G_{xx}^{FM}(\mathbf{r}, \mathbf{r}')\,\mathbf{xx} + G_{yy}^{FM}(\mathbf{r}, \mathbf{r}')\,\mathbf{yy} \right. \\ &\qquad \left. + G_{zz}^{FM}(\mathbf{r}, \mathbf{r}')\,\mathbf{zz}\right) dS' \\ \Rightarrow F_{x_2}(M_\xi \xi(\mathbf{r}')) &= \epsilon\,\mathrm{Cos}[\theta] \int_S M_\xi(\mathbf{r}')\,G_{xx}^{FM}(\mathbf{r}, \mathbf{r}')\,dS' \\ \text{and } F_{z_2}(M_\xi \xi(\mathbf{r}')) &= \epsilon\,\mathrm{Sin}[\theta] \int_S M_\xi(\mathbf{r}')\,G_{zz}^{FM}(\mathbf{r}, \mathbf{r}')\,dS' \end{aligned} \tag{3.55}$$

Substituting the results from (3.55) into (3.54) and then back into (3.53) leads to a compact expression for H_ξ:

$$H_\xi(M_\xi \xi(\mathbf{r}')) = -\frac{j}{\omega\mu}[\mathrm{Cos}[\theta] + \mathrm{Sin}[\theta]]\begin{bmatrix} \frac{\partial^2}{\partial x_2^2} + k^2 & \frac{\partial^2}{\partial z_2 \partial x_2} \\ \frac{\partial^2}{\partial z_2 \partial x_2} & \frac{\partial^2}{\partial z_2^2} + k^2 \end{bmatrix}\begin{bmatrix} \mathrm{Cos}[\theta]\int_S M_\xi(\mathbf{r}')\, G_{xx}^{FM}(\mathbf{r}, \mathbf{r}')\, dS' \\ \mathrm{Sin}[\theta]\int_S M_\xi(\mathbf{r}')\, G_{zz}^{FM}(\mathbf{r}, \mathbf{r}')\, dS' \end{bmatrix}$$

$$\Rightarrow H_\xi(\mathbf{f}_p(\mathbf{r}')) = -\frac{j}{\omega\mu}[\mathrm{Cos}[\theta] + \mathrm{Sin}[\theta]]\begin{bmatrix} \frac{\partial^2}{\partial x_2^2} + k^2 & \frac{\partial^2}{\partial z_2 \partial x_2} \\ \frac{\partial^2}{\partial z_2 \partial x_2} & \frac{\partial^2}{\partial z_2^2} + k^2 \end{bmatrix}\begin{bmatrix} \mathrm{Cos}[\theta]\int_S f_p(\mathbf{r}')\, G_{xx}^{FM}(\mathbf{r}, \mathbf{r}')\, dS' \\ \mathrm{Sin}[\theta]\int_S f_p(\mathbf{r}')\, G_{zz}^{FM}(\mathbf{r}, \mathbf{r}')\, dS' \end{bmatrix} \tag{3.56}$$

Substituting (3.56) into (3.10.6) gives:

$$[Y_2^{22}]_{qp} = \frac{j}{\omega\mu}\frac{1}{W}\int_{S_2} \mathrm{Sin}\left[\frac{p\pi}{L}\left(\xi + \frac{L}{2}\right)\right][\mathrm{Cos}[\theta] + \mathrm{Sin}[\theta]]$$

$$* \begin{bmatrix} \frac{\partial^2}{\partial x_2^2} + k^2 & \frac{\partial^2}{\partial z_2 \partial x_2} \\ \frac{\partial^2}{\partial z_2 \partial x_2} & \frac{\partial^2}{\partial z_2^2} + k^2 \end{bmatrix}\begin{bmatrix} \mathrm{Cos}[\theta]\int_{S_2} f_p(\mathbf{r}')\, G_{xx}^{FM}(\mathbf{r}, \mathbf{r}')\, dS' \\ \mathrm{Sin}[\theta]\int_{S_2} f_p(\mathbf{r}')\, G_{zz}^{FM}(\mathbf{r}, \mathbf{r}')\, dS' \end{bmatrix} dS \tag{3.57}$$

Equation (3.57) can be evaluated to complete the matrix elements for the crossed waveguide coupler.

Chapter 4
Implementation and results

The development of a neural network model to solve the longitudinal slot problem is described in detail in the first part of this chapter. The design decisions and development iterations are presented chronologically to demonstrate how the network evolved. In the second part of the chapter, the neural network technique is compared to an Adaptive Sampling Interpolation (ASI) Technique.

4.1 Development of a neural network model

The design of a neural network can be divided into two parts. The first part constitutes the preliminary decisions about the training parameters, as summarised in Section 2.4. The second part is the iterative design procedure to experiment with different networks and find the best one. These two parts will be dealt with systematically, starting with the preliminary design decisions.

4.1.1 Variables

In order to keep the model relatively simple, only three input variables were chosen, namely the frequency (f), the length of the slot (L) and the offset of the slot from the side of the waveguide (Δ), as defined in Figure 3.4. All other parameters were kept constant. Each input variable was assigned one node. The variable ranges are shown in Table 4.1 together with the constant values of the other dimensions. The variable ranges were chosen to be identical to that used by Lehmensiek [Lehmensiek 2001] for later comparison.

The width of the slot was kept constant at 0.5 mm and standard X-band waveguide dimensions were used. The distance between the slot centre and the ports at which the s-parameters were determined had to be large enough to ensure that the ports did not coincide with the slot. This

Input parameter	Symbol	Minimum value	Maximum value
Frequency	f	8 GHz	12 GHz
Slot length	L	3.5 mm	10 mm
Offset	Δ	1 mm	11 mm
		Constant value	
Slot width	W	0.5 mm	
Slot thickness	T	2.54 mm	
Waveguide width	a	22.86 mm	
Waveguide height	b	10.16 mm	
Distance to ports	$z_{1,2,3,4}$	50 mm	

Table 4.1: Input parameter ranges and constant values for the longitudinal slot.

distance influences the phase of the s-parameters, but not the magnitude. Because of the relationship between phase and wavelength, if the port is further from the excitation, the phase changes more with respect to frequency. The distance was fixed at 50 mm.

The output variables had to represent the scattering parameters of the system. It has already been shown that four scattering parameters are necessary to define the system, each with a real and imaginary part. This called for eight output variables to the network. An example slot was chosen to examine the behaviour of the s-parameters in magnitude/phase form and in real/imaginary form. In Figure 4.1, S_{11} is shown for a test slot with length 5 mm and offset 3 mm. It can be seen from the figure that modelling the magnitude and phase would be simpler

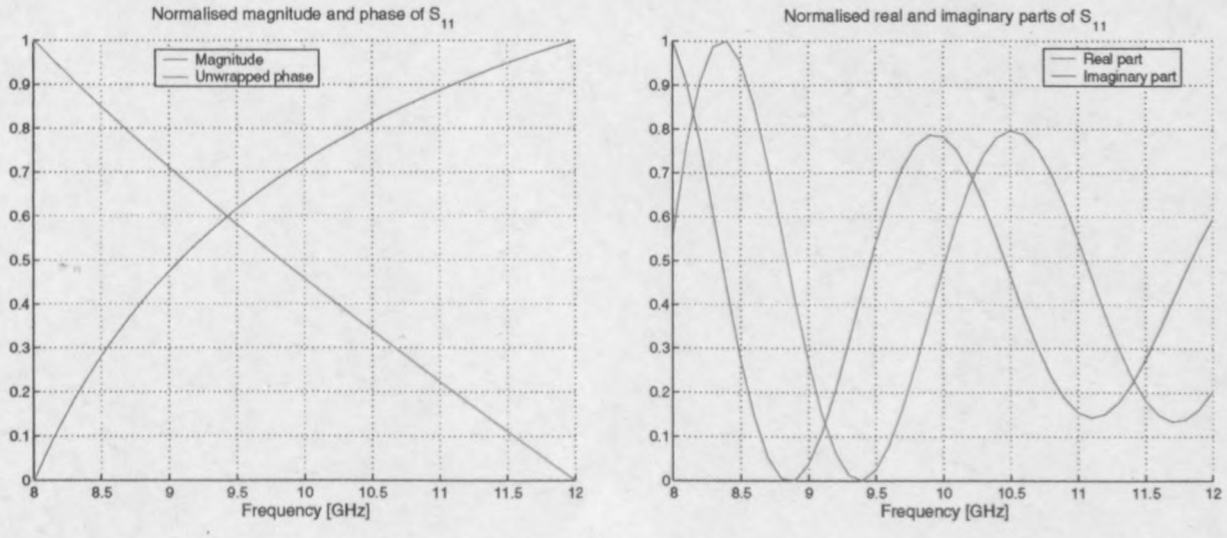

Figure 4.1: The difference between the magnitude-phase and the real-imaginary representation of S_{11} for a slot with L = 5 mm and Δ = 3 mm. The values are normalised to a maximum value of 1.

than modelling the real and imaginary parts. The behaviour of the other s-parameters was similar. In addition, since the sudden jumps in the wrapped phase angles would make the response more unpredictable and therefore make accurate modelling more difficult, the phase angles were unwrapped before they were presented to the network.

It was noted that several of the output variables were so similar that they could be considered equal for modelling purposes. After comparing the s-parameters of a hundred different slots over frequency, the following equations could be formulated:

$$\angle S_{11} \approx \angle S_{21} - 90° \approx \angle S_{31} + 180° \approx \angle S_{41} + 180° \tag{4.1.1}$$

$$|S_{31}| \approx |S_{41}| \tag{4.1.2}$$

where '≈' means closer than 0.62° for the angles, and closer than 0.37 dB for the magnitudes. These equations are not valid for a general coupling slot, but arose for this specific case because the small range chosen for the various slot parameters lead to a structure that was approximately symmetrical. The output variables were therefore set to:

$$|S_{11}| \quad \angle S_{11} \quad |S_{21}| \quad |S_{31}|$$

with the magnitudes in dB and the angle in degrees. Both input and output variables were linearly normalised to the range [0.1, 0.9] before presenting them to the network.

4.1.2 Architecture

Because the response of the slot for the chosen set of input parameters is relatively simple, an MLP network was chosen to model the slot. MLPs are easy to use and there are many examples in the literature of successful models. MLPs also have many well-established training algorithms.

4.1.3 Training algorithm

Table 4.2 contains details of published neural network models of microwave applications. Based on the success of the backpropagation algorithm displayed in Table 4.2, it was considered the best and simplest option for this network.

A parameter required by SNNS (Stuttgart Neural Network Simulator) that is related to the choice of training algorithm, is the update function, indicating the order in which the new activations of the neurons are calculated during training. The *Topological_Order* update function was chosen because it is indicated in the SNNS manual as the most favourable mode for feedforward

Reference	Application	Network structure	Size of training set [examples]	Training parameters
Sagiroglu 1997	resonant frequency of triangular microstrip antenna	5-5-3-1	12	25 000 epochs η=3, μ=0.5
Sagiroglu 1998	resonant frequency of circular microstrip antenna	3-5-5-1	17	2.5 x 10^6 epochs η=0.08, μ=0.1
Watson 1996-1, Watson 1996-2	microstrip via	4-10-4	29 freq sweeps 6 freq points	
Watson 1999	CPW 90° bends	4-10-4	165	
		3-10-4	45	
	CPW transmission lines	3-20-2	265	
	CPW open circuit stub	3-6-4	95	
	CPW short circuit stub	3-5-4	71	
	CPW step in width	4-8-4	95	
	CPW symmetric T-junction	5-15-4	155	
Mishra 1998	square-patch antenna	3-40-1	645	η=0.002, μ=5 η adaptation=1.5
Watson 1996-2	stripline-to-stripline interconnect	3-9-4	17 freq sweeps 6 freq points	
	microstrip-to-microstrip interconnect	3-8-4	17 freq sweeps 6 freq points	
Burrascano 1998	waveguide filter	15-50-1	65 freq sweeps 300 freq points	
Fedi 1998	waveguide filter	15-11-4	70 freq sweeps 101 freq points	

Table 4.2: Examples of microwave applications of neural networks that appeared in the literature, showing the network structure in 'input-hidden-output' format, the size of the training set that was used and parameters of the training algorithm, where given. All the neural networks were trained with the backpropagation algorithm.

networks. In this mode, the outputs of the input neurons are calculated first, then that of the hidden neurons and lastly that of the output neurons.

4.1.4 Initial weight values

A built-in function of SNNS was used to initialise the weights. It is not necessary to convey any knowledge in the assignment of initial values, nor are there any specific requirements for the backpropagation algorithm and therefore a random initialisation was selected. The function *Randomize_Weights* provided distributed random values for the weights and bias in the user-specified range [-1, 1].

4.1.5 Activation functions

Since the input layer is considered only a buffer, the identity function was used as activation function for this layer, while the logistic function was chosen as the non-linear activation

Parameter	Slot 1	Slot 2	Slot 3	Slot 4	Slot 5
L [mm]	9	9	5	9	5
Δ [mm]	2	7	3	10	9

Table 4.3: Five test slots to examine the properties of the scattering parameters.

function of the hidden layer. The activation function of the output layer was not fixed. Both the identity function and the logistic function were to be investigated in the development stage.

4.1.6 Network size

To investigate the complexity of the function, the s-parameters of the five slot configurations detailed in Table 4.3 were plotted over frequency as shown in Figure 4.2. These figures

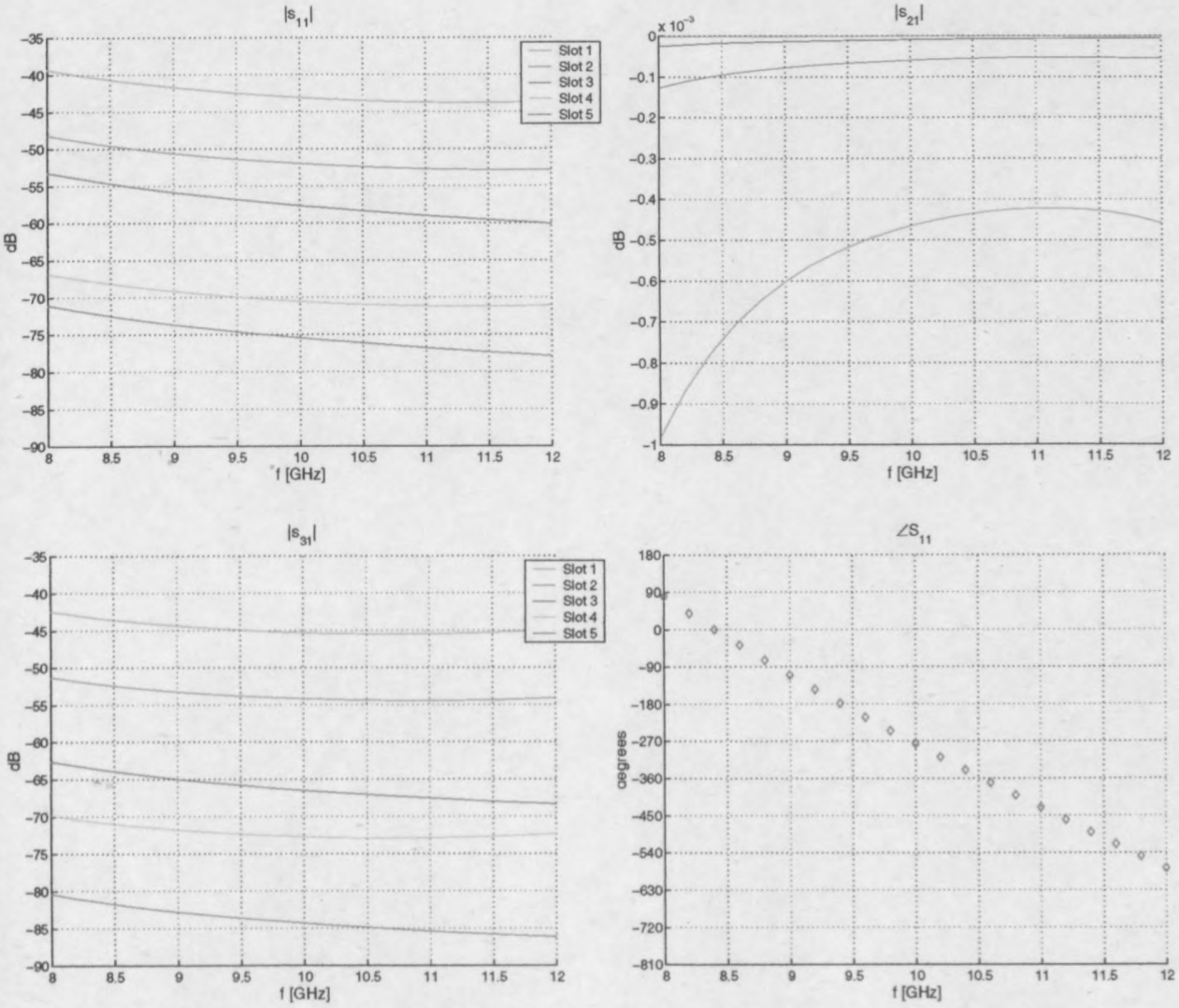

Figure 4.2: The scattering parameters for 5 test slots. The input variables for the slots are: Slot 1: L = 9 mm, Δ = 2 mm. Slot 2: L = 9 mm, Δ = 7 mm. Slot 3: L = 5 mm, Δ = 3 mm. Slot 4: L = 9 mm, Δ = 10 mm. Slot 5: L = 5 mm, Δ = 9 mm.

confirmed that the function to be mapped by the neural network was quite simple. Judging from the network sizes of the models in Table 4.2, a MLP with one hidden layer was chosen to be implemented with six different network sizes: 3-4-4, 3-5-4, 3-6-4, 3-8-4, 3-10-4 and 3-12-4, all fully connected. One of the networks is illustrated in Figure 4.3.

4.1.7 Training data

The importance of the size and composition of the training set was discussed in Section 2.3.4. It is difficult to know beforehand how much training data will be needed and the size of the set might require adjustment during the training process. Because generating training data is generally expensive, the initial training set was small and the size was to be increased if the network could not be trained successfully.

For each of the three input variables, data points were sampled uniformly over the variable range given in Table 4.1. The complete input data set comprised all possible combinations of the sampled points, filling a uniform rectangular grid in the three-dimensional input space. This complete data set was divided into a training and validation set in order to make use of early

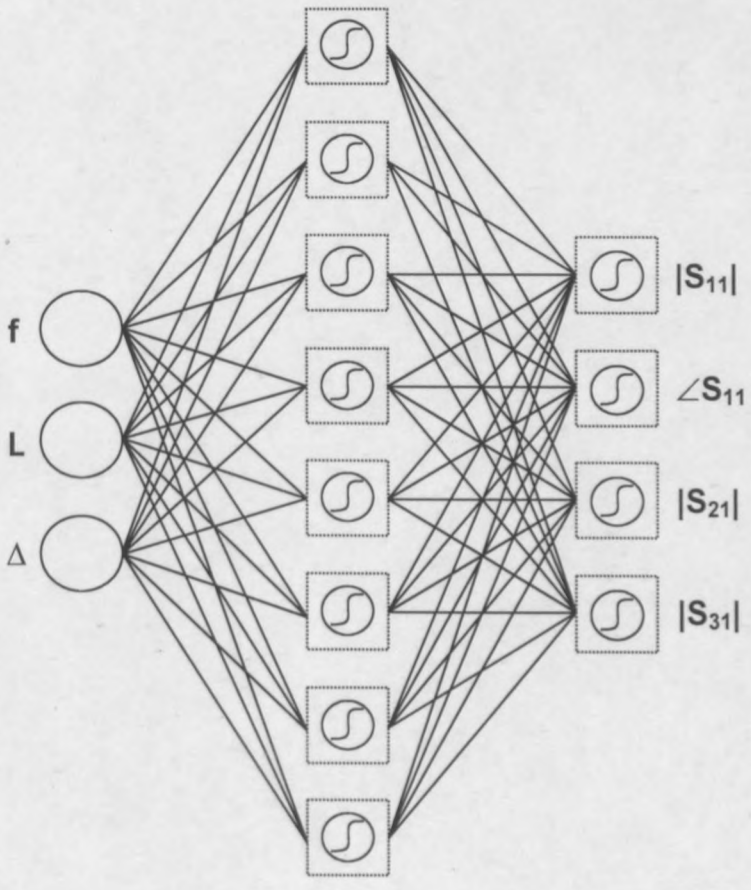

Figure 4.3: The topology of a network with eight hidden neurons.

stopping (cross-validation) as described in Section 2.3.2. An independent test set was generated after the training process had been completed to test the generalisation of the network.

4.1.8 Training process

A batch program to train the neural networks was written in the SNNS batch program language, *Batchman*. In that way, the training could be controlled without user supervision. The core of the program is described in the following paragraphs with reference to the flowchart in Figure 4.4.

In accordance with the principle of early stopping, training has to stop at the point where the validation error starts to rise (see Figure 2.9). Therefore the network is trained one epoch at a time, and after each iteration the previous lowest validation error (*min_val_error*) is compared with the current validation error and updated if necessary. Training stops if no new minimum validation error has been found for *Max_tries* iterations, or if the maximum number of iterations allowed (*Max_epochs*) has been reached.

Every time a new minimum validation error is encountered, the current network (as specified by the values of the weights) is saved as the possible best network (*best_network*). The network output for both the validation and training sets are also saved (*best_val_results* and *best_tr_results*) for error computation later. If the maximum number of epochs, *Max_epochs* (specified by the user) is reached while the validation error is still dropping (or at least has been dropping somewhere in the previous *Max_tries* number of iterations), training is stopped and the current network and results are saved as *last_network*, *last_tr_results* and *last_val_results*. After training has stopped, *best_network* is loaded again and the test set is evaluated for the first time. The network output is saved in *best_tst_results*.

The error used by SNNS to evaluate the performance of a network during training is a sum squared error (SSE). The SSE is equal to the sum of the squared differences between target and actual output of each output neuron for each example in the epoch. For evaluation and comparison of the networks, the SSE is not easy to interpret, since it depends on the number of output variables and also on the size of the training set (epoch). A per-example per-output error is preferred, but merely taking the average of the SSE does not provide a good criterion for the current problem either. More useful information is conveyed by the maximum error, and therefore the maximum error that occurred in the entire data set was used as a basis for comparison. This error was retained in its absolute form in dB or degrees.

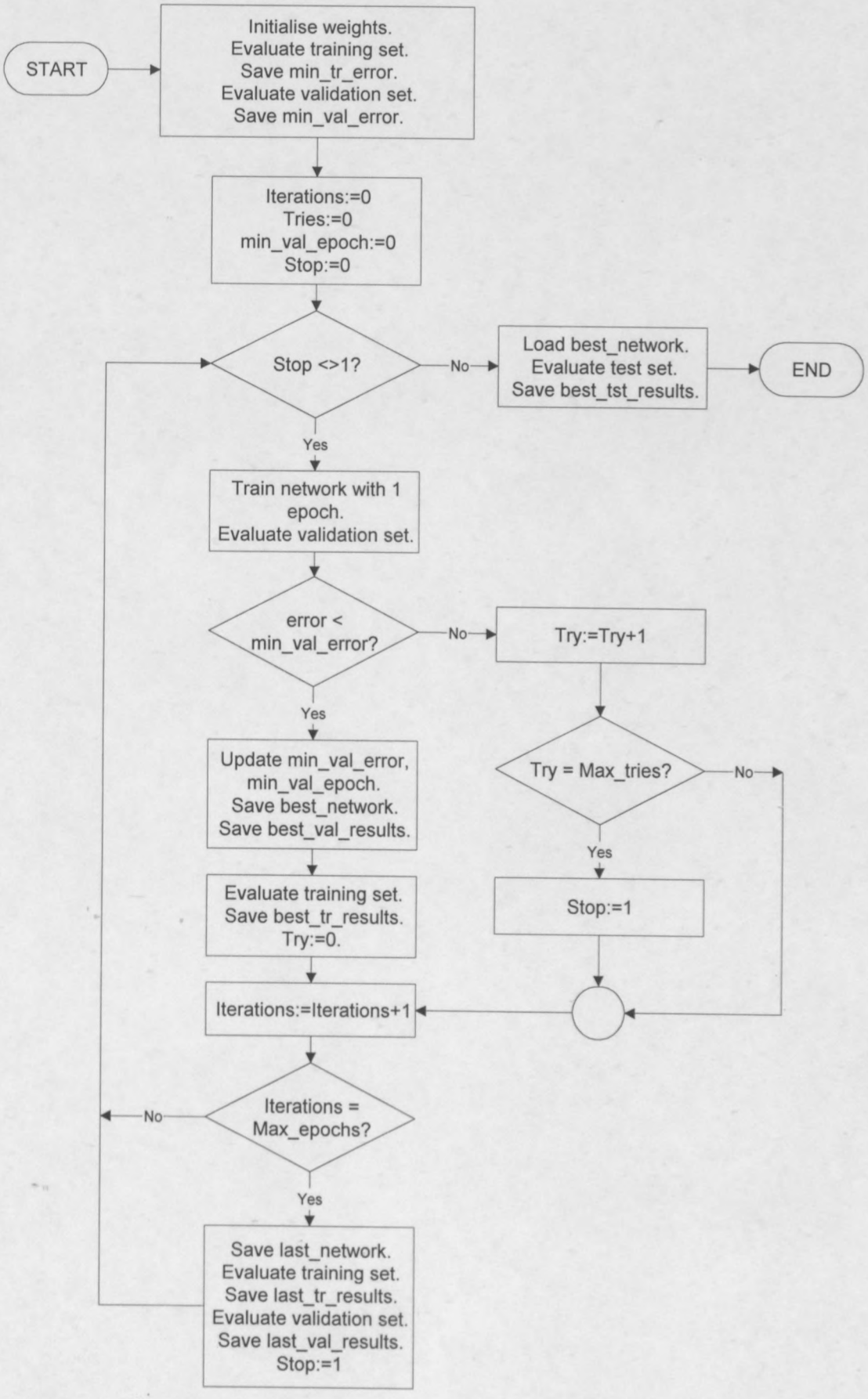

Figure 4.4: Flowchart of the batch program to train neural networks in SNNS using the principle of early stopping.

The batch program was run under Linux on three different computers. Sometimes these resources were also shared with other users and the training times given serve only as an indication. Specifications of the three computers are:

1. AMD 800 MHz CPU with 256 kB cache and 512 MB RAM.
2. AMD 700 MHz CPU with 512 kB cache and 128 MB RAM.
3. Pentium III 450 MHz CPU with 512 kB cache and 512 MB RAM.

The batch programs were not memory intensive and the speed and availability of the CPU had a greater influence on the duration of the training process.

4.1.9 Iteration 1: Learning rate and output activation function

The first iteration was used to investigate both learning rate and output layer activation function. As can be seen in Table 4.2, details about the learning rate are not published frequently. According to the SNNS manual typical values are in the range [0.1, 1.0]. Three values were chosen, namely 0.1, 0.2 and 0.5, and for each of these both the identity function and the logistic function were implemented as activation function. The second training parameter required by SNNS indicates error tolerance between target output and actual output and was set to zero.

A small network with five hidden neurons was chosen for the comparison. The details of the six networks are given in Table 4.4. The composition of the training set, Data Set 1, is given in Table 4.5 and shown in Figure 4.5.

Network	Topology	Data set	Output activation function	Learning rate
Net 1	3-5-4	Data Set 1	Logistic	0.1
Net 2	3-5-4	Data Set 1	Logistic	0.2
Net 3	3-5-4	Data Set 1	Logistic	0.5
Net 4	3-5-4	Data Set 1	Identity	0.1
Net 5	3-5-4	Data Set 1	Identity	0.2
Net 6	3-5-4	Data Set 1	Identity	0.5

Table 4.4: Training and topology details for the networks used to investigate learning rate and output activation function.

	Data Set 1
f points	9
L points	8
Δ points	8
Total data points	**576**
Points in training set	288
Points in validation set	288

Table 4.5: Information about the size and composition of Data Set 1.

The networks were trained with backpropagation using the Batchman program. For each network, the training process was executed for ten different weight initialisations. These will be referred to as the ten runs of the network. The training time for ten runs was between 4 and 8 hours per network. For each network the best run was selected based on a comparison of both the maximum magnitude error and the maximum phase error. Where the smallest magnitude error and the smallest phase error did not occur in the same run, the run with the best compromise between the two was (subjectively) chosen. The maximum errors of the best run of

	Magnitude [dB]						Phase [degrees]	
	$\|S_{11}\|$		$\|S_{21}\|$		$\|S_{31}\|$		$\angle S_{11}$	
	Tr	Val	Tr	Val	Tr	Val	Tr	Val
Net 1	2.86	**5.90**	0.0004	0.0004	3.34	5.76	7.35	**7.97**
Net 2	2.74	**5.74**	0.0004	0.0004	3.38	5.62	7.22	**7.88**
Net 3	2.54	**5.73**	0.0004	0.0004	3.47	5.73	7.31	**7.98**
Net 4	3.16	**5.48**	0.0005	0.0006	2.52	4.16	1.72	**1.92**
Net 5	2.96	**5.39**	0.0005	0.0006	2.52	4.12	1.71	**1.90**
Net 6	2.60	**5.16**	0.0005	0.0006	2.63	3.75	1.88	**1.93**

Table 4.6: The maximum absolute error for each output variable for the training (Tr) and validation (Val) sets. Only the best run for each network is shown. All errors were rounded upwards. The maximum magnitude and phase errors of each network are in bold type.

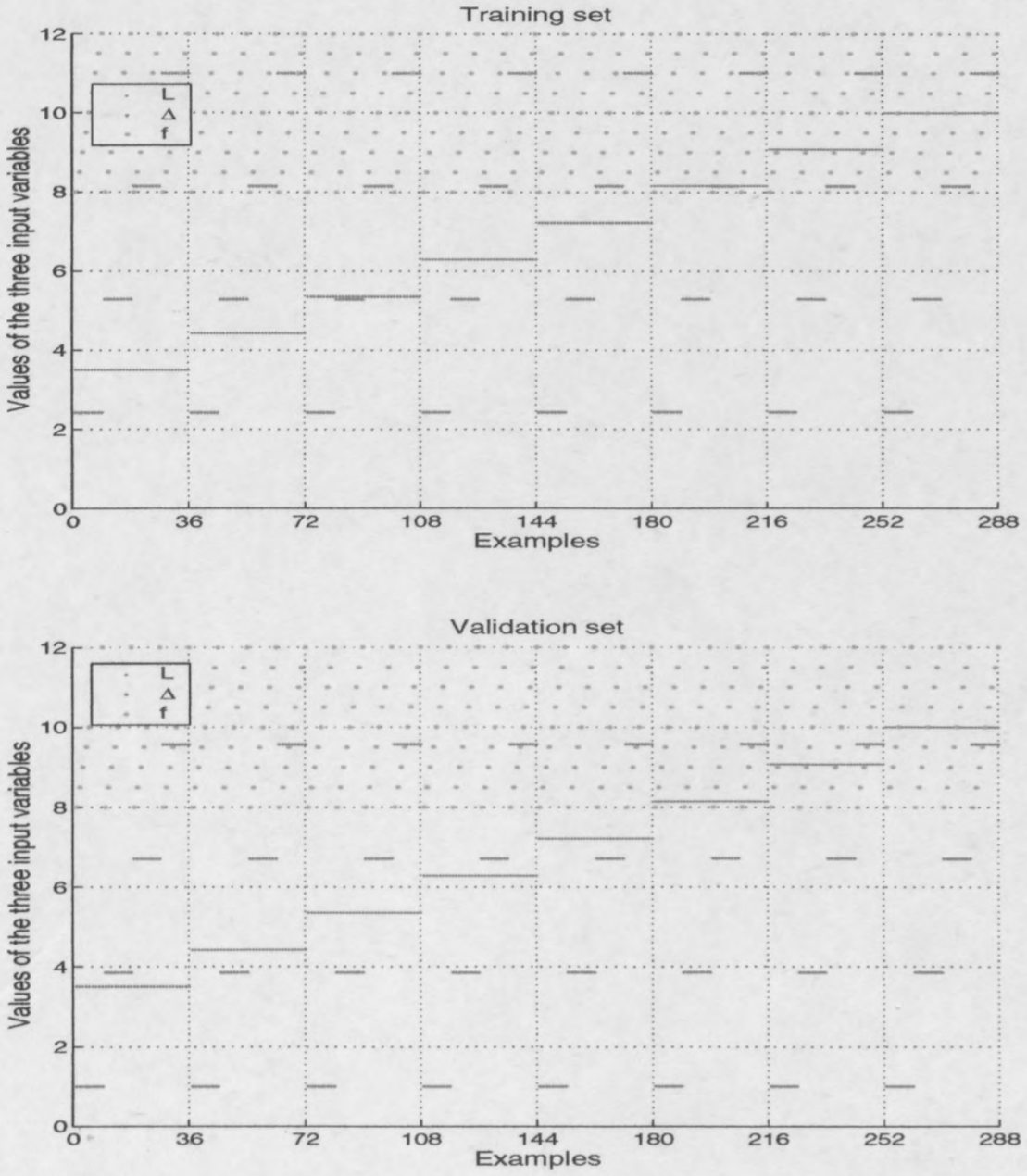

Figure 4.5: Training and validation samples of Data Set 1. The actual values of the frequency (f) is shown in GHz and of the length (L) and offset (Δ) in mm.

each network is given in Table 4.6 and the number of epochs that were presented to each network before it reached its minimum validation SSE is shown in Table 4.7.

The training and validation SSE curves are shown in Figure 4.6 where the difference in training performance resulting from the different activation functions and learning rates can be inspected. The first observation is that the training and validation SSE are not relatively close to each other, indicating that the training set is too small for the network to generalise well.

Network	User-specified epoch limit (*Max_Epochs*)	Epochs for the run that trained the longest	Epochs for the best run
Net 1	500 000	6 runs reached the limit	500 000
Net 2	800 000	2 runs reached the limit	800 000
Net 3	800 000	4 runs reached the limit	441 136
Net 4	500 000	187 331	184 016
Net 5	500 000	91 306	91 306
Net 6	500 000	142 657	142 657

Table 4.7: Details about the number of epochs trained for different networks. The values indicated are the number of epochs at which the validation error was the lowest.

The influence of the learning rate can be seen most clearly when looking at the SSE of Net 4 to Net 6. Net 6 (with a learning rate of 0.5) converged more quickly than Net 4 (with a learning rate of 0.1). The networks have also avoided the potential pitfall of large learning rates leading to poorer results. In this case the results are much the same, as is confirmed in Table 4.6.

To further confirm that the learning rate did not influence the results, the weights of the best networks were examined. They are plotted in Figure 4.7, where the best runs from Net 4 and Net 6 are plotted in solid lines. The values of corresponding weights can be seen to be very similar, indicating that the two networks converged to almost the same system of weights, regardless of the learning rate. In contrast, the weights of a different run from Net 4 do not show good agreement with the other two networks. This network had a maximum magnitude error of 5.52 dB and a maximum phase error of 43.0°. Gaining in training speed and not losing in accuracy, the large learning rate was retained for further iterations.

The influence of the output activation function is not clear from the training figures, but Table 4.7 indicates that Net 4-6 (with the identity output activation function) trained faster, needing less epochs. Furthermore, the maximum phase errors were much smaller for Nets 4-6 according to Table 4.6. Based on these results, the identity function was selected to be used for further iterations.

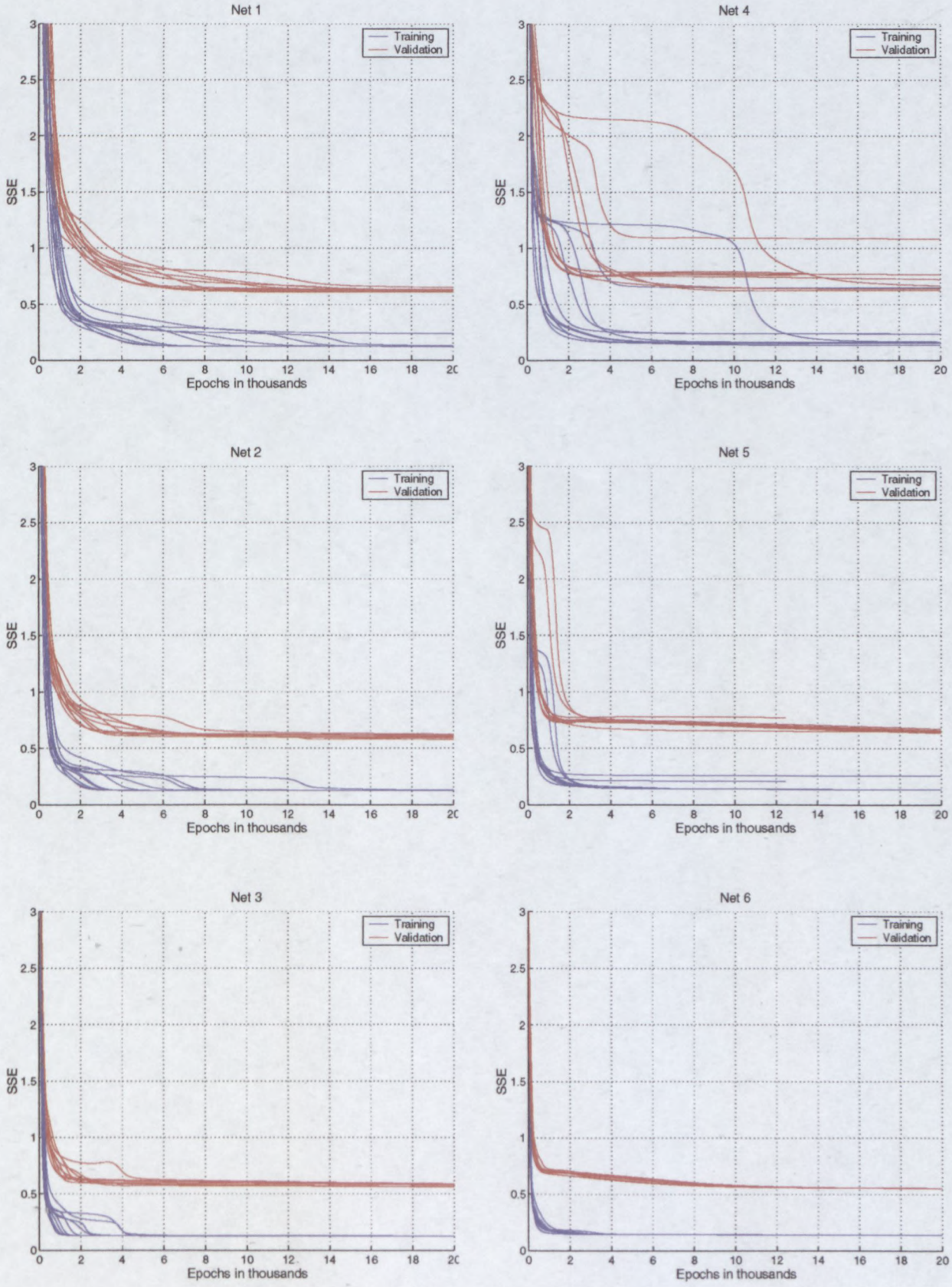

Figure 4.6: Training and validation errors for Net 1 to 6 during the first 20 000 epochs of training. For the three networks on the left the output activation function was the logistic function, and for the three on the right it was the identity function. The leaning rate increases from top to bottom: for the top figures $\eta = 0.1$, for the middle figures $\eta = 0.2$ and for the bottom figures $\eta = 0.5$.

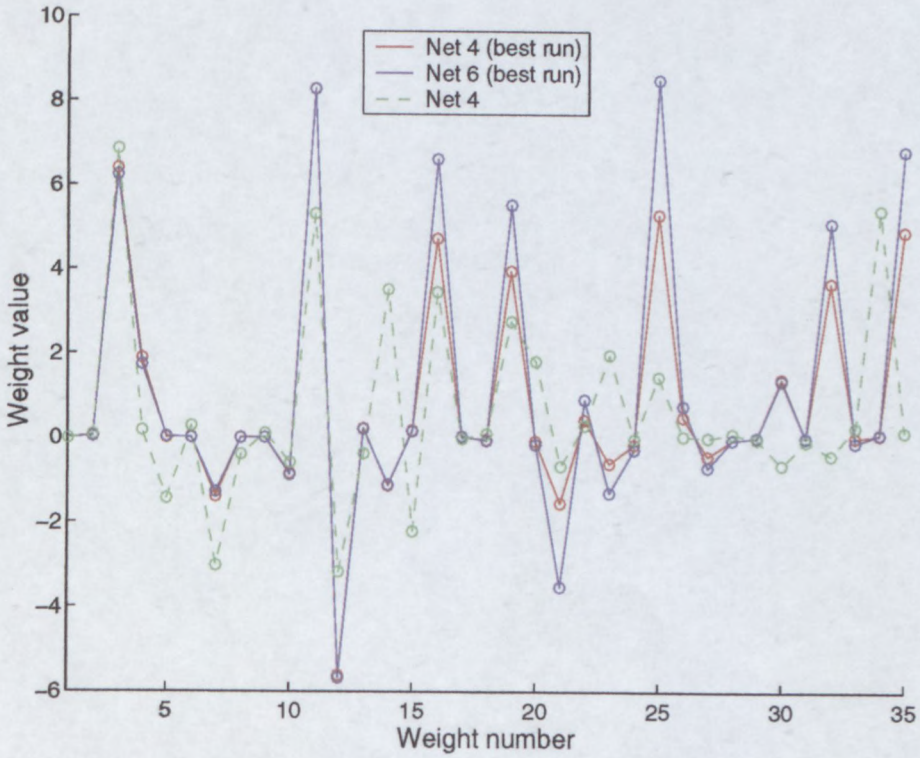

Figure 4.7: A comparison of the weight values of three different networks, all modelled to the same training data. The weights are numbered starting with the 15 input-to-hidden layer weights, followed by the 20 hidden-to-output layer weights.

It should be kept in mind that the errors given in Table 4.6 are for the training and validation sets only, so that they are only an indication of network accuracy. Actual test errors would be larger. There was not much difference in magnitude errors between the six networks already trained, but based on all the available information, Net 6 was selected as the best network trained so far, yielding a magnitude error of less than 5.2 dB and a phase error of less than 2° (for Data Set 1).

Going beyond numbers in a table, the actual response of the network to a set of input parameters was viewed graphically. An example of such a typical network response is shown in Figure 4.8. It shows the target outputs in comparison to the actual network outputs. It should be noted that although the difference between, for example, a –62 dB target value and the –67 dB predicted by the network is not really relevant for performance evaluation, the purpose of this comparison is to evaluate the accuracy of the network irrespective of the absolute values of the output parameters.

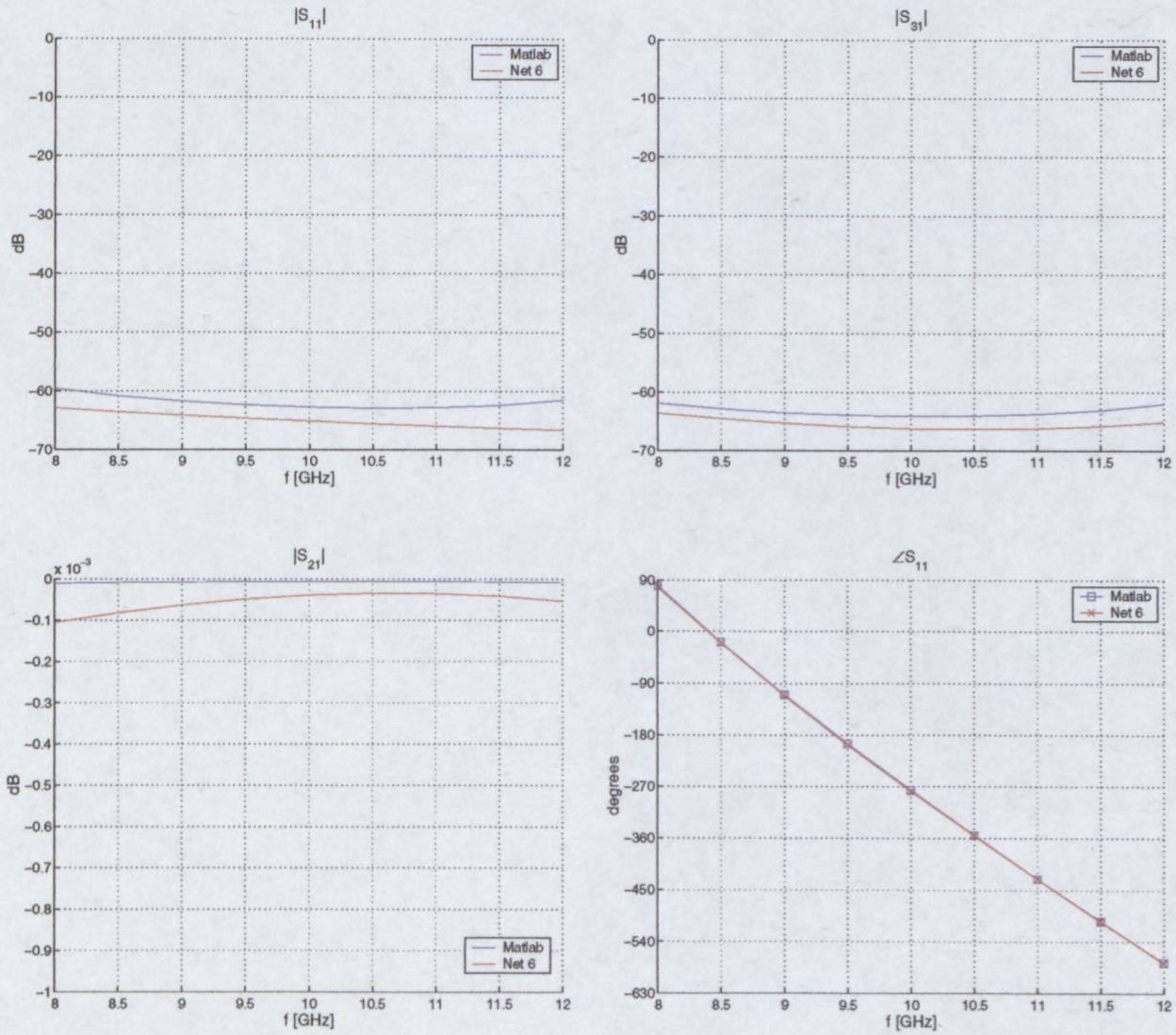

Figure 4.8: An example of the response of the best run from Net 6 for a slot from the validation set. L = 10 mm and Δ = 9.57 mm. This is the slot for which the maximum magnitude error of 5.16 dB occurred.

4.1.10 Iteration 2: Network size

The next important parameter to investigate is network size. The six configurations mentioned in Section 4.1.6 were implemented in Net 6-11 (using Net 6 again from the previous iteration). Their details are given in Table 4.8.

Training times were 1 to 6 hours. Training curves (SSE) are shown in Figure 4.9. As the complexity (size) of the network increases, both the training and validation SSE drops. This is also reflected in the maximum errors given in Table 4.9, where the errors of Nets 9-11 are the lowest.

Network	Topology	Data set	Output activation function	Learning rate
Net 7	3-4-4	Data Set 1	Identity	0.5
Net 6	3-5-4	Data Set 1	Identity	0.5
Net 8	3-6-4	Data Set 1	Identity	0.5
Net 9	3-8-4	Data Set 1	Identity	0.5
Net 10	3-10-4	Data Set 1	Identity	0.5
Net 11	3-12-4	Data Set 1	Identity	0.5

Table 4.8: Training and topology details for the networks used to investigate the influence of the network size.

	Magnitude [dB]						Phase [degrees]	
	$\|S_{11}\|$		$\|S_{21}\|$		$\|S_{31}\|$		$\angle S_{11}$	
	Tr	Val	Tr	Val	Tr	Val	Tr	Val
Net 7	2.77	4.58	0.0005	0.0006	4.74	**6.66**	38.84	**42.84**
Net 6	2.60	**5.16**	0.0005	0.0006	2.63	3.75	1.88	**1.93**
Net 8	2.52	**5.07**	0.0003	0.0005	2.55	3.95	4.99	**5.00**
Net 9	1.59	**3.78**	0.0003	0.0005	1.36	3.59	4.31	**4.52**
Net 10	1.13	3.23	0.0002	0.0006	1.17	**3.30**	3.19	**3.71**
Net 11	0.72	**2.33**	0.0001	0.0006	0.73	2.28	1.71	**1.81**

Table 4.9: The maximum absolute error for each output variable for the training (Tr) and validation (Val) sets. Only the best run for each network is shown. All errors were rounded upwards. The maximum magnitude and phase errors of each network are in bold type.

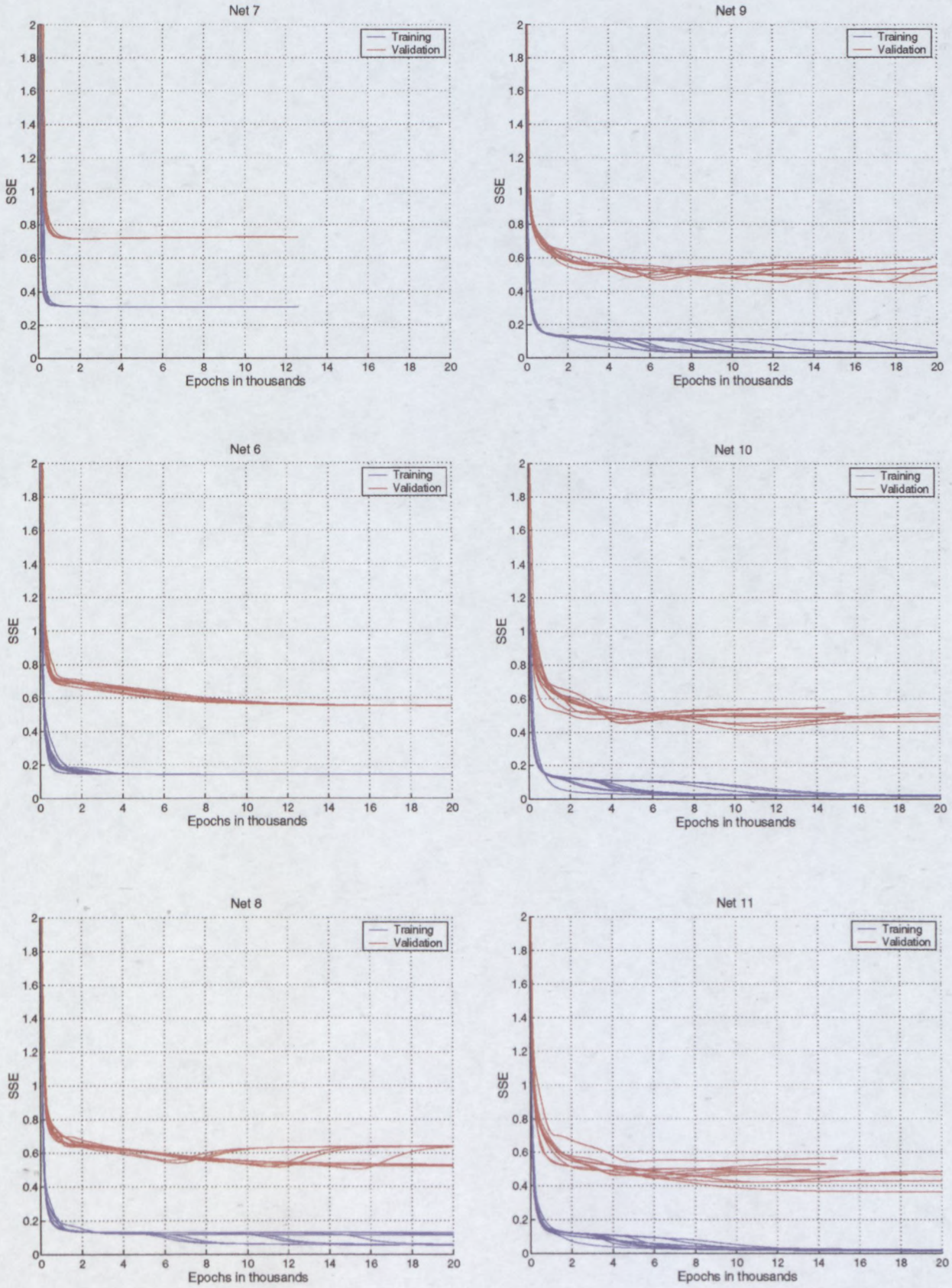

Figure 4.9: Training and validation errors for Net 6 to 11, showing the first 20 000 epochs. The networks have different numbers of hidden neurons: in the left-hand column 4, 5 and 6 respectively, and in the right-hand column 8, 10 and 12.

Training times are compared in Figure 4.10 in terms of the number of epochs trained. The huge difference in training time between Net 7 (4 hidden neurons) and Net 6 (5 hidden neurons) was unexpected, but could possibly indicate that Net 7 was too small to model the problem, as is also indicated in the large errors (Table 4.9). As the network size is increased from 5 hidden neurons upwards, two opposing factors influence the training time. On the one hand, the larger number of weights tends to reduce the SSE more efficiently, *decreasing* training time. On the other hand, with more weights there are more degrees of freedom to be matched to the underlying function, tending to *increase* training time. For the current problem, this causes the training time to first decrease, as the number of hidden neurons h is increased from 5 to 10, and then to rise again as h is set to 12. The number of epochs trained for the best run of each network is summarised in Table 4.10.

Net 11 has the lowest errors and is expected to improve even more if presented with more training data. Both Net 10 and Net 11 will be tried out with larger training sets in the next iteration.

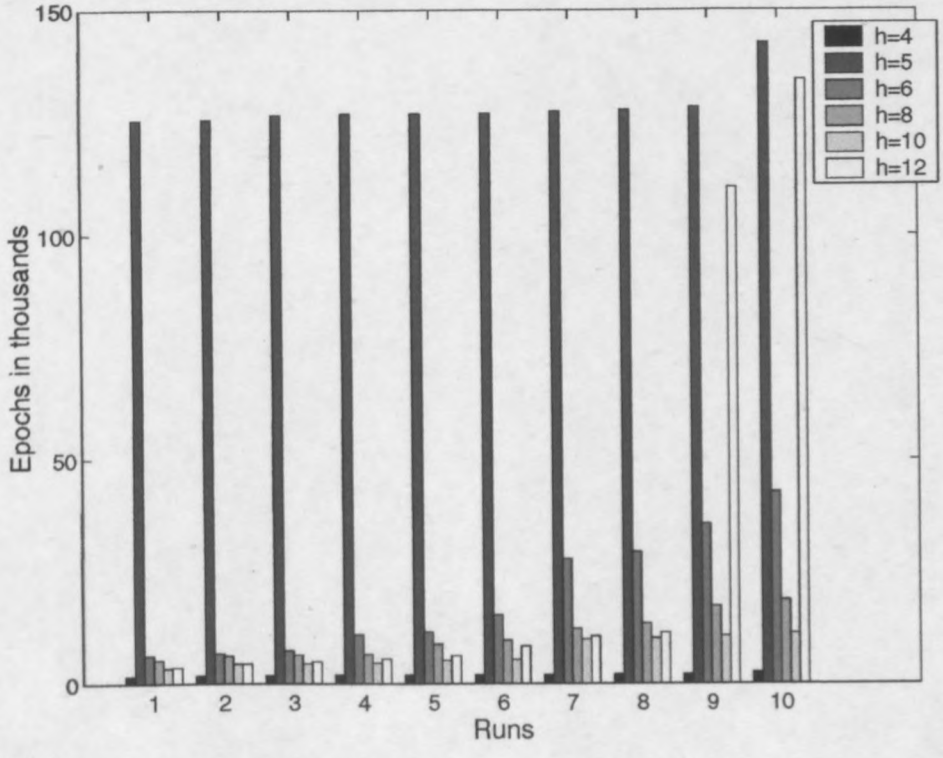

Figure 4.10: The number of epochs needed to train the runs of six different networks (Net 6 to Net 11). The number of hidden neurons h of each network is indicated in the legend.

Network	Epochs for the best run	Epochs for the run that trained the longest
Net 7	2 054	2 599
Net 6	142 657	142 657
Net 8	6 283	42 800
Net 9	6 331	18 660
Net 10	10 176	11 261
Net 11	134 567	134 567

Table 4.10: Details about the number of epochs trained for different networks. The values indicated are the number of epochs at which the validation error was the lowest.

4.1.11 Iteration 3: Training set

Two larger training sets were created and designated Data Sets 2 and 3. The details of the data sets are given in Table 4.11. The two best networks from the previous iteration, one with 10 hidden neurons and one with 12 hidden neurons, were trained with each data set. The four new networks are detailed in Table 4.12.

The training curves are shown in Figure 4.11. With the increase of training data, the training and validation SSE overlapped more, indicating that the network is able to extend its good training data response to an equally good validation data response (generalisation). As expected, the

	Data Set 2	Data Set 3
f points	17	21
L points	8	10
Δ points	9	11
Total data points	**1224**	**2310**
Points in training set	612	1155
Points in validation set	612	1155

Table 4.11: Information about the data sets used for training the networks.

Network	Topology	Data set	Output activation function	Learning rate
Net 12	3-10-4	Data Set 2	Identity	0.5
Net 13	3-12-4	Data Set 2	Identity	0.5
Net 14	3-10-4	Data Set 3	Identity	0.5
Net 15	3-12-4	Data Set 3	Identity	0.5

Table 4.12: Training and topology details for the networks used to investigate the influence of a larger training set.

maximum errors dropped, as can be seen in Table 4.13. Net 15 had a magnitude error of less than 0.5 dB and a phase error of less than 1.1°. Reducing the errors further would be meaningless, since they are approaching the approximations made in equation (4.1) to equate the scattering parameters to each other.

The number of epochs trained for each network is shown in Table 4.14. The networks needed more epochs to train as the size of their training set increased. Looking at the training curves, it is clear that the larger training sets cause the networks to initially improve faster, but then they continue to improve very slowly for a long time before training stops. This could be understood in the light of the fact that the larger training sets also lead to smaller errors, in the end causing the change in weights to become very small and slowing down the final stage of training – a problem that could possibly have been overcome with the use of flat spot elimination (page 27).

	Magnitude [dB]						Phase [degrees]	
	$\lvert S_{11}\rvert$		$\lvert S_{21}\rvert$		$\lvert S_{31}\rvert$		$\angle S_{11}$	
	Tr	Val	Tr	Val	Tr	Val	Tr	Val
Net 12	0.63	0.79	0.0002	0.0001	0.93	**0.97**	**1.87**	1.85
Net 13	**0.60**	0.60	0.0001	0.0001	0.51	0.57	1.70	**1.84**
Net 14	0.45	0.46	0.0001	0.0001	**0.69**	0.61	1.56	**1.57**
Net 15	0.46	**0.49**	0.0001	0.0001	0.40	0.39	1.03	**1.03**

Table 4.13: The maximum absolute error for each output variable for the training (Tr) and validation (Val) sets. Only the best run for each network is shown. All errors were rounded upwards. The maximum magnitude and phase errors of each network are in bold type.

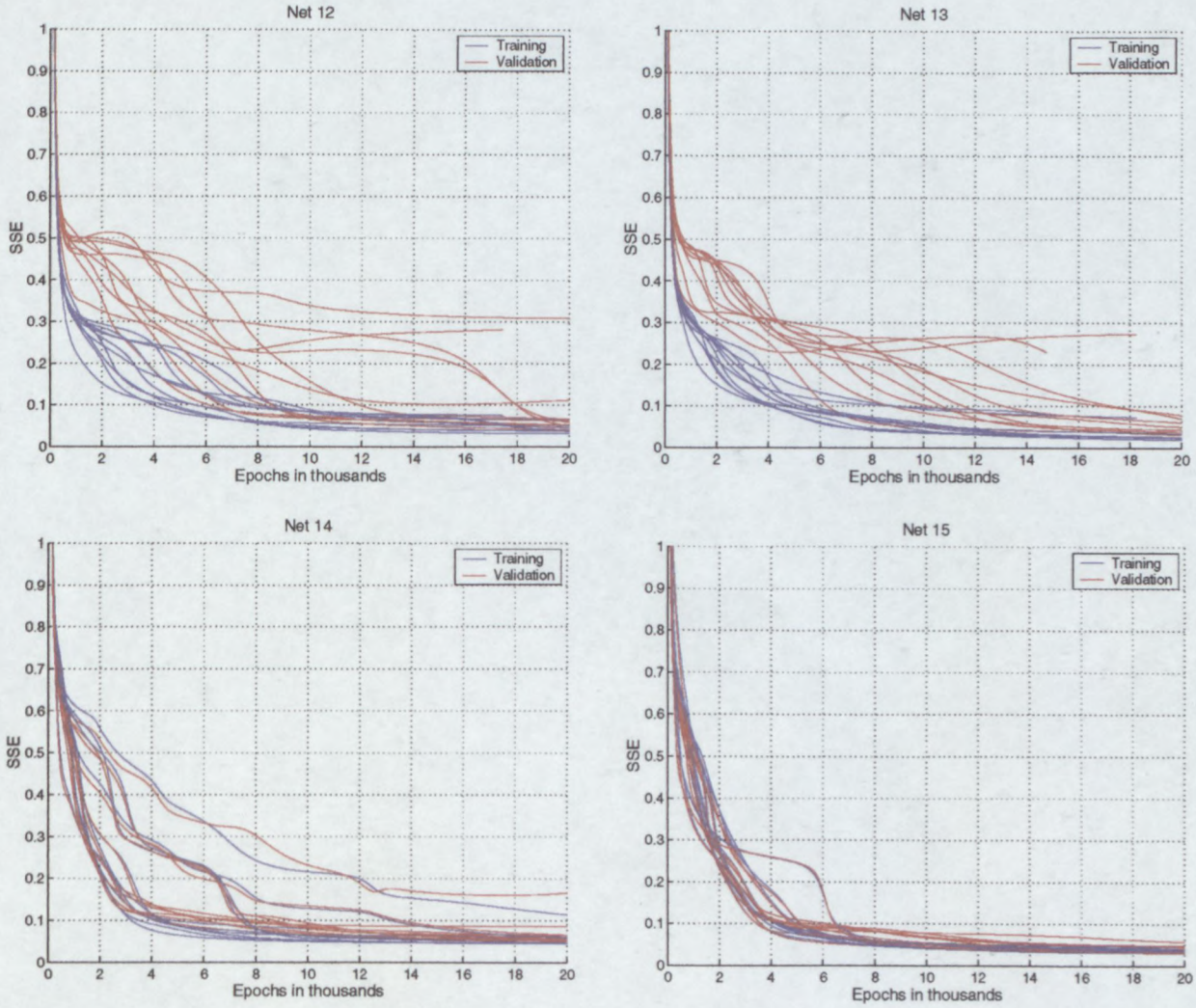

Figure 4.11: Training and validation errors for the first 20 000 epochs of training for Net 12 to 15. The networks on the left-hand side had 10 hidden neurons and the networks on the right-hand side had 12. The top networks were trained with less data than the bottom networks.

Network	Epochs for the best run	Epochs for the run that trained the longest
Net 12	63 316	63 316
Net 13	42 692	132 949
Net 14	60 423	97 759
Net 15	194 144	363 047

Table 4.14: Details about the number of epochs trained for the last four networks. The values indicated are the number of epochs at which the validation error was the lowest.

	Data Set 4
f points	41
L points	16
Δ points	21
Total data points	**13 776**

Table 4.15: Information about Data Set 4, the data set used for testing the final network.

4.1.12 Testing the network

The results of an independent test set served as final criterion for the success of the network. From the errors in Table 4.13, Net 15 was chosen as the best network and it was tested with Data Set 4, the details of which are given in Table 4.15. The test set was designed to be very large to give a reliable demonstration of the network's performance and the range of L was extended in order to get an indication of the network's extrapolating ability: while the trained range was [3.5, 10] mm, the testing range was [3, 10.5] mm.

The testing errors are displayed in Table 4.16 together with the network's training and validation errors. The testing errors are notably larger than the training and validation errors, but the network is still able to produce magnitudes with an error of less than 1 dB and 1.05° within its trained range of input variables. The network errors rise as soon as it is expected to extrapolate, as can be seen from the maximum errors given in Table 4.16.

A different way to look at the network errors, is to consider the complex scattering parameters. Using the four output parameters and equation (4.1), relative percentage errors can be computed with the following equation:

$$E = \frac{|T - A|}{|T|} \times 100$$

where T is the target value of the complex s-parameter and A is the actual network output. The maximum percentage error for each scattering parameter is given in Table 4.17, as well as the mean error for each s-parameter, computed as the arithmetic mean of all the test errors.

	$\|S_{11}\|$ [dB]	$\|S_{21}\|$ [dB]	$\|S_{31}\|$ [dB]	$\angle S_{11}$ [degrees]
Training errors	0.46	0.0001	0.40	1.03
Validation errors	0.49	0.0001	0.39	1.03
Test errors (interpolation only)	0.93	0.0002	0.87	1.03
Test errors (including extrapolation)	1.71	0.0013	1.54	1.32

Table 4.16: A summary of the maximum errors associated with Net 15. The training and validation errors are from Data Set 3, with which the network was trained, and the test errors are from Data Set 4.

	S_{11} [%]	S_{21} [%]	S_{31} [%]
Mean Error	1.13	0.59	1.23
Maximum Error	10.12	1.83	9.45

Table 4.17: Mean and maximum relative percentage errors of the complex s-parameters for Net 15 tested with Data Set 4 (interpolation testing only). The errors of S_{41} were the same as those for S_{31}.

4.2 Comparison with Adaptive Sampling Interpolation Technique

Interpolation techniques offer the same advantages as neural networks with respect to small memory and data set requirements, are fast to evaluate and can be also be faster than neural networks to create [Lehmensiek 2001]. A study by Lehmensiek [op. cit.] investigated the use of an Adaptive Sampling Interpolation (ASI) Technique in multivariate, multiple output models. His technique made use of an iterative procedure that gradually selected more support points where the error was the largest. In one of his examples he made use of the same slotted waveguide configuration that was successfully modelled in the previous section of the current work. In this section a comparison between the performance of neural networks and the ASI Technique will be presented.

Lehmensiek's model contained six output parameters: the complex values of S_{11}, S_{21} and S_{31}. Because a change in the number of output variables can change the behaviour of a neural

network completely, new networks were trained to be compared with Lehmensiek's model. The knowledge gained in the previous section was used to reduce the number of design iterations. For clarity the neural models created in Section 4.1 (Net 1-15) will collectively be referred to as Model A, and the new models to be created in this section as Model B.

4.2.1 Creating the neural network models

The input variables again were frequency, slot length and offset, and the variable ranges were the same as those given in Table 4.1. The output variables were the magnitudes and unwrapped phases of S_{11}, S_{21} and S_{31}. The same normalisation as before was used for both input and output variables. A MLP with the identity output activation function was used again and the training algorithm, update function and weight initialisation were retained as before. A learning rate of 0.5 was used.

The three training data sets from the previous section (Data Set 1-3) were expanded to include the extra scattering parameters and used again (see Table 4.18), but the examples were divided differently between the training and validation sets. In the previous section, for each f-L combination the Δ points were divided between the two sets; in this section for each L-Δ combination the f-points were divided between the sets. This was done because the frequency has less influence on the network response than the offset.

The only parameter experimentally investigated was the size of the network. Three network sizes were implemented for the smallest training set. The three networks are detailed in Table 4.19. The maximum magnitude and phase errors are shown in Table 4.20. It is clear that the network performance improved with increasing network size: Net 18 with 15 hidden neurons had a maximum magnitude error of 0.32 dB and a maximum phase error of 0.63°.

	Data Set 5	**Data Set 6**	**Data Set 7**
f points	9	17	21
L points	8	8	10
Δ points	8	9	11
Total data points	**576**	**1224**	**2310**

Table 4.18: The details of the three training sets used for Model B.

Network	Topology	Data set	Output activation function	Learning rate
Net 16	3-10-6	Data Set 5	Identity	0.5
Net 17	3-12-6	Data Set 5	Identity	0.5
Net 18	3-15-6	Data Set 5	Identity	0.5

Table 4.19: Training and topology details for the networks trained to investigate the influence of the network size.

	Magnitude [dB]		Phase [degrees]	
	Tr	Val	Tr	Val
Net 16	0.52	0.54	1.09	1.11
Net 17	0.39	0.45	1.27	1.25
Net 18	0.32	0.34	0.63	0.60

Table 4.20: The maximum magnitude and phase errors of the best runs for each network. The training (Tr) and validation (Val) errors are given.

Network	Topology	Data set	Output activation function	Learning rate
Net 18	3-15-6	Data Set 5	Identity	0.5
Net 19	3-15-6	Data Set 6	Identity	0.5
Net 20	3-15-6	Data Set 7	Identity	0.5

Table 4.21: Training and topology details for networks to investigate the influence of more training data.

Based on these results, the network with 15 hidden neurons was selected and trained with the two larger training sets, Data Set 6 and Data Set 7. The network details are shown in Table 4.21.

The maximum magnitude and phase errors are shown in Table 4.22 and the training curves in Figure 4.12. A surprising result is that the network performance did not improve as the training set was enlarged. This observation was confirmed as the networks were evaluated with a large test set. The test set, Data Set 8, had 41 f points, 14 L points and 21 Δ points for a total of 12054 examples. In addition, to evaluate the networks' extrapolating ability they were also tested with slots of length 3 mm and 10.5 mm. The results of the test set are shown in Table 4.23.

The difference in performance between Net 19 and Net 20 is negligible. It appears as though the network configuration reached a saturation point as to how much it can improve with more training examples. It is possible that other network parameters are preventing the network from improving, for example the network size.

	Magnitude [dB]		Phase [degrees]	
	Tr	Val	Tr	Val
Net 18	0.32	0.34	0.63	0.60
Net 19	0.36	0.44	0.53	0.54
Net 20	0.48	0.45	0.55	0.54

Table 4.22: The maximum magnitude and phase errors of the best runs for each network. The training (Tr) and validation (Val) errors are given.

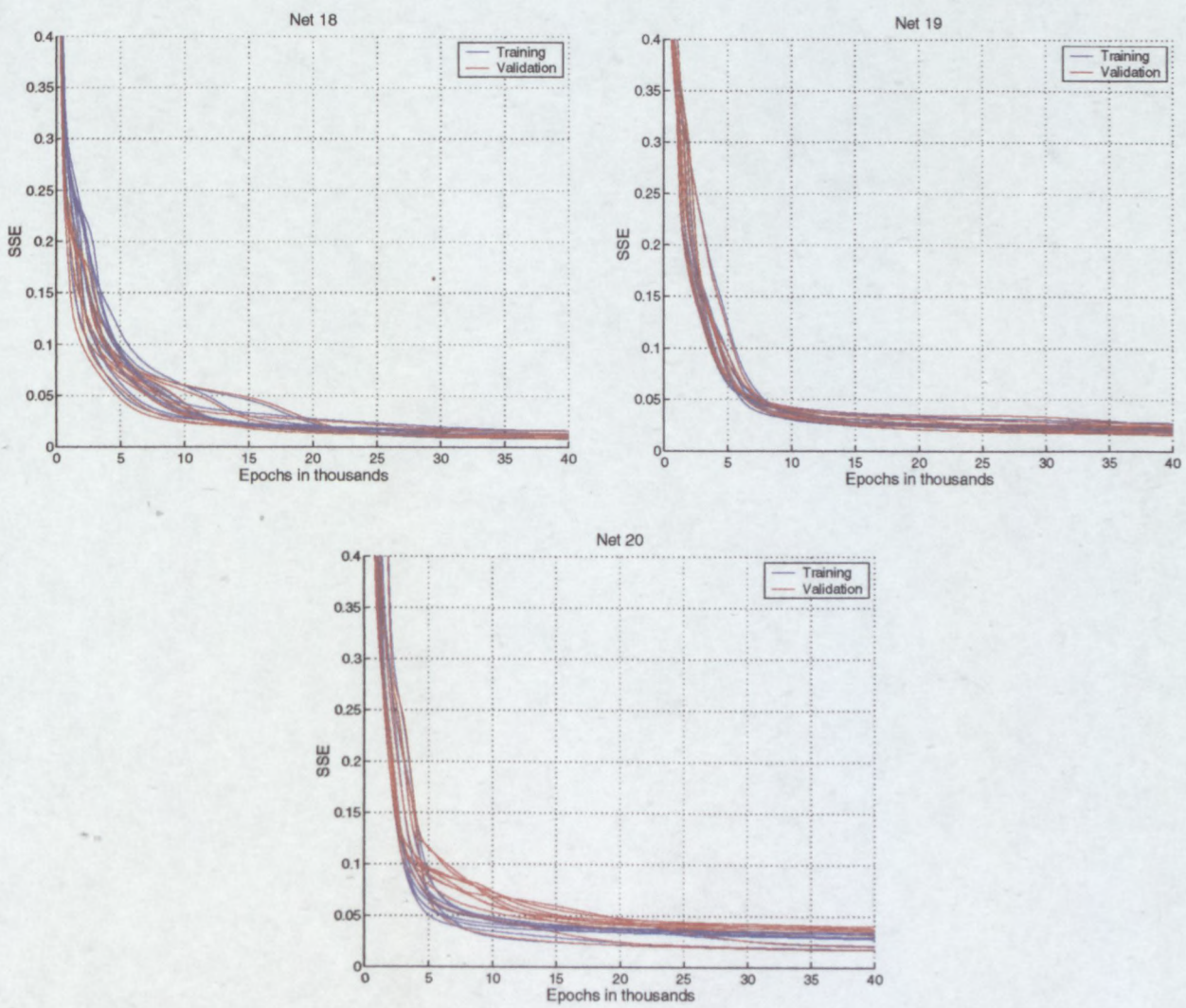

Figure 4.12: Training and validation errors for networks trained with different training sets.

	Magnitude [dB]		Phase [degrees]	
	Mean	Max	Mean	Max
	Interpolating examples only			
Net 18	0.14	1.43	0.23	0.76
Net 19	0.10	1.00	0.13	0.55
Net 20	0.10	1.02	0.13	0.56
	Extrapolating examples included			
Net 18	0.18	1.98	0.23	0.84
Net 19	0.13	1.56	0.14	1.00
Net 20	0.13	1.71	0.16	0.92

Table 4.23: Network errors in response to the test set, Data Set 8. The mean errors were computed as the arithmetic average of the absolute errors in dB or degrees over all the test examples.

4.2.2 Comparison with ASI Technique

Lehmensiek used a different function to compute the model errors. The complex s-parameters were used and the relative squared error computed with the following equations:

$$E = 10\log_{10}\left(\frac{|T-A|^2}{|T|^2}\right)\text{dB}$$

$$E_{mean} = 10\log_{10}\left(\frac{1}{N}\sum_{examples}\frac{|T-A|^2}{|T|^2}\right)\text{dB}$$

where T is the target value for the s-parameter, A is the actual value and N is the number of examples in the test set. The errors of Net 18-20 computed with the above equations are tabulated in Table 4.24 and the errors of the ASI model in Table 4.25.

A comparison of the maximum errors show that the neural network trained with 576 data points (288 training points and 288 validation points) is comparable to the ASI model trained with 301 data points, although the mean error of the neural network is higher than the corresponding ASI error. In further development the neural network did not improve much and the ASI model surpassed its performance easily.

Training and validation points	E_{11} [dB]		E_{21} [dB]		E_{31} [dB]	
	Mean	Max	Mean	Max	Mean	Max
576	-31.0	-16.4	-46.5	-37.6	-30.6	-17.7
1224	-35.9	-19.2	-50.3	-40.5	-35.5	-21.7
2310	-36.2	-19.1	-51.3	-40.3	-35.4	-20.2

Table 4.24: Errors obtained with neural network models (Net 18-20).

Number of support points	E_{11} [dB]		E_{21} [dB]		E_{31} [dB]	
	Mean	Max	Mean	Max	Mean	Max
301	-58.2	-14.2	-62.8	-39.4	-60.3	-17.7
403	-66.0	-35.9	-73.5	-51.8	-70.0	-38.8
536	-71.3	-47.8	-70.6	-48.8	-74.0	-48.0
577	-73.6	-57.7	-78.5	-63.3	-76.8	-59.8

Table 4.25: Model errors obtained with the ASI Technique [Lehmensiek 2001].

Based on these quantitative observations and the experience of the whole training process of the neural networks, it is concluded that the ASI technique can lead to better results with less effort. Improving the neural network to reach the same low errors as those displayed by the ASI model would take more experimenting and training time. The ASI model improves its performance by selecting more support points without teacher supervision.

Chapter 5
Evaluation and conclusion

This thesis describes the application of neural networks to a specific passive microwave structure. The two main components of the work were the generation of the training data and the development of the neural model.

5.1 The moment method solution

For the generation of training data, integral equations were set up that described the problem. They were solved with the Method of Moments (MoM) for a general inclined slot and their validity were confirmed by implementing the results for a longitudinal and transverse slot and comparing them to commercial software results.

The MoM code can be used to solve for longitudinal or transverse slots of variable length, width and offset over a frequency band. The code can be extended to include inclined slots using the equations given in Section 3.4. Further extensions that will require more substantial changes to the program include crossed waveguides and slots in the narrow wall.

5.2 Evaluation of the neural network model

A literature study was performed to investigate the use of neural networks in microwave applications. It was found that although such results are increasingly being published, papers do not provide sufficient design detail to serve as guideline for new designs and the design process had to make extensive use of experimentation.

In Section 4.1 a neural network model was developed for a longitudinal slot coupling two parallel waveguides. The model had three input variables (slot length, slot offset and frequency)

and four output variables ($|S_{11}|$, $\angle S_{11}$, $|S_{21}|$ and $|S_{31}|$). The best network (Net 15) was a MLP with 12 hidden neurons in a single layer that was trained with 1155 training data points and 1155 validation data points.

When a mathematical model is developed to be used as a design tool, the accuracy required is determined by the problem. In the case of narrow-band structures such as waveguide slots, the required accuracy is very high – Josefsson [Josefsson 1987] mentions an accuracy of 0.5% in the determination of resonant length. The accuracy of the best network was tested with a test set consisting of 12 054 uniformly spaced input points. The maximum absolute errors were 0.93 dB for the magnitude outputs and 1.03° for the phase output. When the test set was extended to include slot lengths 0.5 mm smaller and 0.5 mm larger than the trained range of the network, the test errors increased to 1.71 dB and 1.32°. When the errors of the complex scattering parameters relative to the target values were expressed as percentages, the largest maximum percentage error was 10.12 % on S_{11} and the largest mean percentage error was 1.23 % on S_{31}. The maximum errors of the network are too large for frequency-sensitive design applications, although the mean errors are low. It can be concluded that it is difficult to obtain very high accuracy with a neural network without increasing the cost paid in development and training time even further.

The time it takes to develop any model should be realistic in the context of the design environment. The development time must be measured against the time that will be saved on future designs by using the model. Finding the best neural network model for a problem takes a long time. It was found that there are many choices to be made that cannot be arrived at through logical deduction, but that need to be tried out in different combinations to find the best solution. The process needed to be supervised and evaluated constantly in order to determine the changes to be implemented in the next iteration. The current problem was relatively simple and contained no resonance points in its response. Even so, three iterative steps were needed to find a good neural network and fifteen networks had to be trained.

For a more complex problem, just increasing the size of the training set could increase computer training time many times. The fifteen networks trained in this case had training times that ranged from 1 hour to 38 hours per network. Where the generation of training data involves measurement, the time increase for the actual gathering of the data points can also be substantial. A more complex problem can furthermore be expected to place greater demand on the designer's time and effort. There are many more options available for the implementation of a neural network than had been used for this project.

Apart from the actual development time, time had to be spent acquiring enough background knowledge on neural networks to be able to use the technique. In general, the usefulness of a technique also depends on how easy it will be for an engineer with relatively little knowledge of the subject to design such a model successfully. Although the basic principles of neural networks are relatively easy to understand, it seemed as though experience would be the only way to really accelerate the design process by eliminating some of the experimental configurations.

The only real time advantage of neural networks is in the optimisation process: once a trained neural network model exists, evaluating different structures can take place almost instantaneously. Spending a few weeks on finding a good model can be justified if the model would be used frequently after that for evaluations.

5.3 Comparison between neural network and interpolation technique

Solving exactly the same problem, a neural network model was compared to a model created with the Adaptive Sampling Interpolation (ASI) Technique [Lehmensiek 2001]. The models had three input variables (slot length, slot offset and frequency) and three complex output variables: the scattering parameters S_{11}, S_{21} and S_{31}. The best network (Net 19) had 15 hidden neurons in a single layer and was trained with 612 training points and 612 validation points.

When evaluated with a test set containing 12 054 examples, the network had a maximum absolute magnitude error of 1 dB and a maximum absolute phase error of 0.55°. For comparison with the ASI results, relative squared errors in dB were computed. The neural network yielded maximum errors lower than –19.2 dB and mean errors lower than –35.5 dB. In contrast, the ASI model trained with 301 support points yielded maximum errors lower than –14.2 dB and mean errors lower than –58.2 dB. The ASI results for models trained with a larger number of support points, up to 577 points, improved to maximum errors lower than –57.7 dB. The neural network could not be improved by increasing its number of training examples.

Neural networks and the ASI technique share advantages such as the reduced number of CEM evaluations needed for training, the low memory (storage) requirements, their ability to handle multi-dimensional and non-linear problems and handling increasing complexity without an exponential increase in model size. However, the ASI technique needs less user intervention to

reach a solution, while the neural networks need user supervision and input during the training process. The ASI technique can therefore be considered more time-efficient and also easier to use, since little prior knowledge about the technique is necessary.

5.4 Conclusion

A systematic approach to the training of a neural network model was described. It was found that even for a simple problem, finding a suitable neural network was not trivial. This drawback of the technique can outweigh the advantages, especially for complex problems. A comparison between neural networks and an interpolation technique was carried out for the first time. The interpolation technique showed superior accuracy and ease of implementation.

Appendix – Mathematical detail

A. Table of integrals

p and q are integers

Integral	Solution	
$\int_{-\frac{W}{2}}^{\frac{W}{2}} \mathrm{Cos}\left[\frac{m\pi}{a}(\Delta-\eta)\right] d\eta$	$\frac{2a}{m\pi}\mathrm{Cos}\left[\frac{m\pi\Delta}{a}\right]\mathrm{Sin}\left[\frac{m\pi W}{2a}\right], \quad m\neq 0$ $W, \quad m=0$	(A.1)
$\int_{-\frac{L}{2}}^{\frac{L}{2}} \mathrm{Sin}\left[\frac{q\pi}{L}\left(\xi+\frac{L}{2}\right)\right] e^{-\Gamma_{mn}\xi} d\xi$	$\frac{L\pi q}{\pi^2 q^2+L^2\Gamma_{mn}{}^2}\left\{e^{\frac{L}{2}\Gamma_{mn}}-\mathrm{Cos}[\pi q]\, e^{-\frac{L}{2}\Gamma_{mn}}\right\}$	(A.2)
$\int_{-\frac{L}{2}}^{\frac{L}{2}} \mathrm{Sin}\left[\frac{q\pi}{L}\left(\xi+\frac{L}{2}\right)\right] e^{\Gamma_{mn}\xi} d\xi$	$\frac{L\pi q}{\pi^2 q^2+L^2\Gamma_{mn}{}^2}\left\{e^{-\frac{L}{2}\Gamma_{mn}}-\mathrm{Cos}[\pi q]\, e^{\frac{L}{2}\Gamma_{mn}}\right\}$	(A.3)
$\int_{-\frac{L}{2}}^{\frac{L}{2}} \mathrm{Sin}\left[\frac{p\pi}{L}\left(\xi'+\frac{L}{2}\right)\right] e^{-\Gamma_{mn}\lvert\xi-\xi'\rvert} d\xi'$	$\frac{L}{p^2\pi^2+L^2\Gamma_{mn}{}^2}\left\{2L\Gamma_{mn}\mathrm{Sin}\left[\frac{p\pi}{L}\xi+\frac{p\pi}{2}\right]\right.$ $\left.+p\pi e^{-\Gamma_{mn}\left(\xi+\frac{L}{2}\right)}-p\pi\mathrm{Cos}[p\pi]\, e^{\Gamma_{mn}\left(\xi-\frac{L}{2}\right)}\right\}$	(A.4)
$\int_{-\frac{L}{2}}^{\frac{L}{2}} \mathrm{Sin}\left[\frac{q\pi}{L}\left(\xi+\frac{L}{2}\right)\right]\mathrm{Sin}\left[\frac{p\pi}{L}\left(\xi+\frac{L}{2}\right)\right] d\xi$	$\frac{L}{2}\delta_{pq}$	(A.5)
$\int_{-\frac{W}{2}}^{\frac{W}{2}} e^{\Gamma_{mn}\eta} d\eta$	$\frac{2}{\Gamma_{mn}}\mathrm{Sinh}\left[\frac{W}{2}\Gamma_{mn}\right]$	(A.6)
$\int_{-\frac{W}{2}}^{\frac{W}{2}} e^{-\Gamma_{mn}\eta'} d\eta'$	$\frac{2}{\Gamma_{mn}}\mathrm{Sinh}\left[\frac{W}{2}\Gamma_{mn}\right]$	(A.7)

$$\int_{-\frac{W}{2}}^{\frac{W}{2}} e^{-\Gamma_{mn}|-\eta+\eta'|}\, d\eta' \qquad \frac{2}{\Gamma_{mn}}\left(1 - e^{-\frac{W}{2}\Gamma_{mn}}\,\mathrm{Cosh}[\eta\Gamma_{mn}]\right) \tag{A.8}$$

$$\int_{-\frac{L}{2}}^{\frac{L}{2}} \mathrm{Sin}\left[\frac{q\pi}{L}\left(\xi + \frac{L}{2}\right)\right]\mathrm{Sin}\left[\frac{m\pi}{a}(\Delta - \xi)\right] d\xi$$

$$-\frac{aL}{\pi(a^2q^2 - L^2m^2)}\left((Lm + aq)\,\mathrm{Cos}\left[\frac{\pi q}{2} + \frac{m\pi\Delta}{a}\right]\mathrm{Sin}\left[\frac{\pi q}{2} - \frac{m\pi L}{2a}\right]\right.$$

$$\left. + (Lm - aq)\,\mathrm{Cos}\left[\frac{\pi q}{2} - \frac{m\pi\Delta}{a}\right]\mathrm{Sin}\left[\frac{\pi q}{2} + \frac{m\pi L}{2a}\right]\right),\quad Lm \neq aq$$

$$-\frac{L}{2}\,\mathrm{Cos}\left[\frac{q\pi}{2} + \frac{m\pi\Delta}{a}\right],\qquad Lm = aq \tag{A.9}$$

$$\int_{-\frac{W}{2}}^{\frac{W}{2}}\left(1 - e^{-\frac{W}{2}\Gamma_{mn}}\,\mathrm{Cosh}[\eta\Gamma_{mn}]\right) d\eta \qquad W - \frac{2}{\Gamma_{mn}}\, e^{-\frac{W}{2}\Gamma_{mn}}\,\mathrm{Sinh}\left[\frac{W}{2}\Gamma_{mn}\right] \tag{A.10}$$

B. Symmetry of the matrix components

The Lorentz Reciprocity Theorem [Collin 1991, Section 1.10] states for the case where $\mathbf{J}_e = 0$:

$$\oint_S (\mathbf{E}_1 \times \mathbf{H}_2 - \mathbf{E}_2 \times \mathbf{H}_1)\, d\mathbf{S} = \int_V (\mathbf{H}_1 \cdot \mathbf{J}_{m2} - \mathbf{H}_2 \cdot \mathbf{J}_{m1})\, dV \tag{B.1}$$

for a volume V surrounded by surface S and where the magnetic currents $\mathbf{J}_{mi}$ excite fields $\mathbf{E}_i$ and $\mathbf{H}_i$. If the volume V is the equivalent slot, then the surface S is a perfect electric conductor on which

$$\mathbf{n} \times \mathbf{E}_i = 0$$

if $\mathbf{n}$ is the unit vector normal to the surface S. The left-hand side of (B.1) is reduced to zero, and therefore

$$\int_V \mathbf{H}_1 \cdot \mathbf{J}_{m2}\, dV = \int_V \mathbf{H}_2 \cdot \mathbf{J}_{m1}\, dV.$$

Furthermore, the magnetic currents exist only on the surfaces S_1 and S_2, and are known to be $\mathbf{M}_1$ and $-\mathbf{M}_2$ respectively. Therefore

$$-\int_{S_2} \mathbf{H}_1 \cdot \mathbf{M}_2\, dS = \int_{S_1} \mathbf{H}_2 \cdot \mathbf{M}_1\, dS \tag{B.2}$$

The relevant matrix components can be written from (3.10) as

$$\begin{aligned} [Y_1^{32}]_{qp} &= -\int_{S_1} \mathbf{f}_q(\mathbf{r}) \cdot \mathbf{H}_2\, dS \\ [Y_2^{31}]_{qp} &= \int_{S_2} \mathbf{f}_q(\mathbf{r}) \cdot \mathbf{H}_1\, dS \end{aligned} \tag{B.3}$$

Since M_1 and M_2 consist of the same basis functions f_p, which are also the weighting functions f_q, (B.3) can be written in the form

$$\begin{aligned} [Y_1^{32}]_{qp} &= -\int_{S_1} \mathbf{M}_1 \cdot \mathbf{H}_2\, dS \\ [Y_2^{31}]_{qp} &= \int_{S_2} \mathbf{M}_2 \cdot \mathbf{H}_1\, dS \end{aligned}$$

It follows from (B.2) that $\left[\mathbf{Y}_1^{32}\right] = \left[\mathbf{Y}_2^{31}\right]$.

C. Derivation of matrix components for a longitudinal slot

The equations for the matrix components of equation (3.9) as given in (3.40.2) - (3.40.5) can be simplified for the case of the longitudinal slot shown in Figure 3.4 by setting $\theta = 0°$. The detail of that simplification is presented in this section and the resulting equations are repeated in Section 3.6.

The matrix equation and its general solution are:

(3.9):
$$\begin{bmatrix} [Y_1^{11}]+[Y_1^{31}] & [Y_1^{32}] \\ [Y_2^{31}] & [Y_2^{32}]+[Y_2^{22}] \end{bmatrix} \begin{bmatrix} [A] \\ [B] \end{bmatrix} = \begin{bmatrix} [H] \\ [0] \end{bmatrix} \tag{C.1}$$

(3.40.2):
$$[H]_q = \frac{2}{W}\sqrt{\frac{\beta_{10}}{abkZ_0}}\, e^{\Gamma_{10} z_i} \int_{-\frac{L}{2}}^{\frac{L}{2}} \int_{-\frac{W}{2}}^{\frac{W}{2}} e^{-\Gamma_{10}(\mathrm{Cos}[\theta]\xi - \mathrm{Sin}[\theta]\eta)} \mathrm{Sin}\left[\frac{q\pi}{L}\left(\xi + \frac{L}{2}\right)\right]$$
$$\times \Big\{ -\mathrm{Sin}[\theta]\,\mathrm{Sin}\left[\frac{\pi}{a}(-\mathrm{Sin}[\theta]\xi - \mathrm{Cos}[\theta]\eta + \Delta)\right]$$
$$- j\frac{\pi}{a}\frac{1}{\beta_{10}}\,\mathrm{Cos}[\theta]\,\mathrm{Cos}\left[\frac{\pi}{a}(-\mathrm{Sin}[\theta]\xi - \mathrm{Cos}[\theta]\eta + \Delta)\right] \Big\} d\eta\, d\xi \tag{C.2}$$

(3.40.3):
$$[Y_2^{32}]_{qp} = [Y_1^{31}]_{qp} = -\frac{jkL}{2WZ_0}\left(1 - \left(\frac{p\pi}{kL}\right)^2\right)\frac{\mathrm{Cos}[k_{zp}T]}{k_{zp}\,\mathrm{Sin}[k_{zp}T]}\,\delta_{pq} \tag{C.3}$$

(3.40.4):
$$[Y_1^{32}]_{qp} = [Y_2^{31}]_{qp} = \frac{jkL}{2WZ_0}\left(1 - \left(\frac{p\pi}{kL}\right)^2\right)\frac{1}{k_{zp}\,\mathrm{Sin}[k_{zp}T]}\,\delta_{pq} \tag{C.4}$$

(3.40.5):
$$[Y_1^{11}]_{qp} = [Y_2^{22}]_{qp} = \frac{j}{2W^2 ab\omega\mu}\sum_{m=0}^{\infty}\sum_{n=0}^{\infty}\frac{\epsilon_{0m}\epsilon_{0n}}{\Gamma_{mn}}\int_S \mathrm{Sin}\left[\frac{q\pi}{L}\left(\xi + \frac{L}{2}\right)\right][-\mathrm{Sin}[\theta]\ \mathrm{Cos}[\theta]]$$
$$* \begin{bmatrix} \frac{\partial^2}{\partial x^2} + k^2 & \frac{\partial^2}{\partial z\,\partial x} \\ \frac{\partial^2}{\partial z\,\partial x} & \frac{\partial^2}{\partial z^2} + k^2 \end{bmatrix} \begin{bmatrix} -\mathrm{Sin}[\theta]\,S_x \int_S \mathrm{Sin}\left[\frac{p\pi}{L}\left(\xi' + \frac{L}{2}\right)\right] e^{-\Gamma_{mn}|z-z'|} S_x'\, dS' \\ \mathrm{Cos}[\theta]\,C_x \int_S \mathrm{Sin}\left[\frac{p\pi}{L}\left(\xi' + \frac{L}{2}\right)\right] e^{-\Gamma_{mn}|z-z'|} C_x'\, dS' \end{bmatrix} dS \tag{C.5}$$

The four components given in (C.3) and (C.4) are not functions of θ and therefore remain unchanged, but the other components need to be simplified. The incident field is computed first. Setting $\theta = 0°$ in (C.2), gives:

$$[H]_q = -\frac{2\,j\pi}{W\,a\,\beta_{10}}\sqrt{\frac{\beta_{10}}{a\,b\,k\,Z_0}}\;e^{\Gamma_{10}\,z_i}\int_{-\frac{L}{2}}^{\frac{L}{2}}\mathrm{Sin}\left[\frac{q\pi}{L}\left(\xi+\frac{L}{2}\right)\right]e^{-\Gamma_{10}\,\xi}\,d\xi\int_{-\frac{W}{2}}^{\frac{W}{2}}\mathrm{Cos}\left[\frac{\pi}{a}(\Delta-\eta)\right]d\eta$$

which can be evaluated using integrals (A.1) and (A.2) from Appendix A:

$$[H]_q = -\frac{j4\pi q\,L}{W}\;\frac{e^{\Gamma_{10}\,z_i}}{\sqrt{a\,b\,k\,Z_0\,\beta_{10}}}\;\mathrm{Cos}\left[\frac{\pi\Delta}{a}\right]\mathrm{Sin}\left[\frac{\pi W}{2\,a}\right]\frac{e^{\Gamma_{10}\frac{L}{2}}-(-1)^q e^{-\Gamma_{10}\frac{L}{2}}}{\pi^2 q^2+L^2\,\Gamma_{10}{}^2} \qquad \text{(C.6)}$$

This is the final expression for the incident field component.

In order to compute $\left[\mathbf{Y}_1^{11}\right]$ and $\left[\mathbf{Y}_2^{22}\right]$, set $\theta = 0°$ in (C.5):

$$[Y_1^{11}]_{qp} = \frac{j}{2W^2 ab\,\omega\mu}\sum_{m=0}^{\infty}\sum_{n=0}^{\infty}\frac{\epsilon_{0m}\,\epsilon_{0n}}{\Gamma_{mn}}\int_{S_1}\mathrm{Sin}\left[\frac{q\pi}{L}\left(\xi+\frac{L}{2}\right)\right][0\;\;1]$$

$$*\begin{bmatrix}\frac{\partial^2}{\partial x^2}+k^2 & \frac{\partial^2}{\partial z\,\partial x}\\ \frac{\partial^2}{\partial z\,\partial x} & \frac{\partial^2}{\partial z^2}+k^2\end{bmatrix}\begin{bmatrix}0\\ C_x\int_{S_1}\mathrm{Sin}\left[\frac{p\pi}{L}\left(\xi'+\frac{L}{2}\right)\right]e^{-\Gamma_{mn}|z-z'|}\,C_x'\,dS'\end{bmatrix}dS$$

Matrix multiplication gives:

$$[Y_1^{11}]_{qp} = \frac{j}{2W^2 ab\,\omega\mu}\sum_{m=0}^{\infty}\sum_{n=0}^{\infty}\frac{\epsilon_{0m}\,\epsilon_{0n}}{\Gamma_{mn}}\int_{S_1}\mathrm{Sin}\left[\frac{q\pi}{L}\left(\xi+\frac{L}{2}\right)\right]$$

$$*\left(\frac{\partial^2}{\partial z^2}+k^2\right)C_x\int_{S_1}\mathrm{Sin}\left[\frac{p\pi}{L}\left(\xi'+\frac{L}{2}\right)\right]e^{-\Gamma_{mn}|z-z'|}\,C_x'\,dS'\,dS$$

Convert all the variables to integration coordinates, using equations from Table 3.2 with $\theta = 0°$:

$$[Y_1^{11}]_{qp} = \frac{j}{2W^2 ab\,\omega\mu}\sum_{m=0}^{\infty}\sum_{n=0}^{\infty}\frac{\epsilon_{0m}\,\epsilon_{0n}}{\Gamma_{mn}}$$

$$*\int_{-\frac{L}{2}}^{\frac{L}{2}}\int_{-\frac{W}{2}}^{\frac{W}{2}}\mathrm{Sin}\left[\frac{q\pi}{L}\left(\xi+\frac{L}{2}\right)\right]\mathrm{Cos}\left[\frac{m\pi}{a}(\Delta-\eta)\right]\left(\frac{\partial^2}{\partial\xi^2}+k^2\right)$$

$$*\left(\int_{-\frac{W}{2}}^{\frac{W}{2}}\mathrm{Cos}\left[\frac{m\pi}{a}(\Delta-\eta')\right]d\eta'\int_{-\frac{L}{2}}^{\frac{L}{2}}\mathrm{Sin}\left[\frac{p\pi}{L}\left(\xi'+\frac{L}{2}\right)\right]e^{-\Gamma_{mn}|\xi-\xi'|}\,d\xi'\right)d\eta\,d\xi$$

Use integrals (A.1) and (A.4) from Appendix A to solve the integration of the primed variables:

$$[Y_1^{11}]_{qp} = \frac{j2aL}{W^2 ab\pi\omega\mu}\sum_{m=1}^{\infty}\sum_{n=0}^{\infty}\frac{\epsilon_{0n}}{m\Gamma_{mn}}\mathrm{Cos}\left[\frac{m\pi\Delta}{a}\right]\mathrm{Sin}\left[\frac{m\pi W}{2a}\right]\frac{1}{p^2\pi^2+L^2\Gamma_{mn}{}^2}$$

$$*\int_{-\frac{W}{2}}^{\frac{W}{2}}\mathrm{Cos}\left[\frac{m\pi}{a}(\Delta-\eta)\right]d\eta\int_{-\frac{L}{2}}^{\frac{L}{2}}\mathrm{Sin}\left[\frac{q\pi}{L}\left(\xi+\frac{L}{2}\right)\right]\left(\frac{\partial^2}{\partial\xi^2}+k^2\right)$$

$$*\left(2L\Gamma_{mn}\mathrm{Sin}\left[\frac{p\pi}{L}\xi+\frac{p\pi}{2}\right]+p\pi e^{-\Gamma_{mn}\left(\xi+\frac{L}{2}\right)}-p\pi\mathrm{Cos}[p\pi]e^{\Gamma_{mn}\left(\xi-\frac{L}{2}\right)}\right)d\xi$$

$$+\frac{jL}{2Wab\omega\mu}\sum_{n=0}^{\infty}\frac{\epsilon_{0n}}{\Gamma_{0n}}\frac{1}{p^2\pi^2+L^2\Gamma_{0n}{}^2}\int_{-\frac{L}{2}}^{\frac{L}{2}}\int_{-\frac{W}{2}}^{\frac{W}{2}}\mathrm{Sin}\left[\frac{q\pi}{L}\left(\xi+\frac{L}{2}\right)\right]$$

$$*\left(\frac{\partial^2}{\partial\xi^2}+k^2\right)\left(2L\Gamma_{0n}\mathrm{Sin}\left[\frac{p\pi}{L}\xi+\frac{p\pi}{2}\right]+p\pi e^{-\Gamma_{0n}\left(\xi+\frac{L}{2}\right)}\right.$$

$$\left.-p\pi\mathrm{Cos}[p\pi]e^{\Gamma_{0n}\left(\xi-\frac{L}{2}\right)}\right)d\eta d\xi$$

In the course of evaluating the integrals, distinction has been made between the cases m = 0 and m ≠ 0, as can be seen in the summation formulation.

The integrals over η and the derivatives with respect to ξ are evaluated next:

$$[Y_1^{11}]_{qp} = \frac{j4aL}{W^2 b\pi^2\omega\mu}\sum_{m=1}^{\infty}\sum_{n=0}^{\infty}\frac{\epsilon_{0n}}{m^2\Gamma_{mn}}\mathrm{Cos}^2\left[\frac{m\pi\Delta}{a}\right]\mathrm{Sin}^2\left[\frac{m\pi W}{2a}\right]\frac{1}{p^2\pi^2+L^2\Gamma_{mn}{}^2}$$

$$*\int_{-\frac{L}{2}}^{\frac{L}{2}}\mathrm{Sin}\left[\frac{q\pi}{L}\left(\xi+\frac{L}{2}\right)\right]\left(2\Gamma_{mn}L\left(k^2-\left(\frac{p\pi}{L}\right)^2\right)\mathrm{Sin}\left[\frac{p\pi}{L}\xi+\frac{p\pi}{2}\right]\right.$$

$$\left.+p\pi\left(\Gamma_{mn}{}^2+k^2\right)\left(e^{-\Gamma_{mn}\left(\xi+\frac{L}{2}\right)}-\mathrm{Cos}[p\pi]e^{\Gamma_{mn}\left(\xi-\frac{L}{2}\right)}\right)\right)d\xi$$

$$+\frac{jL}{2ab\omega\mu}\sum_{n=0}^{\infty}\frac{\epsilon_{0n}}{\Gamma_{0n}}\frac{1}{p^2\pi^2+L^2\Gamma_{0n}{}^2}\int_{-\frac{L}{2}}^{\frac{L}{2}}\mathrm{Sin}\left[\frac{q\pi}{L}\left(\xi+\frac{L}{2}\right)\right]$$

$$*\left(2\Gamma_{0m}L\left(k^2-\left(\frac{p\pi}{L}\right)^2\right)\mathrm{Sin}\left[\frac{p\pi}{L}\xi+\frac{p\pi}{2}\right]\right.$$

$$\left.+p\pi\left(\Gamma_{0n}{}^2+k^2\right)\left(e^{-\Gamma_{0n}\left(\xi+\frac{L}{2}\right)}-\mathrm{Cos}[p\pi]e^{\Gamma_{0n}\left(\xi-\frac{L}{2}\right)}\right)\right)d\xi$$

The remaining integral is broken up into smaller parts:

$$[Y_1^{11}]_{qp} = \frac{j4aL}{W^2 b \pi^2 \omega\mu} \sum_{m=1}^{\infty}\sum_{n=0}^{\infty} \frac{\epsilon_{0n}}{m^2 \Gamma_{mn}} \mathrm{Cos}^2\left[\frac{m\pi\Delta}{a}\right] \mathrm{Sin}^2\left[\frac{m\pi W}{2a}\right] \frac{1}{p^2\pi^2 + L^2\Gamma_{mn}{}^2}$$

$$* \Bigg(2\Gamma_{mn} L\left(k^2 - \left(\frac{p\pi}{L}\right)^2\right) \int_{-\frac{L}{2}}^{\frac{L}{2}} \mathrm{Sin}\left[\frac{q\pi}{L}\left(\xi + \frac{L}{2}\right)\right] \mathrm{Sin}\left[\frac{p\pi}{L}\left(\xi + \frac{L}{2}\right)\right] d\xi$$

$$+ p\pi\left(\Gamma_{mn}{}^2 + k^2\right) e^{-\Gamma_{mn}\frac{L}{2}} \int_{-\frac{L}{2}}^{\frac{L}{2}} \mathrm{Sin}\left[\frac{q\pi}{L}\left(\xi + \frac{L}{2}\right)\right] e^{-\Gamma_{mn}\xi} d\xi$$

$$- \mathrm{Cos}[p\pi]\, p\pi\left(\Gamma_{mn}{}^2 + k^2\right) e^{-\Gamma_{mn}\frac{L}{2}} \int_{-\frac{L}{2}}^{\frac{L}{2}} \mathrm{Sin}\left[\frac{q\pi}{L}\left(\xi + \frac{L}{2}\right)\right] e^{\Gamma_{mn}\xi} d\xi \Bigg)$$

$$+ \frac{jL}{2ab\omega\mu} \sum_{n=0}^{\infty} \frac{\epsilon_{0n}}{\Gamma_{0n}} \frac{1}{p^2\pi^2 + L^2\Gamma_{0n}{}^2}$$

$$* \Bigg(2\Gamma_{0n} L\left(k^2 - \left(\frac{p\pi}{L}\right)^2\right) \int_{-\frac{L}{2}}^{\frac{L}{2}} \mathrm{Sin}\left[\frac{q\pi}{L}\left(\xi + \frac{L}{2}\right)\right] \mathrm{Sin}\left[\frac{p\pi}{L}\left(\xi + \frac{L}{2}\right)\right] d\xi$$

$$+ p\pi\left(\Gamma_{0n}{}^2 + k^2\right) e^{-\Gamma_{0n}\frac{L}{2}} \int_{-\frac{L}{2}}^{\frac{L}{2}} \mathrm{Sin}\left[\frac{q\pi}{L}\left(\xi + \frac{L}{2}\right)\right] e^{-\Gamma_{0n}\xi} d\xi$$

$$- \mathrm{Cos}[p\pi]\, p\pi\left(\Gamma_{0n}{}^2 + k^2\right) e^{-\Gamma_{0n}\frac{L}{2}} \int_{-\frac{L}{2}}^{\frac{L}{2}} \mathrm{Sin}\left[\frac{q\pi}{L}\left(\xi + \frac{L}{2}\right)\right] e^{\Gamma_{0n}\xi} d\xi \Bigg)$$

The integrals are solved using (A.2), (A.3) and (A.5) from Appendix A, as well as the fact that

$$\mathrm{Cos}[n\pi] = (-1)^n$$

if n is an integer.

$$[Y_1^{11}]_{qp} = \frac{j4aL^2}{W^2 b \pi^2 \omega\mu} \sum_{m=1}^{\infty}\sum_{n=0}^{\infty} \frac{\epsilon_{0n}}{m^2 \Gamma_{mn}} \mathrm{Cos}^2\left[\frac{m\pi\Delta}{a}\right] \mathrm{Sin}^2\left[\frac{m\pi W}{2a}\right] \frac{1}{p^2\pi^2 + L^2\Gamma_{mn}{}^2}$$

$$* \Bigg(pq\pi^2 \frac{\Gamma_{mn}{}^2 + k^2}{\pi^2 q^2 + L^2\Gamma_{mn}{}^2} \left(1 - ((-1)^q + (-1)^p) e^{-\Gamma_{mn} L} + (-1)^{p+q}\right)$$

$$+ \Gamma_{mn} L\left(k^2 - \left(\frac{p\pi}{L}\right)^2\right) \delta_{pq} \Bigg)$$

$$+ \frac{jL^2}{2ab\omega\mu} \sum_{n=0}^{\infty} \frac{\epsilon_{0n}}{\Gamma_{0n}} \frac{1}{p^2\pi^2 + L^2\Gamma_{0n}{}^2} \Bigg(\Gamma_{0n} L\left(k^2 - \left(\frac{p\pi}{L}\right)^2\right) \delta_{pq}$$

$$+ pq\pi^2 \frac{\Gamma_{0n}{}^2 + k^2}{\pi^2 q^2 + L^2\Gamma_{0n}{}^2} \left(1 - ((-1)^q + (-1)^p) e^{-\Gamma_{0n} L} + (-1)^{p+q}\right) \Bigg) \qquad \text{(C.7)}$$

Since $\left[\mathbf{Y}_2^{22}\right]=\left[\mathbf{Y}_1^{11}\right]$, this completes the derivation of the matrix elements for the longitudinal slot. The complete set of simplified matrix components is:

$$(C.6): \quad [H]_q = -\frac{j4\pi q L}{W}\frac{e^{\Gamma_{10} z_i}}{\sqrt{abkZ_0\beta_{10}}}\mathrm{Cos}\left[\frac{\pi\Delta}{a}\right]\mathrm{Sin}\left[\frac{\pi W}{2a}\right]\frac{e^{\Gamma_{10}\frac{L}{2}}-(-1)^q e^{-\Gamma_{10}\frac{L}{2}}}{\pi^2 q^2 + L^2\Gamma_{10}{}^2}$$

$$(C.3): \quad [Y_2^{32}]_{qp} = [Y_1^{31}]_{qp} = -\frac{jkL}{2WZ_0}\left(1-\left(\frac{p\pi}{kL}\right)^2\right)\frac{\mathrm{Cos}[k_{zp}T]}{k_{zp}\,\mathrm{Sin}[k_{zp}T]}\delta_{pq}$$

$$(C.4): \quad [Y_1^{32}]_{qp} = [Y_2^{31}]_{qp} = \frac{jkL}{2WZ_0}\left(1-\left(\frac{p\pi}{kL}\right)^2\right)\frac{1}{k_{zp}\,\mathrm{Sin}[k_{zp}T]}\delta_{pq}$$

$$(C.7): \quad [Y_1^{11}]_{qp} = [Y_2^{22}]_{qp} = \frac{j4aL^2}{W^2 b\pi^2\omega\mu}\sum_{m=1}^{\infty}\sum_{n=0}^{\infty}\frac{\epsilon_{0n}}{m^2\Gamma_{mn}}\mathrm{Cos}^2\left[\frac{m\pi\Delta}{a}\right]\mathrm{Sin}^2\left[\frac{m\pi W}{2a}\right]$$

$$* \frac{1}{p^2\pi^2 + L^2\Gamma_{mn}{}^2}\left\{\Gamma_{mn}L\left(k^2-\left(\frac{p\pi}{L}\right)^2\right)\delta_{pq}\right.$$

$$\left. + pq\pi^2\frac{\Gamma_{mn}{}^2 + k^2}{\pi^2 q^2 + L^2\Gamma_{mn}{}^2}\left(1-((-1)^q+(-1)^p)e^{-\Gamma_{mn}L}+(-1)^{p+q}\right)\right\}$$

$$+\frac{jL^2}{2ab\omega\mu}\sum_{n=0}^{\infty}\frac{\epsilon_{0n}}{\Gamma_{0n}}\frac{1}{p^2\pi^2 + L^2\Gamma_{0n}{}^2}\left\{\Gamma_{0n}L\left(k^2-\left(\frac{p\pi}{L}\right)^2\right)\delta_{pq}\right.$$

$$\left. + pq\pi^2\frac{\Gamma_{0n}{}^2 + k^2}{\pi^2 q^2 + L^2\Gamma_{0n}{}^2}\left(1-((-1)^q+(-1)^p)e^{-\Gamma_{0n}L}+(-1)^{p+q}\right)\right\}$$

The s-parameters for the longitudinal slot can be obtained by substituting

$$\theta = 0°$$
$$x = \Delta - \eta$$
$$z = \xi$$

into (3.47) which are the equations for the scattering parameters for the general slot.

The resulting equations are:

$$S_{11} = \frac{j}{2W\sqrt{abkZ_0\beta_{10}}}\frac{\pi}{a}e^{\Gamma_{10}z_i}\sum_{p=1}^{N}A_p\int_{-\frac{W}{2}}^{\frac{W}{2}}\mathrm{Cos}\left[\frac{\pi}{a}(\Delta-\eta')\right]d\eta'$$

$$* \int_{-\frac{L}{2}}^{\frac{L}{2}}\mathrm{Sin}\left[\frac{p\pi}{L}\left(\xi'+\frac{L}{2}\right)\right]e^{-\Gamma_{10}\xi'}\,d\xi'$$

$$S_{21} = e^{-\Gamma_{10}(z_2 - z_i)} - \frac{j}{2W\sqrt{abkZ_0\beta_{10}}} \frac{\pi}{a} e^{-\Gamma_{10} z_2} \sum_{p=1}^{N} A_p \int_{-\frac{W}{2}}^{\frac{W}{2}} \mathrm{Cos}\left[\frac{\pi}{a}(\Delta - \eta')\right] d\eta'$$

$$* \int_{-\frac{L}{2}}^{\frac{L}{2}} \mathrm{Sin}\left[\frac{p\pi}{L}\left(\xi' + \frac{L}{2}\right)\right] e^{\Gamma_{10}\xi'} d\xi'$$

$$S_{31} = \frac{j}{2W\sqrt{abkZ_0\beta_{10}}} \frac{\pi}{a} e^{-\Gamma_{10} z_3} \sum_{p=1}^{N} B_p \int_{-\frac{W}{2}}^{\frac{W}{2}} \mathrm{Cos}\left[\frac{\pi}{a}(\Delta - \eta')\right] d\eta'$$

$$* \int_{-\frac{L}{2}}^{\frac{L}{2}} \mathrm{Sin}\left[\frac{p\pi}{L}\left(\xi' + \frac{L}{2}\right)\right] e^{\Gamma_{10}\xi'} d\xi'$$

$$S_{41} = -\frac{j}{2W\sqrt{abkZ_0\beta_{10}}} \frac{\pi}{a} e^{\Gamma_{10} z_4} \sum_{p=1}^{N} B_p \int_{-\frac{W}{2}}^{\frac{W}{2}} \mathrm{Cos}\left[\frac{\pi}{a}(\Delta - \eta')\right] d\eta'$$

$$* \int_{-\frac{L}{2}}^{\frac{L}{2}} \mathrm{Sin}\left[\frac{p\pi}{L}\left(\xi' + \frac{L}{2}\right)\right] e^{-\Gamma_{10}\xi'} d\xi'$$

Analytical integration can be carried out using the integral formulas (A.1), (A.2) and (A.3) from Appendix A. The final equations for the scattering parameters are:

$$S_{11} = \frac{j}{W\sqrt{abkZ_0\beta_{10}}} \mathrm{Cos}\left[\frac{\pi\Delta}{a}\right] \mathrm{Sin}\left[\frac{\pi W}{2a}\right] e^{\Gamma_{10} z_i}$$

$$* \sum_{p=1}^{N} A_p \frac{\pi p L}{\pi^2 p^2 + L^2 \Gamma_{10}^2} \left(e^{\frac{L}{2}\Gamma_{10}} - (-1)^p e^{-\frac{L}{2}\Gamma_{10}}\right)$$

$$S_{21} = e^{-\Gamma_{10}(z_2 - z_i)} - \frac{j}{W\sqrt{abkZ_0\beta_{10}}} \mathrm{Cos}\left[\frac{\pi\Delta}{a}\right] \mathrm{Sin}\left[\frac{\pi W}{2a}\right] e^{-\Gamma_{10} z_2}$$

$$* \sum_{p=1}^{N} A_p \frac{L\pi p}{\pi^2 p^2 + L^2 \Gamma_{10}^2} \left(e^{-\frac{L}{2}\Gamma_{10}} - (-1)^p e^{\frac{L}{2}\Gamma_{10}}\right)$$

$$S_{31} = \frac{j}{W\sqrt{abkZ_0\beta_{10}}} \mathrm{Cos}\left[\frac{\pi\Delta}{a}\right] \mathrm{Sin}\left[\frac{\pi W}{2a}\right] e^{-\Gamma_{10} z_3}$$

$$* \sum_{p=1}^{N} B_p \frac{L\pi p}{\pi^2 p^2 + L^2 \Gamma_{10}^2} \left(e^{-\frac{L}{2}\Gamma_{10}} - (-1)^p e^{\frac{L}{2}\Gamma_{10}}\right)$$

$$S_{41} = -\frac{j}{W\sqrt{a\,b\,k\,Z_0\,\beta_{10}}}\,\mathrm{Cos}\left[\frac{\pi\Delta}{a}\right]\mathrm{Sin}\left[\frac{\pi W}{2\,a}\right]e^{\Gamma_{10}\,z_4}$$

$$*\sum_{p=1}^{N} B_p\,\frac{\pi\,p\,L}{\pi^2 p^2 + L^2\Gamma_{10}{}^2}\left(e^{\frac{L}{2}\Gamma_{10}} - (-1)^p e^{-\frac{L}{2}\Gamma_{10}}\right)$$

D. Derivation of matrix components for a transverse slot

To solve the matrix elements for the transverse slot shown in Figure 3.7, it is necessary to set $\theta = 90°$ in the equations for the general slot that was repeated in Appendix C.

For the incident field, set $\theta = 90°$ in (C.2):

$$[H]_q = -\frac{2}{W}\sqrt{\frac{\beta_{10}}{abkZ_0}}\, e^{\Gamma_{10} z_i} \int_{-\frac{W}{2}}^{\frac{W}{2}} e^{\Gamma_{10}\eta}\, d\eta \int_{-\frac{L}{2}}^{\frac{L}{2}} \mathrm{Sin}\left[\frac{q\pi}{L}\left(\xi + \frac{L}{2}\right)\right] \mathrm{Sin}\left[\frac{\pi}{a}(\Delta - \xi)\right] d\xi$$

which can be evaluated using integrals (A.6) and (A.9) from Appendix A:

$$[H]_q = \frac{4}{\Gamma_{10}}\frac{L}{W}\sqrt{\frac{\beta_{10}}{abkZ_0}}\, \mathrm{Sinh}\left[\frac{W}{2}\Gamma_{10}\right] e^{\Gamma_{10} z_i} * \begin{cases} \frac{a}{\pi(a^2q^2 - L^2)}\left((L + aq)\mathrm{Cos}\left[\frac{\pi q}{2} + \frac{\pi\Delta}{a}\right]\mathrm{Sin}\left[\frac{\pi q}{2} - \frac{\pi L}{2a}\right]\right. \\ \qquad \left. + (L - aq)\mathrm{Cos}\left[\frac{\pi q}{2} - \frac{\pi\Delta}{a}\right]\mathrm{Sin}\left[\frac{\pi q}{2} + \frac{\pi L}{2a}\right]\right), & L \neq aq \\ \frac{1}{2}\mathrm{Cos}\left[\frac{q\pi}{2} + \frac{\pi\Delta}{a}\right], & L = aq \end{cases} \tag{D.1}$$

This is the final expression for the incident field component. The only other components dependent on θ are $\left[Y_1^{11}\right]$ and $\left[Y_2^{22}\right]$, which can be computed by setting $\theta = 90°$ in (C.5):

$$[Y_1^{11}]_{qp} = \frac{j}{2W^2 ab\omega\mu}\sum_{m=0}^{\infty}\sum_{n=0}^{\infty}\frac{\epsilon_{0m}\epsilon_{0n}}{\Gamma_{mn}}\int_S \mathrm{Sin}\left[\frac{q\pi}{L}\left(\xi + \frac{L}{2}\right)\right][-1\ \ 0] * \begin{bmatrix} \frac{\partial^2}{\partial x^2} + k^2 & \frac{\partial^2}{\partial z\,\partial x} \\ \frac{\partial^2}{\partial z\,\partial x} & \frac{\partial^2}{\partial z^2} + k^2 \end{bmatrix} \begin{bmatrix} -S_x \int_S \mathrm{Sin}\left[\frac{p\pi}{L}\left(\xi' + \frac{L}{2}\right)\right] e^{-\Gamma_{mn}|z - z'|} S_x'\, dS' \\ 0 \end{bmatrix} dS$$

Matrix multiplication gives

$$[Y_1^{11}]_{qp} = \frac{j}{2W^2 ab\omega\mu}\sum_{m=0}^{\infty}\sum_{n=0}^{\infty}\frac{\epsilon_{0m}\epsilon_{0n}}{\Gamma_{mn}}\int_S \mathrm{Sin}\left[\frac{q\pi}{L}\left(\xi + \frac{L}{2}\right)\right] * \left(\frac{\partial^2}{\partial x^2} + k^2\right)\left(S_x \int_S \mathrm{Sin}\left[\frac{p\pi}{L}\left(\xi' + \frac{L}{2}\right)\right] e^{-\Gamma_{mn}|z - z'|} S_x'\, dS'\right) dS$$

Convert all the variables to integration coordinates, using equations from Table 3.2 with $\theta = 90°$:

$$[Y_1^{11}]_{qp} = \frac{j}{2W^2 ab\omega\mu}\sum_{m=0}^{\infty}\sum_{n=0}^{\infty}\frac{\epsilon_{0m}\epsilon_{0n}}{\Gamma_{mn}}\int_{-\frac{L}{2}}^{\frac{L}{2}}\int_{-\frac{W}{2}}^{\frac{W}{2}}\mathrm{Sin}\left[\frac{q\pi}{L}\left(\xi+\frac{L}{2}\right)\right]$$

$$*\int_{-\frac{W}{2}}^{\frac{W}{2}} e^{-\Gamma_{mn}|-\eta+\eta'|}\,d\eta'\int_{-\frac{L}{2}}^{\frac{L}{2}}\mathrm{Sin}\left[\frac{p\pi}{L}\left(\xi'+\frac{L}{2}\right)\right]\mathrm{Sin}\left[\frac{m\pi}{a}(\Delta-\xi')\right]d\xi'$$

$$*\left(\frac{\partial^2}{\partial\xi^2}+k^2\right)\mathrm{Sin}\left[\frac{m\pi}{a}(\Delta-\xi)\right]d\eta\,d\xi$$

Use integrals (A.9) and (A.8) from Appendix A to solve the integration of the primed variables:

$$[Y_1^{11}]_{qp} = \frac{j}{W^2 ab\omega\mu}\sum_{m=0}^{\infty}\sum_{n=0}^{\infty}\frac{\epsilon_{0m}\epsilon_{0n}}{\Gamma_{mn}^2}\int_{-\frac{W}{2}}^{\frac{W}{2}}\left(1-e^{-\frac{W}{2}\Gamma_{mn}}\mathrm{Cosh}[\eta\Gamma_{mn}]\right)d\eta$$

$$*\int_{-\frac{L}{2}}^{\frac{L}{2}}\mathrm{Sin}\left[\frac{q\pi}{L}\left(\xi+\frac{L}{2}\right)\right]\left(\frac{\partial^2}{\partial\xi^2}+k^2\right)\left(\mathrm{Sin}\left[\frac{m\pi}{a}(\Delta-\xi)\right]\right)d\xi$$

$$*\begin{cases} -\frac{aL}{\pi(a^2p^2-L^2m^2)}\left((Lm+ap)\mathrm{Cos}\left[\frac{\pi p}{2}+\frac{m\pi\Delta}{a}\right]\mathrm{Sin}\left[\frac{\pi p}{2}-\frac{m\pi L}{2a}\right]\right. \\ \qquad\left.+(Lm-ap)\mathrm{Cos}\left[\frac{\pi p}{2}-\frac{m\pi\Delta}{a}\right]\mathrm{Sin}\left[\frac{\pi p}{2}+\frac{m\pi L}{2a}\right]\right), & Lm\neq ap \\ -\frac{L}{2}\mathrm{Cos}\left[\frac{p\pi}{2}+\frac{m\pi\Delta}{a}\right], & Lm=ap \end{cases}$$

The derivatives with respect to ξ are evaluated next, followed by the remaining integrals from (A.9) and (A.10) in Appendix A:

$$[Y_1^{11}]_{qp} = \frac{jL^2}{W^2 ab\omega\mu}\sum_{m=0}^{\infty}\sum_{n=0}^{\infty}\frac{\epsilon_{0m}\epsilon_{0n}}{\Gamma_{mn}^2}\left(k^2-\left(\frac{m\pi}{a}\right)^2\right)\sigma(p)\sigma(q)\left(W-\frac{2}{\Gamma_{mn}}e^{-\frac{W}{2}\Gamma_{mn}}\mathrm{Sinh}\left[\frac{W}{2}\Gamma_{mn}\right]\right)$$

(D.2.1)

where:

$$\sigma(p) = \begin{cases} \frac{a}{\pi(a^2p^2-L^2m^2)}\left((Lm+ap)\mathrm{Cos}\left[\frac{\pi p}{2}+\frac{m\pi\Delta}{a}\right]\mathrm{Sin}\left[\frac{\pi p}{2}-\frac{m\pi L}{2a}\right]\right. \\ \qquad\left.+(Lm-ap)\mathrm{Cos}\left[\frac{\pi p}{2}-\frac{m\pi\Delta}{a}\right]\mathrm{Sin}\left[\frac{\pi p}{2}+\frac{m\pi L}{2a}\right]\right), & Lm\neq ap \\ \frac{1}{2}\mathrm{Cos}\left[\frac{p\pi}{2}+\frac{m\pi\Delta}{a}\right], & Lm=ap \end{cases} \qquad \text{(D.2.2)}$$

This completes the derivation of the matrix elements for the transverse slot. The complete set of equations is given below:

$$[H]_q = \frac{4}{\Gamma_{10}} \frac{L}{W} \sqrt{\frac{\beta_{10}}{abkZ_0}} \operatorname{Sinh}\left[\frac{W}{2}\Gamma_{10}\right] e^{\Gamma_{10} z_i}$$

(D.1):
$$* \begin{cases} \frac{a}{\pi(a^2 q^2 - L^2)} \left((L + aq) \operatorname{Cos}\left[\frac{\pi q}{2} + \frac{\pi \Delta}{a}\right] \operatorname{Sin}\left[\frac{\pi q}{2} - \frac{\pi L}{2a}\right] \right. \\ \qquad \left. + (L - aq) \operatorname{Cos}\left[\frac{\pi q}{2} - \frac{\pi \Delta}{a}\right] \operatorname{Sin}\left[\frac{\pi q}{2} + \frac{\pi L}{2a}\right] \right), & L \neq aq \\ \frac{1}{2} \operatorname{Cos}\left[\frac{q\pi}{2} + \frac{\pi \Delta}{a}\right], & L = aq \end{cases}$$

(C.3):
$$[Y_2^{32}]_{qp} = [Y_1^{31}]_{qp} = -\frac{jkL}{2WZ_0} \left(1 - \left(\frac{p\pi}{kL}\right)^2\right) \frac{\operatorname{Cos}[k_{zp} T]}{k_{zp} \operatorname{Sin}[k_{zp} T]} \delta_{pq}$$

(C.4):
$$[Y_1^{32}]_{qp} = [Y_2^{31}]_{qp} = \frac{jkL}{2WZ_0} \left(1 - \left(\frac{p\pi}{kL}\right)^2\right) \frac{1}{k_{zp} \operatorname{Sin}[k_{zp} T]} \delta_{pq}$$

(D.2):
$$[Y_1^{11}]_{qp} = [Y_2^{22}]_{qp} = \frac{jL^2}{W^2 ab\omega\mu} \sum_{m=0}^{\infty} \sum_{n=0}^{\infty} \frac{\epsilon_{0m} \epsilon_{0n}}{\Gamma_{mn}^2} \left(k^2 - \left(\frac{m\pi}{a}\right)^2\right) \sigma(p) \sigma(q)$$
$$* \left\{ W - \frac{2}{\Gamma_{mn}} e^{-\frac{W}{2}\Gamma_{mn}} \operatorname{Sinh}\left[\frac{W}{2}\Gamma_{mn}\right] \right\}$$

where:

$$\sigma(p) = \begin{cases} \frac{a}{\pi(a^2 p^2 - L^2 m^2)} \left((Lm + ap) \operatorname{Cos}\left[\frac{\pi p}{2} + \frac{m\pi\Delta}{a}\right] \operatorname{Sin}\left[\frac{\pi p}{2} - \frac{m\pi L}{2a}\right] \right. \\ \qquad \left. + (Lm - ap) \operatorname{Cos}\left[\frac{\pi p}{2} - \frac{m\pi\Delta}{a}\right] \operatorname{Sin}\left[\frac{\pi p}{2} + \frac{m\pi L}{2a}\right] \right), & Lm \neq ap \\ \frac{1}{2} \operatorname{Cos}\left[\frac{p\pi}{2} + \frac{m\pi\Delta}{a}\right], & Lm = ap \end{cases}$$

The s-parameters for the transverse slot can be obtained by substituting

$$\theta = 90°$$
$$x = \Delta - \xi$$
$$z = -\eta$$

into (3.47) which are the equations for the scattering parameters for the general slot. The resulting equations are:

$$S_{11} = \frac{j}{2W\sqrt{abkZ_0\beta_{10}}} e^{\Gamma_{10} z_i} \sum_{p=1}^{N} A_p \frac{1}{\Gamma_{10}} \left(k^2 - \left(\frac{\pi}{a}\right)^2\right)$$
$$* \int_{-\frac{L}{2}}^{\frac{L}{2}} \operatorname{Sin}\left[\frac{p\pi}{L}\left(\xi' + \frac{L}{2}\right)\right] \operatorname{Sin}\left[\frac{\pi}{a}(\Delta - \xi')\right] d\xi' \int_{-\frac{W}{2}}^{\frac{W}{2}} e^{\Gamma_{10}\eta'} d\eta'$$

$$S_{21} = e^{-\Gamma_{10}(z_2 - z_i)} - \frac{j}{2W\sqrt{abkZ_0\beta_{10}}} e^{-\Gamma_{10} z_2} \sum_{p=1}^{N} A_p \frac{1}{\Gamma_{10}} \left(k^2 - \left(\frac{\pi}{a}\right)^2\right)$$

$$* \int_{-\frac{L}{2}}^{\frac{L}{2}} \mathrm{Sin}\left[\frac{p\pi}{L}\left(\xi' + \frac{L}{2}\right)\right] \mathrm{Sin}\left[\frac{\pi}{a}(\Delta - \xi')\right] d\xi' \int_{-\frac{W}{2}}^{\frac{W}{2}} e^{-\Gamma_{10}\eta'} d\eta'$$

$$S_{31} = \frac{j}{2W\sqrt{abkZ_0\beta_{10}}} e^{-\Gamma_{10} z_3} \sum_{p=1}^{N} B_p \frac{1}{\Gamma_{10}} \left(k^2 - \left(\frac{\pi}{a}\right)^2\right)$$

$$* \int_{-\frac{L}{2}}^{\frac{L}{2}} \mathrm{Sin}\left[\frac{p\pi}{L}\left(\xi' + \frac{L}{2}\right)\right] \mathrm{Sin}\left[\frac{\pi}{a}(\Delta - \xi')\right] d\xi' \int_{-\frac{W}{2}}^{\frac{W}{2}} e^{-\Gamma_{10}\eta'} d\eta'$$

$$S_{41} = -\frac{j}{2W\sqrt{abkZ_0\beta_{10}}} e^{\Gamma_{10} z_4} \sum_{p=1}^{N} B_p \frac{1}{\Gamma_{10}} \left(k^2 - \left(\frac{\pi}{a}\right)^2\right)$$

$$* \int_{-\frac{L}{2}}^{\frac{L}{2}} \mathrm{Sin}\left[\frac{p\pi}{L}\left(\xi' + \frac{L}{2}\right)\right] \mathrm{Sin}\left[\frac{\pi}{a}(\Delta - \xi')\right] d\xi' \int_{-\frac{W}{2}}^{\frac{W}{2}} e^{\Gamma_{10}\eta'} d\eta'$$

Analytical integration can be carried out using the integral formulas (A.6), (A.7) and (A.9) from Appendix A, also noting that

$$\Gamma_{10}^2 = -\left(k^2 - \left(\frac{\pi}{a}\right)^2\right).$$

The final expressions are:

$$S_{11} = -\frac{jL}{W\sqrt{abkZ_0\beta_{10}}} \mathrm{Sinh}\left[\frac{W}{2}\Gamma_{10}\right] e^{\Gamma_{10} z_i}$$

$$* \sum_{p=1}^{N} A_p \begin{cases} \frac{a}{\pi(ap-L)(ap+L)} \left((ap+L)\mathrm{Cos}\left[\frac{p\pi}{2} + \frac{\pi\Delta}{a}\right]\mathrm{Sin}\left[\frac{p\pi}{2} - \frac{L\pi}{2a}\right]\right. \\ \qquad \left. - (ap-L)\mathrm{Cos}\left[\frac{p\pi}{2} - \frac{\pi\Delta}{a}\right]\mathrm{Sin}\left[\frac{p\pi}{2} + \frac{L\pi}{2a}\right]\right), & L \neq ap \\ \frac{1}{2}\mathrm{Cos}\left[\frac{p\pi}{2} + \frac{\pi\Delta}{a}\right], & L = ap \end{cases}$$

$$S_{21} = e^{-\Gamma_{10}(z_2 - z_i)} + \frac{jL}{W\sqrt{abkZ_0\beta_{10}}} \mathrm{Sinh}\left[\frac{W}{2}\Gamma_{10}\right] e^{-\Gamma_{10} z_2}$$

$$* \sum_{p=1}^{N} A_p \begin{cases} \frac{a}{\pi(ap-L)(ap+L)} \left((ap+L)\mathrm{Cos}\left[\frac{p\pi}{2} + \frac{\pi\Delta}{a}\right]\mathrm{Sin}\left[\frac{p\pi}{2} - \frac{L\pi}{2a}\right]\right. \\ \qquad \left. - (ap-L)\mathrm{Cos}\left[\frac{p\pi}{2} - \frac{\pi\Delta}{a}\right]\mathrm{Sin}\left[\frac{p\pi}{2} + \frac{L\pi}{2a}\right]\right), & L \neq ap \\ \frac{1}{2}\mathrm{Cos}\left[\frac{p\pi}{2} + \frac{\pi\Delta}{a}\right], & L = ap \end{cases}$$

$$S_{31} = -\frac{jL}{W\sqrt{abkZ_0\beta_{10}}}\,\mathrm{Sinh}\left[\frac{W}{2}\Gamma_{10}\right]e^{-\Gamma_{10}z_3}$$

$$*\sum_{p=1}^{N} B_p \begin{cases} \frac{a}{\pi(ap-L)(ap+L)}\left((ap+L)\,\mathrm{Cos}\left[\frac{p\pi}{2}+\frac{\pi\Delta}{a}\right]\mathrm{Sin}\left[\frac{p\pi}{2}-\frac{L\pi}{2a}\right]\right. \\ \qquad\left. -(ap-L)\,\mathrm{Cos}\left[\frac{p\pi}{2}-\frac{\pi\Delta}{a}\right]\mathrm{Sin}\left[\frac{p\pi}{2}+\frac{L\pi}{2a}\right]\right), & L\neq ap \\ \frac{1}{2}\,\mathrm{Cos}\left[\frac{p\pi}{2}+\frac{\pi\Delta}{a}\right], & L=ap \end{cases}$$

$$S_{41} = \frac{jL}{W\sqrt{abkZ_0\beta_{10}}}\,\mathrm{Sinh}\left[\frac{W}{2}\Gamma_{10}\right]e^{\Gamma_{10}z_4}$$

$$*\sum_{p=1}^{N} B_p \begin{cases} \frac{a}{\pi(ap-L)(ap+L)}\left((ap+L)\,\mathrm{Cos}\left[\frac{p\pi}{2}+\frac{\pi\Delta}{a}\right]\mathrm{Sin}\left[\frac{p\pi}{2}-\frac{L\pi}{2a}\right]\right. \\ \qquad\left. -(ap-L)\,\mathrm{Cos}\left[\frac{p\pi}{2}-\frac{\pi\Delta}{a}\right]\mathrm{Sin}\left[\frac{p\pi}{2}+\frac{L\pi}{2a}\right]\right), & L\neq ap \\ \frac{1}{2}\,\mathrm{Cos}\left[\frac{p\pi}{2}+\frac{\pi\Delta}{a}\right], & L=ap \end{cases}$$

Bibliography

[Ackley 1985] D.H. Ackley, G.E. Hinton, T.J. Sejnowski, "A learning algorithm for Boltzmann machines", *Cognitive Science*, Vol.9, p. 147-169, 1985.

[Aspray 1986] W. Aspray, A. Burks, *Papers of John von Neumann on computing and computer theory*, Charles Babbage Institute Reprint Series for the History of Computing, Vol. 12, MIT Press, 1986.

[Bakr 2000] M.H. Bakr, J.W. Bandler, M.A. Ismail, J.E. Rayas-Sánchez, Q.J. Zhang, "Neural space mapping EM optimization of microwave structures", *IEEE Microwave Theory and Techniques Symposium Digest*, 2000.

[Balanis 1989] C.A. Balanis, *Advanced engineering electromagnetics*, John Wiley & Sons, 1989.

[Bandler 1999] J.W. Bandler, M.A. Ismail, J.E. Rayas-Sánchez, Q.J. Zhang, "Neuromodeling of microwave circuits exploiting space mapping technology", *IEEE Microwave Theory and Techniques Symposium Digest*, p. 149-152, 1999.

[Barto 1983] A.G. Barto, R.S. Sutton, C.W. Anderson, "Neuronlike adaptive elements that can solve difficult learning control problems", *IEEE Transactions on Systems, Man, and Cybernetics*, Vol. SMC-13, p. 834-846, 1983.

[Bethe 1944] H.A. Bethe, "Theory of diffraction by small holes", *Physical Review*, Vol. 66, p. 163-182, October 1944.

[Bila 1999] S. Bila, Y. Harkouss, M. Ibrahim, J. Rousset, E. N'Goya, D. Baillargeat, S. Verdeyme, M. Aubourg, P. Guillon, "An accurate wavelet neural-network-based model for electromagnetic optimization of microwave circuits", *International Journal of RF and Microwave Computer-Aided Engineering*, Vol. 9, Issue 3, p. 297-306, May 1999.

[Broomhead 1988] D.S. Broomhead, D. Lowe, "Multivariable functional interpolation and adaptive networks", *Complex Systems*, Vol. 2, p.321-355, 1988.

[Burrascano 1998] P. Burrascano, M. Dionigi, C. Fancelli, M. Mongiardo, "A neural network model for CAD and optimization of microwave filters", *IEEE Microwave Theory and Techniques Symposium Digest*, p. 13-16, 1998.

[Cavalieri 1999] S. Cavalieri, O. Mirabella, "A novel learning algorithm which improves the partial fault tolerance of multilayer neural networks", *Neural Networks 12*, p. 91-106, Elsevier Science Ltd., 1999.

[Cohn 1952] S.B. Cohn, "Microwave coupling by large apertures", *Proceedings of the IRE*, Vol. 40, p. 696-699, June 1952.

[Collin 1969] R.E. Collin, F.J. Zucker, *Antenna Theory Part 1*, McGraw-Hill, Inc., 1969.

[Collin 1973] R.E. Collin, "On the incompleteness of E and H modes in wave guides", *Canadian Journal of Physics*, Vol. 51, p. 1135-1140, 1973.

[Collin 1991] R.E. Collin, *Field theory of guided waves*, 2nd Edition, IEEE Press, New York, 1991.

[Collin 1992] R. E. Collin, *Foundations for microwave engineering*, 2nd Edition, McGraw-Hill, Inc., 1992.

[Creech 1996] G.L. Creech, B. Paul, C. Lesniak, T. Jenkins, R. Lee, M. Calcatera, "Artificial neural networks for accurate microwave CAD applications", *IEEE Microwave Theory and Techniques Symposium Digest*, p. 733-736, 1996.

[Datta 1995] A. Datta, A.M. Rajeek, A. Chakrabarty, B.N. Das, "S matrix of a broad wall coupler between dissimilar rectangular waveguides", *IEEE Transactions on Microwave Theory and Techniques*, Vol. 43, No. 1, p. 56-62, January 1995.

[Dennis 1983] J.E. Dennis, Jr., R.B. Schnabel, *Numerical methods for unconstrained optimization and nonlinear equations*, Prentice-Hall, Inc., 1983.

[Devabhaktuni 1999] V.K. Devabhaktuni, C. Xi, F. Wang, Q. Zhang, "Robust training of microwave neural models", *IEEE Microwave Theory and Techniques Symposium Digest*, p. 145-148, 1999.

[Fahlman 1990] S.E. Fahlman, C. Lebiere, "The cascade-correlation learning architecture", *Advances in neural information processing systems 2*, D.S. Touretzky, Ed., Morgan Kaufmann Publishers, Inc., p. 524-532, 1990.

[Fedi 1998] G. Fedi, A. Gaggelli, S. Manetti, G. Pelosi, "A finite-element neural-network approach to microwave filter design", *Microwave and Optical Technology Letters*, Vol. 19, No. 1, p. 36-38, September 1998.

[Fukumizu 2000] K. Fukumizu, "Statistical active learning in multilayer perceptrons", *IEEE Transactions on Neural Networks*, Vol. 11, No. 1, p. 17-26, January 2000.

[Goasguen 1999] S. Goasguen, S.M. Hammadi, S.M. El-Ghazaly, "A global modeling approach using artificial neural network", *IEEE Microwave Theory and Techniques Symposium Digest*, p. 153-156, 1999.

[Harkouss 1999] Y. Harkouss, J. Rousset, H. Chéhadé, E. Ngoya, D. Barataud, J.P. Teyssier, "The use of artificial neural networks in nonlinear microwave devices and circuits modeling: an application to telecommunication system design", *International Journal of RF and Microwave Computer-Aided Engineering*, Vol. 9, Issue 3, p. 198-215, May 1999.

[Haykin 1999] S. Haykin, *Neural networks: a comprehensive foundation*, Prentice Hall, 1999.

[Hebb 1949] D.O. Hebb, *The organization of behavior: a neuropsychological theory*, John Wiley, 1949.

[Hildebrand 1996] L.T. Hildebrand, *Full-wave analysis of a new microstrip-to-waveguide interconnect configuration*, Ph.D. thesis, University of Pretoria, South Africa, October 1996.

[Hopfield 1982] J.J. Hopfield, "Neural networks and physical systems with emergent collective computational abilities", *Proceedings of the National Academy of Sciences of the USA*, Vol. 79, p.2554-2558, 1982.

[Horng 1993] T. Horng, C. Wang, N. Alexopoulos, "Microstrip circuit design using neural networks", *IEEE Microwave Theory and Techniques Symposium Digest*, p. 413-416, 1993.

[Josefsson 1987] L.G. Josefsson, "Analysis of longitudinal slots in rectangular waveguides", *IEEE Transactions on Antennas and Propagation*, Vol. AP-35, No. 12, p. 1351-1357, December 1987.

[Karystinos 2000] G.N. Karystinos, D.A.Pados, "On overfitting, generalization, and randomly expanded training sets", *IEEE Transactions on Neural Networks*, Vol. 11, No. 5, p. 1050-1057, September 2000.

[Kohonen 1982] T. Kohonen, "Self-organized formation of topologically correct feature maps", *Biological Cybernetics*, Vol. 43, p.59-69, 1982.

[Kruger 1998] J.C. Kruger, *Design of wideband, low loss, high power waveguide couplers and transitions for implementation in power combiners and dividers*, Masters Thesis, University of Stellenbosch, October 1998.

[Langhaar 1980] H.L. Langhaar, *Dimensional analysis and theory of models*, Robert E. Krieger Publishing Company, 1980 (Reprint).

[Lee 1980] S-W. Lee, J. Boersma, C-L. Law, G.A. Deschamps, "Singularity in Green's Function and its numerical evaluation", *IEEE Transactions on Antennas and Propagation*, Vol. AP-28, No. 3, p. 311-317, May 1975.

[Lehmensiek 2001] R. Lehmensiek, *Efficient adaptive sampling applied to multivariate, multiple output rational interpolation models, with applications in electromagnetics-based device modelling*, Ph. D thesis, University of Stellenbosch, March 2001.

[Levenberg 1944] K. Levenberg, "A method for the solution of certain non-linear problems in least squares", *Quarterly of Applied Mathematics*, Vol. 2, No. 2, p. 164-168, 1944.

[Levy 1979] R. Levy, "Improved large aperture waveguide coupling theory", *IEEE Microwave Theory and Techniques Symposium Digest*, p.431-433, 1979.

[Levy 1980] R. Levy, "Improved single and multiaperture waveguide coupling theory, including explanation of mutual interactions", *IEEE Transactions on Microwave Theory and Techniques*, Vol. MTT-28, No. 4, p. 331-338, April 1980.

[Lewin 1960] L. Lewin, "Some observations on waveguide coupling through medium-sized slots", *Proceedings of the IEE*, Vol. 107C, p. 171-178, September 1960.

[Lyon 1981] R.W. Lyon, A.J. Sangster, "Efficient moment method analysis of radiating slots in a thick-walled rectangular waveguide", *IEE Proceedings*, Vol. 128, Pt. H, No. 4, p. 197-205, August 1981.

[Mah 1998] M.Y. Mah, L.L. Liou, R.L. Ewing, A.M. Ferendeci, "Design methodology of microstrip lines using dimensional analysis", *IEEE Microwave and Guided Wave Letters*, Vol. 8, No.7, p. 248-250, July 1998.

[Marquardt 1963] D.W. Marquardt, "An algorithm for least-squares estimation of nonlinear parameters", *Journal of the Society for Industrial and Applied Mathematics*, Vol. 11, No.2, p. 431-441, June 1963.

[McCulloch 1943] W.S. McCulloch, W. Pitts, "A logical calculus of the ideas imminent in nervous activity", *Bulletin of Mathematical Biophysics*, Vol.5, p. 115-133.

[McDonald 1972] N.A. McDonald, "Electric and magnetic coupling through small apertures in shield walls of any thickness", *IEEE Transactions on Microwave Theory and Techniques*, Vol. MTT-20, No. 10, p. 689-695, October 1972.

[Minsky 1969] M.L. Minsky, S.A. Papert, *Perceptrons*, MIT Press, 1969.

[Mishra 1998] R.K. Mishra, A. Patnaik, "Neural network-based CAD model for the design of square-patch antennas", *IEEE Transactions on Antennas and Propagation*, Vol.46, No.12, p. 1890-1891, December 1998.

[Pandharipande 1978] V.M. Pandharipande, B.N. Das, "Coupling of waveguides through large apertures", *IEEE Transactions on Microwave Theory and Techniques*, Vol. MTT-26, No. 3, p. 209-212, March 1978.

[Pandharipande 1979] V.M. Pandharipande, B.N. Das, "Comments on 'Coupling of waveguides through large apertures'", *IEEE Transactions on Microwave Theory and Techniques*, Vol. MTT-27, No. 7, p. 707-708, July 1979.

[Park 1998-1] M. Park, J. Park, S. Nam, "Efficient calculation of the Green's Function for the rectangular cavity", *IEEE Microwave and Guided Wave Letters*, Vol. 8, No. 3, p. 124-126, March 1998.

[Park 1998-2] M. Park, S. Nam, "Rapid summation of the Green's Function for the rectangular waveguide", *IEEE Transactions on Microwave Theory and Techniques*, Vol. 46, No. 12, p.2164-2166, December 1998.

[Piel 1999] P. Piel, J. Griffith, T. Lam, G.W. Pan, "Fast hybrid integral equation-neural network method for the modeling of multiconductor transmission lines", *IEEE Microwave Theory and Techniques Symposium Digest*, p. 1673-1676, 1999.

[Qian 1999] N. Qian, "On the momentum term in gradient descent learning algorithms", *Neural Networks 12*, p. 145-151, Elsevier Science Ltd., 1999.

[Rahmat-Samii 1975] Y. Rahmat-Samii, "On the question of computation of the dyadic Green's Function at the source region in waveguides and cavities", *IEEE Transactions on Microwave Theory and Techniques*, Vol. 23, No. 9, p. 762-765, September 1975.

[Reed 1993] R. Reed, "Pruning algorithms – a survey", *IEEE Transactions on Neural Networks*, Vol. 4, No.5, p. 740-747, September 1993.

[Rengarajan 1989-1] S.R. Rengarajan, "Analysis of a centered-inclined waveguide slot coupler", *IEEE Transactions on Microwave Theory and Techniques*, Vol. 37, No. 5, p. 884-889, May 1989.

[Rengarajan 1989-2] S.R. Rengarajan, "Characteristics of a longitudinal / transverse coupling slot in crossed rectangular waveguides", *IEEE Transactions on Microwave Theory and Techniques*, Vol. 37, No. 8, p. 1171-1177, August 1989.

[Rengarajan 1989-3] S.R. Rengarajan, "Compound radiating slots in a broad wall of a rectangular waveguide", *IEEE Transactions on Antennas and Propagation*, Vol. 37, No. 9, p. 1116-1123, September 1989.

[Riblet 1948] H.J. Riblet, T.S. Saad, "A new type of waveguide directional coupler", *Proceedings of the IRE*, Vol. 36, p. 61-64, January 1948.

[Riedmiller 1993] M. Riedmiller, H. Braun, "A direct adaptive method for faster backpropagation learning: The RProp algorithm", *IEEE International Conference on Neural Networks*, p. 586-591, 1993.

[Rosenblatt 1958] F. Rosenblatt, "The perceptron: A probabilistic model for information storage and organization in the brain", *Psychological Review*, Vol. 65, p. 386-408, 1958.

[Rumelhart 1986-1] D.E. Rumelhart, J.L. McClelland, eds., *Parallel distributed processing: explorations in the microstructure of cognition*, Vol.1 and 2, MIT Press, 1986.

[Rumelhart 1986-2] D.E. Rumelhart, G.E. Hinton, R.J. Williams, "Learning representations by back-propagating errors", *Nature (London)*, Vol. 323, p. 533-536, 1986.

[Sagiroglu 1997] S. Sagiroglu, K. Güney, "Calculation of resonant frequency for an equilateral triangular microstrip antenna with the use of artificial neural networks", *Microwave and Optical Technology Letters*, Vol. 14, No. 2, p. 89-93, February 1997.

[Sagiroglu 1998] S. Sagiroglu, K. Güney, M. Erler, "Resonant frequency calculation for circular microstrip antennas using artificial neural networks", *International Journal of RF and Microwave Computer-aided Engineering*, Vol. 8, p.270-277, 1998.

[Sangster 1965] A.J. Sangster, "Variational method for the analysis of waveguide coupling", *Proceedings of the IEE*, Vol. 112, No. 12, p. 2171-2179, December 1965.

[Sangster 1979] A.J. Sangster, "Slot coupling between uniform rectangular waveguides", *IEEE Transactions on Microwave Theory and Techniques*, Vol. MTT-27, No. 7, p. 705-707, July 1979.

[Sarle] W.S. Sarle, *Neural networks FAQ*, ftp://ftp.sas.com/pub/neural/FAQ.html, updated 2000.

[Shewchuk 1994] J.R. Shewchuk, *An introduction to the conjugate gradient method without the agonizing pain*, School of Computer Science, Carnegie Mellon University, 1994. Available on the internet at http://www.cs.cmu.edu/~jrs/jrspapers.html#cg.

[Shirakawa 1998] K. Shirakawa, M. Shimizu, N. Okubo, Y. Daido, "Structural determination of multilayered large-signal neural-network HEMT model", *IEEE Transactions on Microwave Theory and Techniques*, Vol. 46, No. 10, p. 1367-1375, October 1998.

[Sinha 1987] S.N. Sinha, "A generalised network formulation for a class of waveguide coupling problems", *IEE Proceedings*, Vol. 134, Pt. H, No. 6, p. 502-508, December 1987.

[Smith 1993] M. Smith, *Neural networks for statistical modeling*, Van Nostrand Reinhold, New York, 1993.

[SNNS manual] User manual for the Stuttgart Neural Network Simulator, Version 4.2, University of Stuttgart and University of Tübingen, http://www.informatik.uni-stuttgart.de/ipvr /bv/projekte/snns/snns.html.

[Sollich 1994] P. Sollich, "Query construction, entropy, and generalization in neural-network models", *Physical Review E*, Vol. 49, p. 4637-4651, 1994.

[Stevenson 1948] A.F. Stevenson, "Theory of slots in rectangular waveguides", *Journal of Applied Physics*, Vol. 19, p. 24-38, January 1948.

[Stutzman 1998] W.L. Stutzman, G.A. Thiele, *Antenna theory and design*, 2nd Edition, John Wiley & Sons, Inc., 1998.

[Tai 1994] C. Tai, *Dyadic Green Functions in electromagnetic theory*, 2nd Edition, IEEE Press, 1994.

[Treadgold 1999] N.K. Treadgold, T.D. Gedeon, "Exploring constructive cascade networks", *IEEE Transactions on Neural Networks*, Vol.10, No.6, p. 1335-1350, November 1999.

[Vai 1993] M. Vai, S. Prasad, "Automatic impedance matching with a neural network", *IEEE Microwave and Guided wave Letters*, Vol. 3, No. 10, p. 353-354, October 1993.

[Vai 1998] M.M. Vai, S. Wu, B. Li, S. Prasad, "Reverse modeling of microwave circuits with bidirectional neural network models", *IEEE Transactions on Microwave Theory and Techniques*, Vol. 46, No. 10, p. 1492-1494, October 1998.

[Vu Khac 1972] T. Vu Khac, C.T. Carson, "Coupling by slots in rectangular waveguides with arbitrary wall thickness", *Electronics Letters*, Vol. 8, No. 18, p. 456-458, September 1972.

[Vu Khac 1973] T. Vu Khac, C.T. Carson, "Impedance properties of a longitudinal slot antenna in the broad face of a rectangular waveguide", *IEEE Transactions on Antennas and Propagation*, Vol. 21, p. 708-710, September 1973.

[Wang 1997] F. Wang, Q.J. Zhang, "Knowledge-based neural models for microwave design", *IEEE Transactions on Microwave Theory and Techniques*, Vol. 45, No. 12, p. 2333-2343, December 1997.

[Wang 1999] F. Wang, V.K. Devabhaktuni, C. Xi, Q.J. Zhang, "Neural network structures and training algorithms for RF and microwave applications", *International Journal of RF and Microwave Computer-Aided Engineering*, Vol. 9, Issue 3, p. 216-240, May 1999.

[Watson 1996-1] P. Watson, K.C. Gupta, "EM-ANN models for via interconnects in microstrip circuits", *IEEE Microwave Theory and Techniques Symposium Digest*, p. 1819-1822, 1996.

[Watson 1996-2] P.M. Watson, K.C. Gupta, "EM-ANN models for microstrip vias and interconnects in dataset circuits", *IEEE Transactions on Microwave Theory and Techniques*, Vol. 44, No. 12, p. 2495-2503, December 1996.

[Watson 1997] P.M. Watson, K.C. Gupta, "Design and optimization of CPW circuits using EM-ANN models for CPW components", *IEEE Transactions on Microwave Theory and Techniques*, Vol. 45, No. 12, p. 2515-2523, December 1997.

[Watson 1998] P.M. Watson, K.C. Gupta, R.L. Mahajan, "Development of knowledge based artificial neural network models for microwave components", *IEEE Microwave Theory and Techniques Symposium Digest*, p. 9-12, 1998.

[Watson 1999] P.M. Watson, M.Y. Mah, L.L. Liou, "Input variable space reduction using dimensional analysis for artificial neural network modeling", *IEEE Microwave Theory and Techniques Symposium Digest*, p. 269-272, 1999.

[Widrow 1960] B. Widrow, M.E. Hoff Jr., "Adaptive switching circuits", *IRE Western Electric Show and Convention Record*, Part 4, p. 96-104, 1960.

[Wu 1999] C. Wu, E.A. Navarro, J. Navasquillo, J. Litva, "FDTD signal extrapolation using a finite impulse response neural network model", *Microwave and Optical Technology Letters*, Vol. 21, No. 5, p. 325-330, June 1999.

[Zaabab 1994] A.H. Zaabab, Q.J. Zhang, M. Nakhla, "Analysis and optimization of microwave circuits & devices using neural network models", *IEEE Microwave Theory and Techniques Symposium Digest*, p. 393-396, 1994.

[Zaabab 1997] A.H. Zaabab, Q. Zhang, M.S. Nakhla, "Device and circuit-level modeling using neural networks with faster training based on network sparsity", *IEEE Transactions on Microwave Theory and Techniques*, Vol. 45, No. 10, p. 1696-1704, October 1997.

[Zhang 2000] Q.J. Zhang, K.C. Gupta, *Neural networks for RF and microwave design*, Artech House, Inc., 2000.

[Zurada 1992] J.M. Zurada, *Introduction to artificial neural systems*, West Publishing Company, 1992.